The Solution and Solid State Analysis of Xylylic Di-copper Complexes as Receptors for Encapsulating Anions

James Rawiri Stevens

2011

A thesis presented in partial fulfillment of the requirements for the degree of

Master of Science

in Chemistry at Massey University, Palmerston North, New Zealand

Abstract

The investigation into neutral aryl-linked oxime dicopper helicates encapsulating a number of anions was carried out. Two dicopper aryl-linked salicyloxime derived complexes were synthesized and studied which contained either *p*-xylylic (**1**) or *m*-xylylic (**2**) incorporated spacer groups. UV-visible spectroscopy was used to determine the binding stability constants of the anion complexes. Complex binding, encapsulation of anions and the conformational flexibility of **1** and **2** was supported and ascertained by the crystal structural data obtained. Receptor **1** expressed an exceptional binding strength for sulfate in THF where a log *K* value of 5.5 ± 0.3 was acquired. Receptor **2** could form both helical and non-helical structures. This was able to bind bromide selectively in a 2:1 stoichiometry of anion:receptor with a log K_2 value of 9.2 ± 0.1 and showed an unexpectedly high association constant for the perchlorate anion in a 1:1 stoichiometry with a log *K* value of 4.6 ± 0.2 (presumably in a helical structure).

Acknowledgements

Firstly, I wish to give a great big shout out to everyone that has contributed towards this project. The ever helpful knowledge, assistance and insight into synthetic techniques, crystal growth and formation and spectroscopic analysis provided by my supervisor Dr Paul Plieger has helped me immensely to complete my project and thesis. Another great big thank you goes out to Dr Marco Wenzel and Ross Davidson for all their help and knowledge in the lab and office whenever I needed it.

A very special thanks goes to my girlfriend Kelsey, for her love, understanding and support during all the long boring nights of thesis writing. She has also provided focus to the work at hand through her heartening smile and love throughout the last few years.

Many thanks must go towards my dependable and steadfast friend Liam. Without his protective roof over my head and the continually enjoyable evenings together, I believe we gained a lot of mutual respect and understanding of each other.

I also wish to express appreciation to Geoff Jameson, who assisted in X-ray crystallography assignment; Pat Edwards for providing excellent knowledge of NMR; Dave Lun for his help in expanding my knowledge of the ESMS system and lastly but not in the least to all my fellow co-workers and friends I have made along this perilous journey to which the advice and support has been encouraging.

I express sincere appreciation to all, as there is no doubt that the project would not have been successful without their efforts.

Contents

List of Figures

List of Tables

Abbreviations

⊂	Indicates encapsulation of a guest molecule within a host molecule/complex.
1	Anion-free complex formed between Cu(II) acetate and ligand **L[1]**. It is used within this report to represent the unprotonated complex $[Cu_2(L^1\text{-}2H)_2]$.
1a	N, N'-dimethyl-p-xylylenediamine.
1b	3, 3'-(1, 4-phenylenebis(methylene))bis(methylazanediyl)bis (methylene)bis(5-*tert*-butyl-2-hydroxybenzaldehyde).
2	Anion-free complex formed between Cu(II) acetate and ligand **L[2]**, representing the unprotonated form $[Cu_2(L^2\text{-}2H)_2]$.
2a	N, N'-dimethyl-m-xylylenediamine.
2b	3, 3'-(1, 3-phenylenebis(methylene))bis(methylazanediyl)bis (methylene)bis(5-*tert*-butyl-2-hydroxybenzaldehyde).
3	$[ClO_4{\subset}(Cu_2L^1{}_2)](ClO_4)_3$; the zwitterionic form with a captured perchlorate anion.
4	$[BF_4{\subset}(Cu_2L^1{}_2)](BF_4)_3$; the zwitterionic form with a captured tetrafluoroborate anion.
5	$[NO_3{\subset}(Cu_2L^2{}_2)](NO_3)_3$; the zwitterionic form with a captured nitrate anion.
6	$[2Br{\subset}(Cu_2L^2{}_2)](Br)_2$; the zwitterionic form with two captured bromide anions and two counter bromide anions.
7	$[2Br{\subset}(Cu_2L^2{}_2)](BF_4)_2$; the zwitterionic form with two captured bromide anions and two counter tetrafluoroborate anions.
CCDC	Cambridge Crystallographic Data Centre.
$CHCl_3$	Chloroform.
DCE	1,2-dichloroethane.
DMSO-d_6	Deuterated dimethyl sulfoxide.

ESMS	Electrospray Ionization Mass Spectrometry.
IPA	Isopropanol.
IR	Infrared spectroscopy.
K	Formation constant. The equilibrium constant for the formation of a complex in solution. Also referred to as the binding, stability or association constant throughout the text.
L^1	(1*E*, 1'*E*)-5-*tert*-butyl-3-(((4-(((5-*tert*-butyl-2-hydroxy-3-((*E*)-(hydroxyimino)methyl)benzyl)(methyl)amino)methyl)benzyl)(methyl)amino)methyl)-2-hydroxybenzaldehyde oxime.
L^2	(1*E*, 1'*E*)-5-*tert*-butyl-3-(((3-(((5-*tert*-butyl-2-hydroxy-3-((*E*)-(hydroxyimino)methyl)benzyl)(methyl)amino)methyl)benzyl)(methyl)amino)methyl)-2-hydroxybenzaldehyde oxime.
MeOH	Methanol.
MeCN	Acetonitrile.
NMR	Nuclear magnetic resonance.
THF	Tetrahydrofuran.
TBABr	Tetra-*n*-butylammonium bromide.
t-Bu	tertiary butyl group or 1,1-dimethylethyl group ($(CH_3)_3C$–).
UV-vis	Ultraviolet-visible spectroscopy.

Chapter 1

Introduction

1.1 Anion Binding Systems

1.1.1 Anion Background

Anions are ever present throughout the environment[1-3] and are important in a wide variety of living systems and organisms. Examples of anion interactions within systems can be found throughout the literature. The Cl^- channel ClC-3 has been implicated to be responsible for biological processes within cells, including cell volume, migration, apoptosis and cell pH.[4] Other examples of biological processes involving anions include sulfate binding to the active site of enzymes[5] (Figure 1) and proteins[6] and the transport of Cl^-/HCO_3^- in anionic transporters[7-10]. Anions are also involved in medicine[11, 12] and as catalysts (Figure 2).[13]

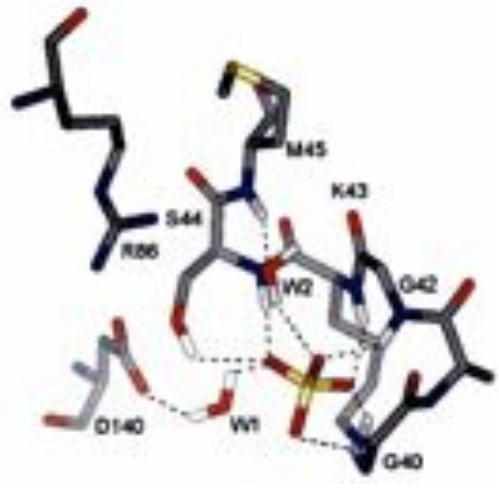

Figure 1. Schematic view of the ATPase active site showing the interactions of the bound sulfate anion with various P-loop residues.[5]

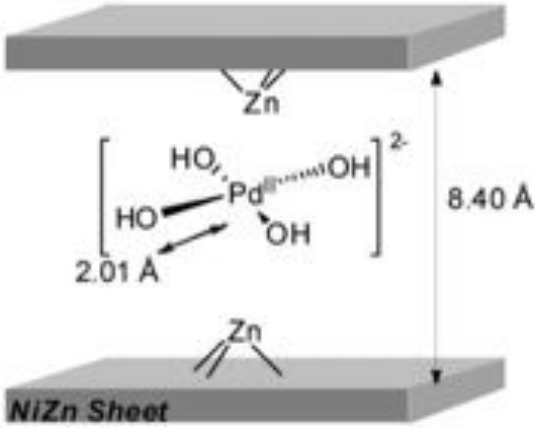

Figure 2. Proposed structure of a NiZn–Pd nanocomposite catalyst, showing an intercalated anionic Pd(II) hydroxide complex. This acts as an efficient heterogeneous catalyst for the oxidation of alcohols under an air atmosphere.[13]

As such, there is an increasing need for the application of anion binding systems for detection and binding of anions and research into the mechanisms and structure of potential systems is required.

Cation binding has received considerable attention due to the inherently more favorable properties of cations (e.g. many possible oxidation states for transition metals), but is more likely due to the wide variety and importance of metal activity. To a lesser extent anion binding has been studied. This lack of attention is due to the fundamental complications of binding anions. As a consequence of the weak coordinating ability of anions, many such as CH_3COO^-, BF_4^- and NO_3^- have been labeled as non-coordinating based on their behavior in aqueous media. In non-aqueous media these anions can be found to show coordination.[14] The weaker binding of anions can be accredited to the many difficulties of binding anions compared to cation binding.[15] Anions are larger than their corresponding isoelectronic cations; therefore the charge density for anions will be lower than the isoelectronic cations and electrostatic interactions will have less of an effect. Anions have a wide range of geometries, sizes and charges and they possess varying degrees of hydrophobicity. The pH dependence must be taken into account when binding anions, as electrostatic and H-bonding interactions will be affected by the protonation state of the anion. H-bonding displays a high degree of regioselectivity.[16] Hence, when setting out to design anion receptors, one must try to account for these differences and incorporate appropriate functional groups in order to maximize effective favorable interactions towards anions, such as electrostatic, H-bonding and metal-anion interactions.[17]

1.1.2 Anion Receptor Evolution

In 1968, the field of anion receptor chemistry was brought to light by Park and Simmons[18-20] with the encapsulation of halide anions within macrobicyclic amine receptors. They consisted of two ammonium bridged centres connected by three alkyl linkers. The chloride anion was found to be

the most strongly bound within the cavity of the positively charged receptor. This was further evidenced by the crystal structure in 1975.[21]

Anion recognition can be accomplished in a number of ways. The usual methods used to bind anions include H-bonding, electrostatic interactions, ion-pair recognition, metal-ion coordination and combinations of these interactions working together.[22] A more recent and less conventional mode of anion binding is with electron deficient π–orbital systems,[23-27] leading to even more possibilities when designing anion receptors. This amounts to a large number of possible functionalities that may be considered to be incorporated into an anion receptor and equates to receptors having many different forms. Early examples of anion receptors displayed simple designs such as the macrobicyclic amine receptors of Park and Simmons[18-20] and the spherical cryptates of Lehn[28, 29] based on polyammonium ion structures. These early examples have since evolved into more complex anionic receptors. An example of this is Young and coworkers' cyclic peptide-thiourea cryptands (Figure 3).[30] These organic receptors still possess the cyclic structure but now possesses thiourea functionalities in the radial arms. ^{1}H-NMR titration studies were carried out in 0.5% v/v H_2O/DMSO-d_6. In this solvent mixture, cryptand 1 demonstrated larger binding constants for the smaller halide ions (F^-, Cl^-) over cryptand 2 (Figure 3). The greater range of binding anions to cryptand 1 over cryptand 2 is possibly due to the more flexible tren-cap in cryptand 1 over the more rigid 1,3,5-triethylbenzene-cap in cryptand 2 thus allowing some flexibility to accommodate a variety of differently shaped and sized monovalent anions (e.g. the halides, $H_2PO_4^-$ and AcO^-). In contrast, cryptand 2 shows a very high selectivity for the acetate anion with a binding constant of $>10^4$ M^{-1}, over three orders of magnitude higher than any of the other anions investigated.

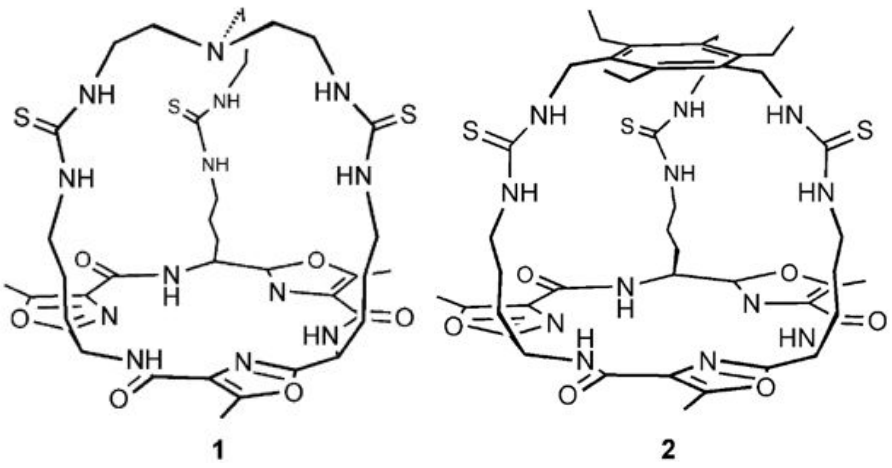

Figure 3. Young and co-workers' flexible tren-capped cryptand 1 and the more rigid 1,3,5-triethylbenzene-capped cryptand 2.[30]

Another example of a more complex anion receptor can be seen with a steroid based compound, cholic acid, used as a backbone scaffold that can be further functionalized to provide anion binding motifs (Figure 4).[31]

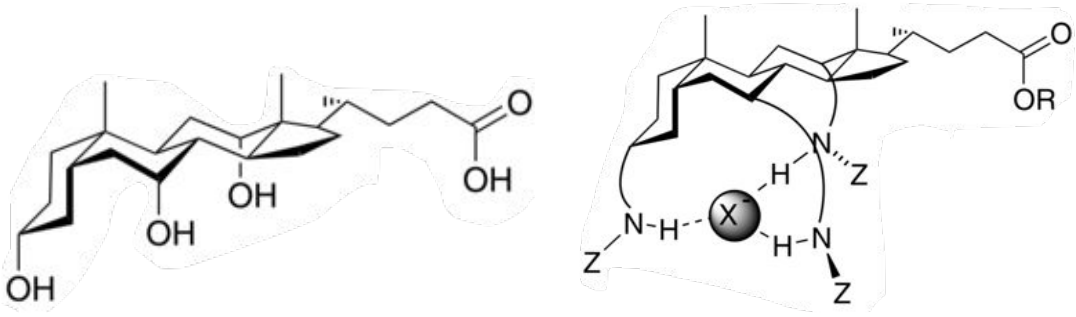

Figure 4. Cholic Acid (left) and an example of a modified cholic acid anion receptor derivative (right).[31]

Simple receptors incorporating polyamine functionalities are also effective at binding anions. An example are the macrocyclic polyamine receptors (Figure 5 and 6) that contain six amine moieties separated by either alkyl or ether spacers. These flexible polyamines can bind anions above and below their cyclic planes to form 1:2 receptor:anion stoichiometry binding complexes, like receptor **17** with $H_2PO_4^-$ at low pH.[32, 33]

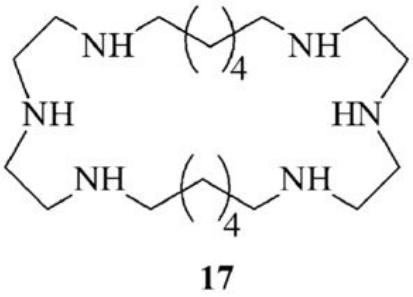

17

Figure 5. Macrocyclic polyamine **17** with an akyl chain spacer.[32]

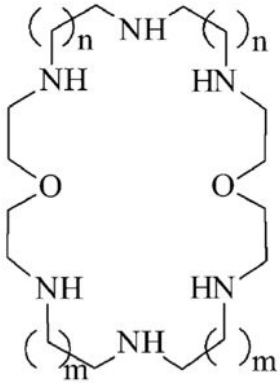

18: n = 1, m = 1
19: n = 1, m = 2
20: n = 2, m = 2

Figure 6. Macrocyclic polyamines **18-20** with an ether spacer.[32]

Incorporating aromatic spacers into cyclic polyamines is a way to provide rigidity, increase sites for additional π–π stacking interactions, increase electrostatic and hydrophobic interactions, complement H-bond forces in biologically important anions and put in place an element of pre-organization.[32] Ligands **21**-**23** and **P3** (Figure 7) exemplify these added effects. These ligands now have the added ability of being able to fully surround, or encompass an anion when protonated. This is shown by the work carried out by Martell[34, 35] and co-workers' where the bromide and pyrophosphate anions are shown to be bound within the cavity of the receptors via a combination of H-bonding and ion-pairing interactions. Ligands **21** and **22** are able to form 1:1 ratios of anion to receptor complexes with the pyrophosphate anion ($P_2O_7^{4-}$). Substituting aryl functionalities into alkyl receptors does not necessarily increase the binding strength of receptors. The alkyl receptors **18** and **20** were found to bind anions more strongly in 1:1 complexes than the more rigid structural analogues **22** and **23**, as was the case with the $P_3O_{10}^{5-}$ anion where the pentaprotonated receptor $(H_5\mathbf{20})^{5+}$ has a log *K* binding constant of 7.06 compared to $(H_5\mathbf{23})^{5+}$ which had a log *K* binding constant of 6.61. This is most likely due to the higher/increased flexibility of the alkyl ligands, allowing them to better surround the anions.

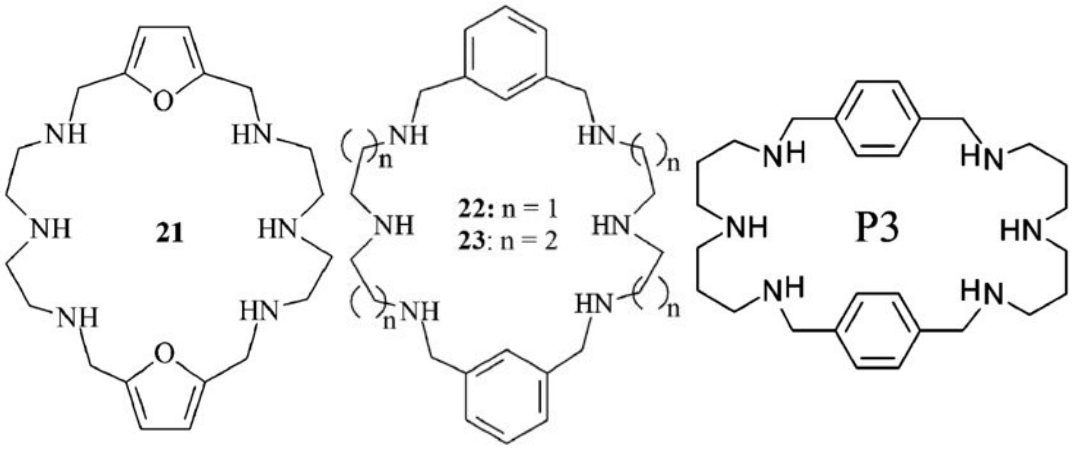

Figure 7. Cyclic aryl-linked polyamines **21**, **22**, **23** and **P3**; rigid analogues of the alkyl-linked cyclic polyamines in Fig. 5 and 6.[32, 34-36]

One way to gain a higher strength of binding an anion within a receptor is to alter the restricting/rigid aryl-linker in the receptor to form an isomeric ligand. This can be achieved by incorporating either ortho-, meta- or para-xylylic linkers. This was shown by comparison of the anion binding properties of the **23** (*m*-xylylic) and **P3** (*p*-xylylic) isomeric ligands (Figure 7). It was found that **23** bound the diphosphate anion more strongly than **P3** over the pH range of 4-7. This was thought to be because of the slight change in the shape and size of the cavity between the two ligands; **23** has a smaller cavity than **P3** and was better able to fit the anion inside, thus providing stronger interactions resulting in a more strongly bound anion.[36]

A further modification that can be utilized for stronger anion binding is to increase the dimensionality of the receptor. Encapsulation of a molecule, whether it is cationic, anionic or neutral, within the central cavity of a supramolecular host molecule is known as molecular encapsulation. Due to the differing interactions of the host environment, the guest molecule experiences a different chemical environment than the free molecules. Cage-like arrangements help to increase the selectivity and strength of binding anionic guests. They provide opportunities for more anion-receptor interactions and can have slow anion transfer rates. Examples of cage-like

receptors are the *p*-xylylic and *m*-xylylic cryptands (Figures 8).[32, 39] The openings between the aryl linkers give enough space to allow cations and anions through and are even able to encapsulate multiple ions, whereas some larger tetrahedral anions were not able to enter the cavities of these receptors, excluding them from within the cavity and binding instead on the periphery of the ligand (Figure 8).[37, 39] The *p*-xylylic cryptand is able to encapsulate most large anions like I^- and ClO_4^- at room temperature while the larger $H_2PO_4^-$ ion is unable to pass the aryl arms and instead multiple $H_2PO_4^-$ ions are situated on the outside of the protonated receptor. If the temperature is increased (100 °C), the increase in the thermal motion then allows $H_2PO_4^-$ to be encapsulated and held in place by multiple H-bonds from the protonated amine groups.[32, 37]

Comparing the *p*-xylylic linker to the *m*-xylylic isomer (Figure 8), the binding properties of the receptor are changed. The *m*-xylylic cryptand, with a smaller central cavity, is now unable to encapsulate the large I^- anion (Figure 8). In contrast, the *m*-xylyl ligand is able to bind fluoride more strongly at pH 5 (log *K* of 3.64) than the slightly larger sized *p*-xylylic ligand (log *K* of 3.15).[38, 39]

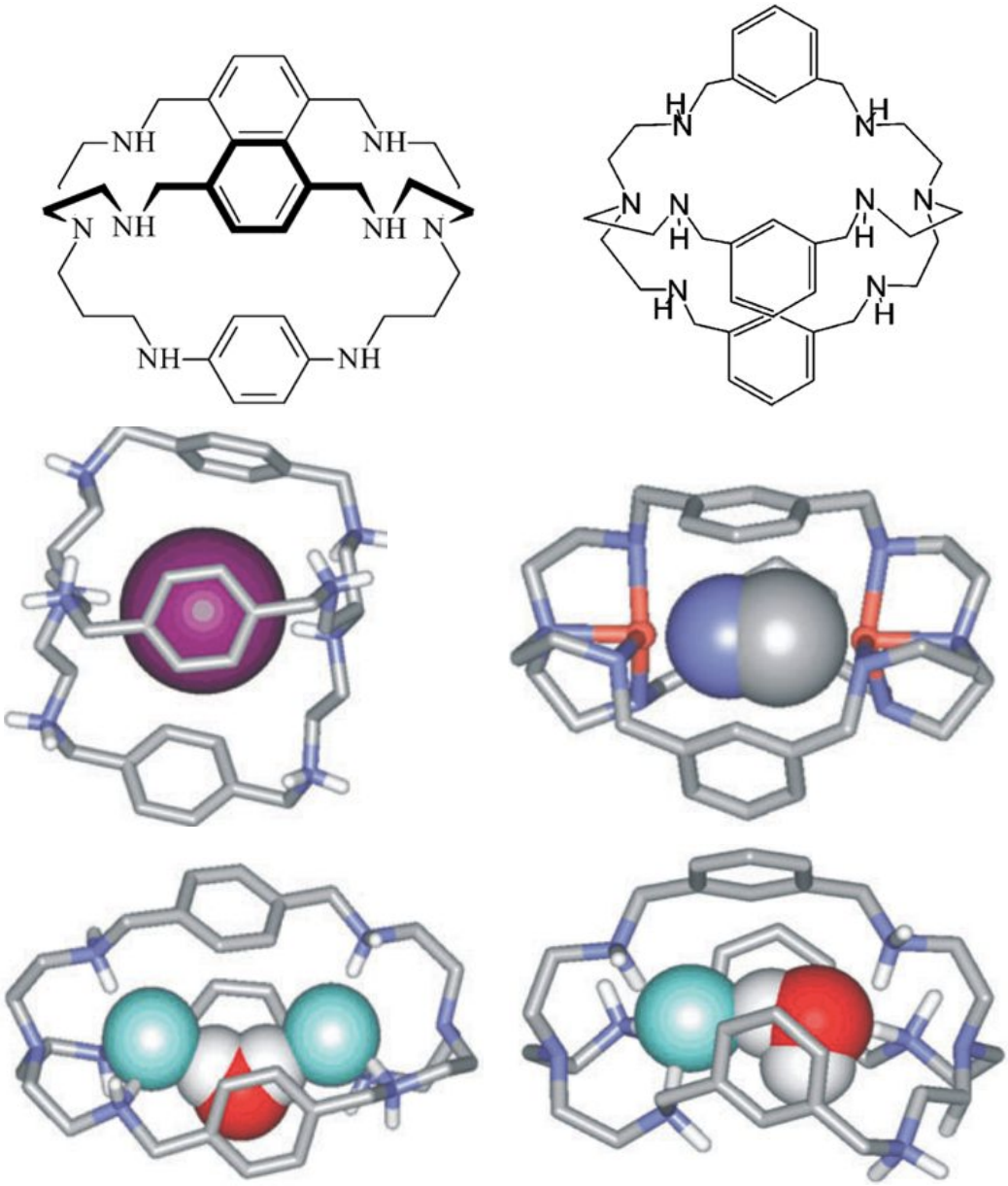

Figure 8. The octaaza cryptands; *p*-xylylic cryptand (left column), *m*-xylylic cryptand (right column), X-ray structure encapsulating I^- (middle left), X-ray structure encapsulating a bridging CN^- anion between two Cu(II) cations in the dinuclear complex (middle right), X-ray structure encapsulating two F^- anions with a bridging H_2O (bottom left) and the X-ray structure encapsulating one F^- anion and one H_2O (bottom right).[32, 37-39]

By incorporating aryl ring systems into anion receptors, a new anion–π interaction is able to come into play to bind anions. Chen *et al's* ditopic receptor is able to bind cations through the calixazacrown ether functionality.[40] The fluorescence and ^{1}H-NMR titrations performed led them to

conclude that the anions investigated are bound via anion–π interactions to the V-shaped cleft formed by the two triazine rings. When zinc(II) was coordinated to the receptor, the complex was able to strongly bind chloride, bromide and nitrate anions, whereas the metal-free complex was not able to bind these anions.[40]

Anions have the ability to induce different conformations in binding receptors depending on a particular anion's shape and size. An example is the urea functionalized isoquinoline Pt(II) complex (Figure 9) of Gale.[41] The ligands bound to the Pt(II) centre are flexible enough to be able to give the complex different conformations upon complexing with spherical halides and tetrahedral oxoanions. In the crystal structure containing the chloride anion (Cl^-) the complex forms a 1:2 receptor:anion complex, with each Cl^- bound by two pairs of adjacent urea functionalities and positioned directly above and below the Pt(II) centre. In contrast, the X-ray structure of the SO_4^{2-}–containing complex has all of the urea ligands on the same face of the anion which fully surround and encapsulate it utilising eight H-bonds, forming a new 1:1 receptor:anion complex conformation.

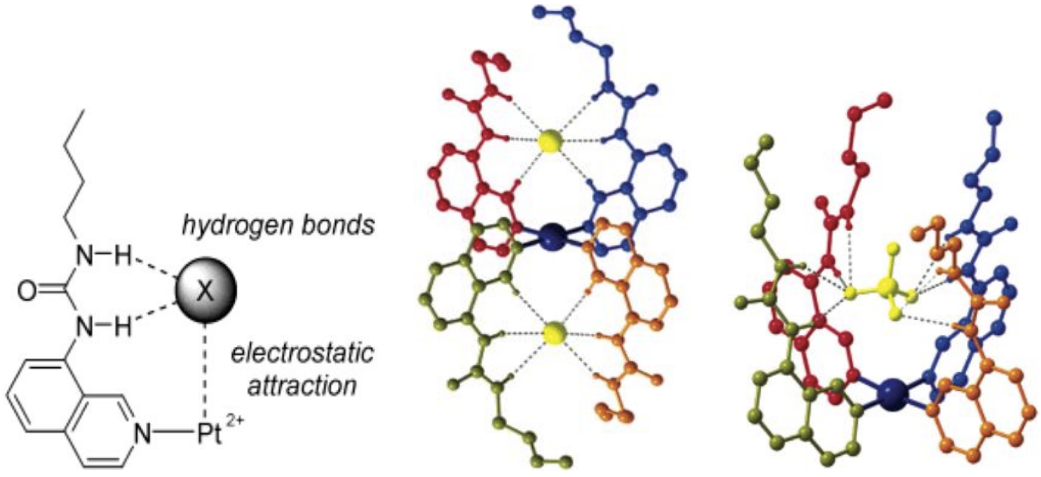

Figure 9. Schematic of the interactions in the urea/Pt(II) complex (left), X-ray structure of the 1:2 receptor:chloride complex (middle) and the x-ray structure of the 1:1 receptor:sulfate complex (right).[41] (colour scheme; ligands are red, blue, green and orange, Pt(II) is dark blue and the anions Cl^-/SO_4^- are both yellow).

Sequential binding of a cationic metal and its attendant anion by a single receptor/complex is an effective method of binding anions. Such a receptor needs to have at least two special binding sites; one for metal coordination and a second for the binding of anions. An example of this is shown in Figure 9 with the urea based complex. Another simpler ditopic receptor is the salen-derived receptor (Figure 10) used by Tasker[42] and colleagues in 1999, where the metal dianionic coordination site is made up of phenol and imine moieties and the anion dicationic binding site the amine moiety. Upon complexation with Cu(II) or Ni(II), the phenols are deprotonated and the protons are transferred to the tertiary amine groups, simultaneously templating the binding of its attendant anion (e.g. SO_4^{2-}), forming a zwitterionic complex.[43] The protonated nitrogen atoms encourage binding of the anion via electrostatic and H-bonding interactions.

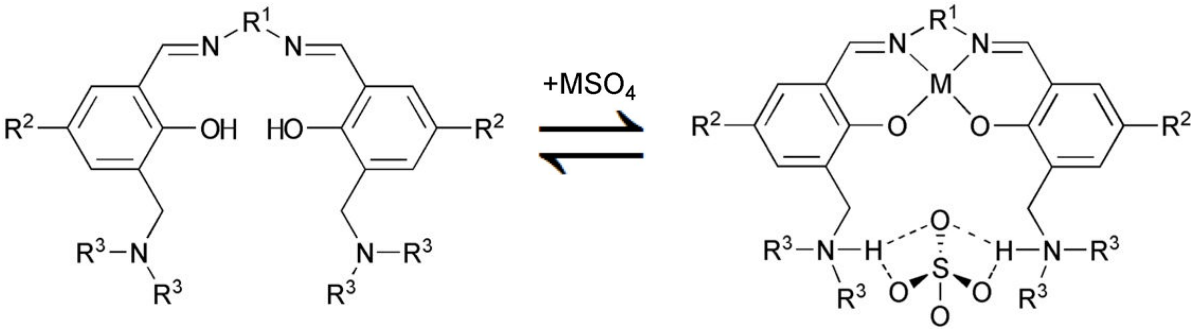

Figure 10. Salen-derived ligands of Tasker and co-workers', able to bind both a metal cation and its attendant anion. (Typical R^1 group = (CH_2CH_2), typical R^2 = CH_3 or *t*-Bu and typical R^3 groups = morpholine or C_6H_{13} alkyl chains).[42]

A related system was used by Plieger[44] throughout the last decade (Figure 11). The ligand replaces the ethylenediimine linker instead with un-linked iminophenyl groups and has also incorporated an *N,N'*-dimethylhexane-1,6-diamine (C6 alkyl) strap. When copper salts of SO_4^{2-} or BF_4^- are added to solutions of the ligand, a helicate structure forms with a 2:2 metal to ligand ratio. Both metals bind to an N_2O_2 binding site, made up of phenolate and imino donors from each ligand. The amine

containing alkyl straps form the sides of the central cavity that separate the metal binding centres. Upon metal coordination, the phenol becomes deprotonated and the protons are transferred to the tertiary amines to form a zwitterionic complex. The cavity has shown it is able to encapsulate a variety of anions, including SO_4^{2-}, BF_4^- and I^-, by either covalent bonds to the metals or by electrostatic and H-bond interactions to the protonated amines.[44-48]

More recently, the anion-free complex with the oxime containing ligand L2 (Figure 11) had been shown to have a large empty cavity with a Cu – Cu distance of 10.191(3) Å. With the addition of an acid, for example HBF_4, the central cavity contracts to accommodate the encapsulation of the anion to give a shorter Cu – Cu distance of 6.938(2) Å, which increases the complex's helical twist by 34°. Upon encapsulation of the BF_4^- ion, the interactions of the complex with it results in a change in the electronic spectrum, allowing the uptake to be followed spectrophotometrically, to give a log *K* value of 4.0 ± 0.1 in a 1:1 mixture of IPA/DCE.[46] In this solvent system, the helical complex shows a general trend of an increase in the association constants with an increase in the size of the captured anion; however, there was not much discrimination in binding strength between the anions studied (log *K* range of 3.5 – 4.5). This was due to more efficient H-bonding and electrostatic interactions with the protonated amines of the complex with the increase in the size of the anion. The higher binding constants for the sulfate and phosphate anions are a direct consequence of coordination to the copper centres.[45, 46] This helicate system has shown that it is highly selective for the sulfate anion from extraction studies carried out from aqueous solutions into a water-immiscible organic phase, even in the presence of high concentrations of other potential binding anions, including chloride, nitrate and the structurally similar yet more hydrophobic dihydrogenphosphate anion.[47]

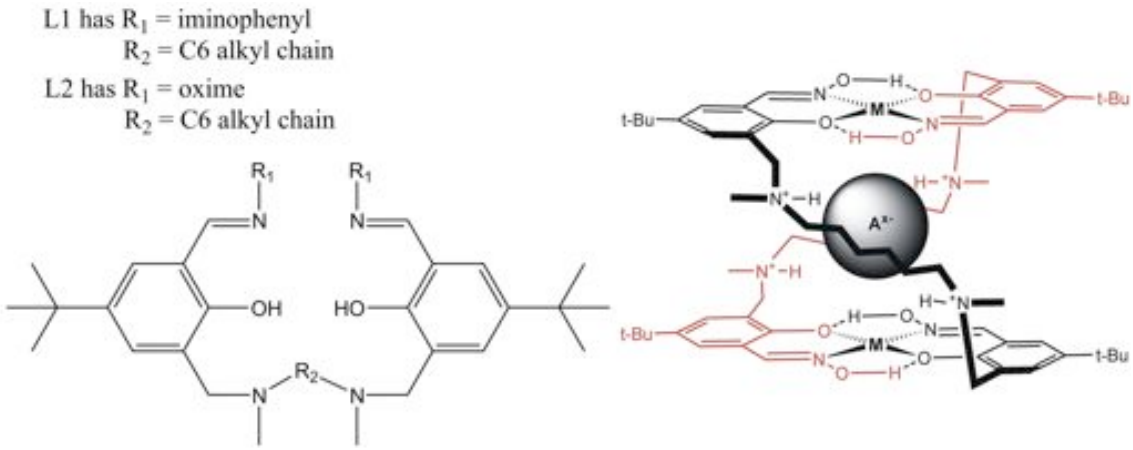

Figure 11. The general alkyl-chain linked ligand (left) used by Plieger and co-workers' to form the Cu(II) helicate complex with an encapsulated anion with L2 (right).[44-48]

A series of L1 derived helical complexes have also been investigated and shows a general trend of an increase in the stability constants with an increase in the size of the captured anion. It was noted that a larger difference in the binding constants between sulfate and the other anions investigated exists.[48]

1.2 Assessment of Anion Receptor Systems

Following an anion receptor's successful synthesis, it is essential to discover how effective anions are bound by the receptor. A range of methods are available to accomplish this. ESMS is one such technique that can be used to analyze large non-volatile macromolecules including proteins and supramolecular complexes.[49] ESMS involves pumping a dilute solution of analyte through a capillary with a large potential (2-5kV) across the capillary tip. The potential may be positive or negative and results in charge separation at the liquid surface. Then droplets with excess charge are ejected from the capillary into the mass spectrometer. These droplets are divided until vapour phase ions are created. These ions are analysed by the mass to charge

ratio.[50] The technique has been shown to be exceedingly useful in analyzing large complexes with multiple counter ions. This is because of the weak ionizing features of ESMS that allows the identification of fragments that contain encapsulated anions but are free of the peripheral counter anions. A number of peaks are then observed. These peaks represent the parent ion(s) with a mass to charge ratio dependent on the number of ions removed. Knapp's work on dicopper helicates with a range of counter ions demonstrates this well.[45]

It is useful to establish just how strongly an anion is bound by a particular receptor. This can be achieved by calculating the stability constants for the association of the anion guest. If acid is titrated into a solution containing a receptor which has the ability to interact and bind with the anion, then the equilibrium;

$$r\mathrm{R} + a\mathrm{A}b\mathrm{H} \rightleftharpoons [\mathrm{R}_r\mathrm{A}_a\mathrm{H}_b]$$

Equation 1.1

is established, where AH and R represent the acid and receptor molecules respectively. The values of *a* and *r* can be established by formulating a mole-ratio plot or through the method of continuous variation.[51, 52] The mole-ratio plot is made by monitoring a physical change that occurs when anions interact with the receptor as a function of the equivalents of anion added. If the binding is strong enough, a noticeable change in this property should occur at the stoichiometric binding ratio. However, weaker binding doesn't cause as much change, thus resulting in a curve over which the tangents can be extrapolated to determine the main species. The method of continuous variation, often referred to as a Job plot, involves plotting the changes in the measured property as a function of the mole equivalents of either the anion or receptor so that the total concentration of both at any point are constant. Once adjusted for the presence of reactants, the plot will show a maximum or minimum at the receptor-anion stoichiometry, corresponding to

the product. The most commonly used visible changes in determining binding constants are with ^{1}H-NMR shifts and UV-visible absorbance measurements.

From equation 1.1, the overall stability constant between the anion and receptor binding is given by the equation;[52]

$$\beta_{rab} = \frac{[R_rA_aH_b]}{[R]^r\,[AH]^{ab}}$$

Equation 1.2

To calculate the association constant, the concentration of either the anion or the receptor must be known. By titrating a solution of an anion into a solution of receptor, the appropriate concentration for a series of solutions of known reactant concentration is determined. The concentrations in the above equation can then be calculated. The stability constants are obtained by best-fitting the experimental data with a chemical model of the equilibrium system. These preliminary values are then refined using a non-linear least squares analysis. NMR chemical shift measurements and spectrophotometry, including UV-visible absorbance and fluorescence measurements are the most routinely used experimental methods for calculating formation constants.[51]

For receptors that possess nuclei with non-zero quantum spin, NMR spectroscopy measurements can be exploited. This would involve analyzing the change in the chemical shifts of protons as they are altered by the binding anion(s). As chemical exchange is fairly rapid on the NMR time-scale, the chemical shifts ($\bar{\delta}$) represent the mole-fractions weighted average of the shifts of the nuclei involved. The observed change in the chemical shifts can again be analysed by best-fitting the experimental data to a suitable model. The model will be based on the determined reaction stoichiometry, which can be calculated from the method of continuous variation or mole-ratio plots. These involve the observed change in the chemical shift of affected protons which is multiplied by the mole-ratio of receptor for the Job plot.[51] A great advantage

of using NMR shifts is that the information about individual H-bond donors is measured, giving a vast amount of information indicating where the binding is taking place in solution. However, due to some limitations of NMR, such as the high solubility of the complex needed in specific deuterated solvents and the lack of being able to study paramagnetic receptors, UV-visible spectroscopy exceeds NMR as the most widely used technique for determining binding constants.[51]

Assessment and calculation of stability constants and stoichiometries by UV-visible spectroscopy is frequently used, due to the fact that many receptors have incorporated in them functionalities that display absorbance over the wavelengths of 200 to 900 nm. A major benefit upon an anion interacting with a receptor that has UV-visible absorption capabilities is that the electronic environment of the complex/receptor may be altered enough to show a change in the UV-visible spectrum. The change can be monitored as a function of added anion that can be used to give information about how strongly or weakly the anion(s) is interacting with a receptor.

The stability constant can be calculated at a single wavelength at which the complex species produces a change in absorbance. If the absorbing compounds present are spectroscopically similar, or they interact with one another, the use of a single wavelength becomes less dependable. When this happens, using data from the entire UV-visible spectrum to calculate stability constants is more reliable and information about the anion-receptor complex system is thus comprised over the full range of the measured spectrum. With this technique, each digitised data point can be considered as a separate variable. Multivariate analysis can be applied to these data and can help in identifying patterns that represent the desired information.[53] SPECFIT/32^{TM} is a program that can analyse and extrapolate multivariate data from UV-visible titration data. It allows the analysis of data sets consisting of simultaneous measurements of absorbance as a function of wavelength and an independent variable, such as time, pH or titrant concentration resulting in reliable stability constant values.

The techniques mentioned above involve analysing the receptor-anion interaction in solution. Complementary techniques exist to study the interactions between the anion and receptor system in the solid state. X-ray crystallography is a method used to study how a particular receptor and its attendant anion(s) interact in the solid state. This technique allows for an accurate and descriptive visualisation of the spatial arrangement of atoms in a chemical compound in its crystalline state.

The spatial data amassed concern the connectivity, bond lengths, angles and the conformation of the molecules in the unit cell as well the stoichiometry, density, symmetry and the three dimensional packing of atoms in the solid state. Owing to this repeating quality, irradiating the crystal lattice with radiation and recording the angles of diffraction allows for the resolution of the interatomic distances using the Bragg equation; [54]

$$(2d\sin\theta = n\lambda)$$

Equation 1.3

The interactions and conformations seen between the receptor and anion(s) are assumed to simulate the interactions that occur in solution. This technique is limited by the ability to grow acceptable crystals of the required receptor complex.

1.3 Project Objectives

The aim of this project was to investigate the effect of change in spacer on anion binding strength within aryl-linked dicopper oxime helicates. These are structurally similar to Plieger's alkyl-linked helicates (Figure 13), which their anion binding strengths will be compared. As Cu(II) is paramagnetic, ^{1}H-NMR was not able to be utilised. Instead, both UV-visible studies and

X-ray structural analysis were undertaken for two structurally different oxime copper(II) containing complexes **1** = $[Cu_2(L^1\text{-}2H)_2]$ and **2** = $[Cu_2(L^2\text{-}2H)_2]$.

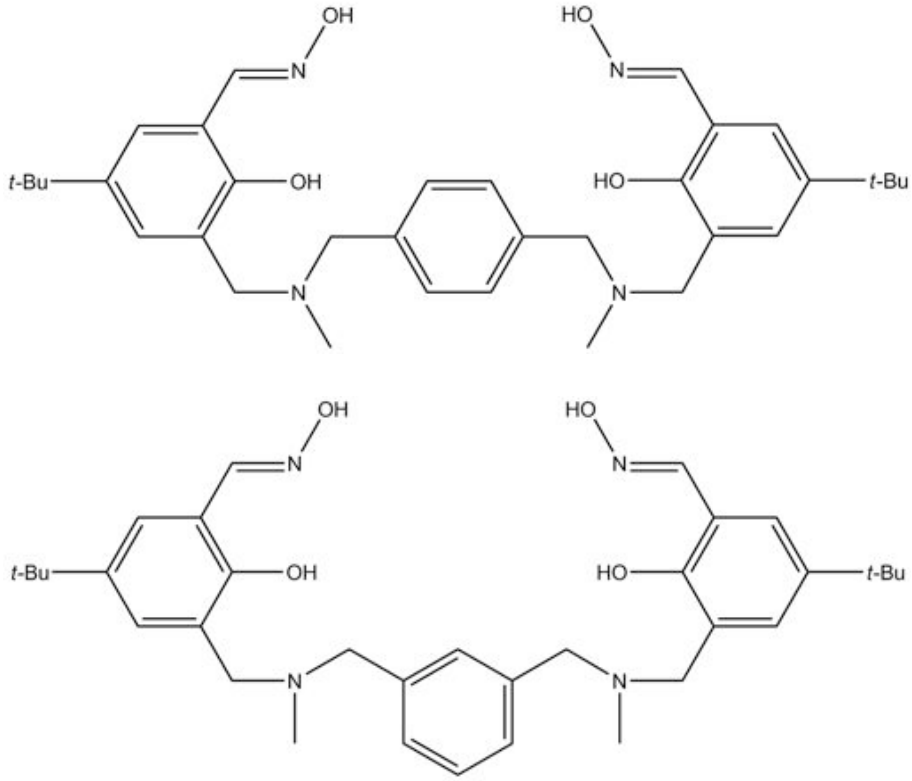

Figure 12. The *p*-xylylic $\mathbf{L^1}$ ligand (top) used to produce complex **1** and the *m*-xylylic $\mathbf{L^2}$ ligand (bottom) utilised to create complex **2**.

Crystallization attempts were made to discern the solid state properties of the complexes formed with a variety of anions. X-ray crystal structural studies of the aryl-linked helicates containing the anions perchlorate, tetrafluoroborate, nitrate and bromide were performed.

Chapter 2

Titrations of $[Cu_2(L^1\text{-}2H)_2]$

2.1 Introduction

Knapp investigated the solution interactions between the C6 alkyl linked salicylaldoxime and salicylaldiminophenyl dicopper helicates (A and B in Figure 13) with a variety of anions in a 50% (v/v) DCE-IPA solution and in an IPA solution respectively. The binding constants for the anions phosphate, sulfate, nitrate, perchlorate, tetrafluoroborate, iodide and bromide were determined.[45] The present thesis was aimed at investigating the solid state and solution interactions between a selection of anions and a more restrictive dicopper helicate **1** (C in Figure 13) in THF.

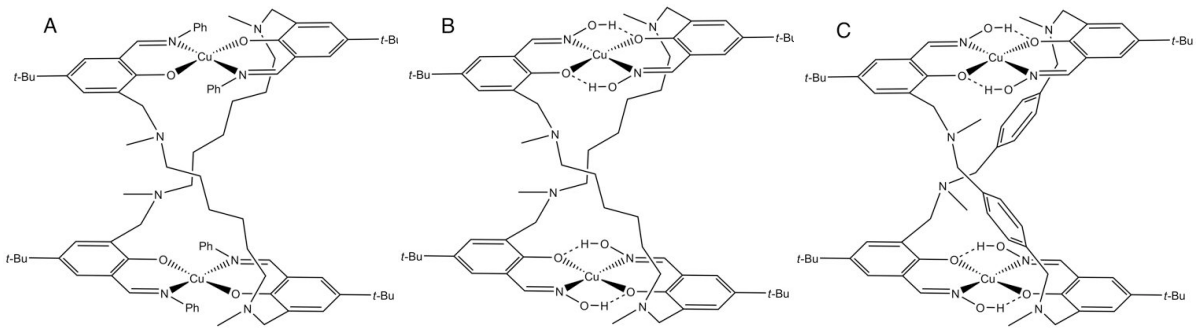

Figure 13. The previously studied 1st generation iminophenyl (A) and 2nd generation oxime (B) hexylene-linked dicopper helicates and the currently studied 3rd generation *p*-xylylic helicate **1** (C).[45]

Salicylaldoxime ligands are known to form 14-membered pseudomacrocyclic structures (as seen in Figure 13 above). The resulting Cu(II) complexes formed by these ligands have a very high stability.[55] The

intermolecular H-bonds between the oxime hydroxyl groups and the phenolate oxygen results in a high hydrolytic stability even in very acidic medium.[55]

By replacing the hexylene linker with a more restrictive 1,4-aryl linker, $\mathbf{L^1}$ was envisioned (Figure 14). Reacting the diamine N, N'-dimethyl-p-xylylenediamine (**1a**) with two equivalents of 3-(bromomethyl)-5-*tert*-butyl-2-hydroxybenzaldehyde, the dialdehyde **1b** was synthesised and was further converted to the oxime $\mathbf{L^1}$ ligand via reaction with hydroxylamine (discussed in Chapter 6). The reaction of $\mathbf{L^1}$ with copper acetate produces an anion free helicate **1** (synthesis outlined in Chapter 6). In the reactant solution, the helicate complex **1** is in equilibrium between its protonated and neutral form. Due to the proximity of the protonated tertiary amines to the phenolate oxygen atoms in its protonated state, the H-bonding causes a weakening of the H-N bond. This effectively lowers the pK_a value of the tertiary amines and hence the acetate is more easily able to acquire the protons from the complex. The resulting neutral anion free helicate **1** produced through recrystallisation was analogous to the hexylene linked helicates, as evidenced by the X-ray crystal structure (see section 2.3.2). The large visible changes in the UV-visible spectral data upon the addition of anionic acids to **1**, as well as the crystal X-ray structures produced, suggest the encapsulation of anions within **1**. Thus this technique has been employed to study the ability of a selection of anions to bind to the protonated form of **1**.

A comparison of the binding constants for anion encapsulation of **1** against previously studied helicates will allow the effect of introducing the *p*-xylylic functionality into the structure to be analysed. In particular, whether the more rigid 1,4-aryl spacer will result in a marked decrease in flexibility of the complex and how this will affect anion binding strength.

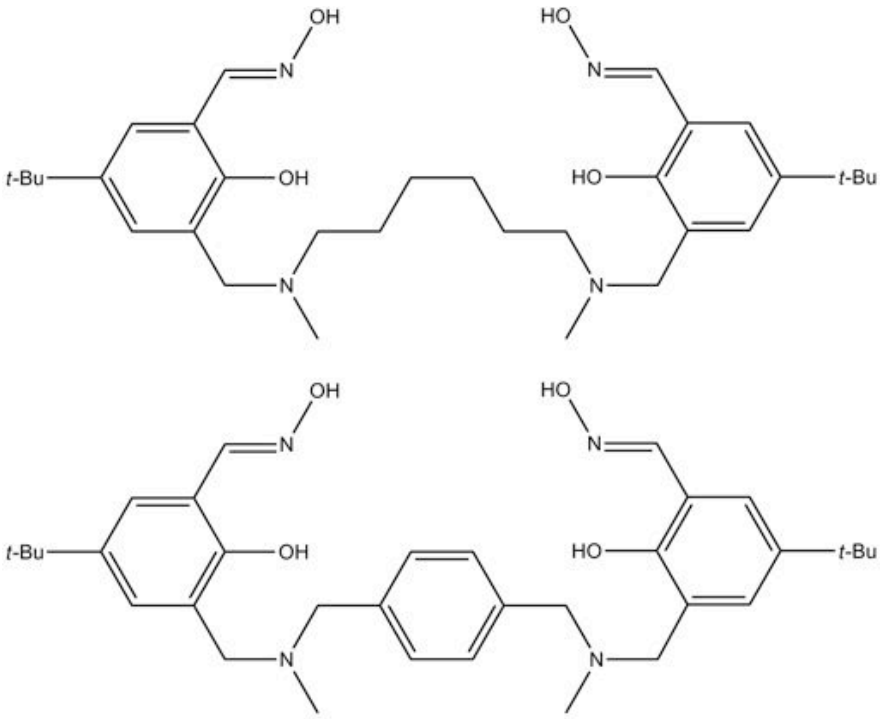

Figure 14. The hexylene-linked oxime analogue (top) vs. $\mathbf{L^1}$ (bottom) which was used to produce the anion free complex **1**.

2.2 Results and Discussion

2.2.1 Synthesis of Complexes

Refer to Chapter 6.

*2.2.2 Absorption Spectra of $[Cu_2(L^1\text{-}2H)_2]$ (**1**)*

Preliminary attempts to dissolve **1** in either IPA, DCE or in a mixture of the two resulted in un-dissolved material. Upon the addition of THF however, the solution took on a coloured appearance. A fully dissolved solution of **1** was achieved by first adding a small amount of chloroform (1-2 mL), which helped dissolve the solid, then adding THF to make up the stock solution. The

final chloroform composition of the solutions that were used in the UV-visible titration studies were less than 0.01%, which is inconsequential for the purposes of the UV-visible titration study.

The spectrum of complex **1** (Figure 15) shows a broad UV-visible band with a maximum at 350 nm and a large shoulder band at 273 and 256 nm. These bands have been assigned as ligand based.[56] The broad shoulder band at 273 nm could be assigned as the $\pi \longrightarrow \pi_2^*$ electronic transition band while the 350 nm band, which is also responsible for the yellow colour of the ligand solutions, was assigned as the characteristic phenolate related $\pi \longrightarrow \pi_1^*$ electron transfer.[56] As a result, any interaction of the anions with the coordinated metal would be expected to affect this absorption band due to perturbation of the phenolate π system. At lower wavelengths between 200-250 nm, the spectrum exhibited inconsistent and unreliable peaks under identical experimental conditions. As a result the spectrum was recorded from 250 → 900 nm for the titration experiments.

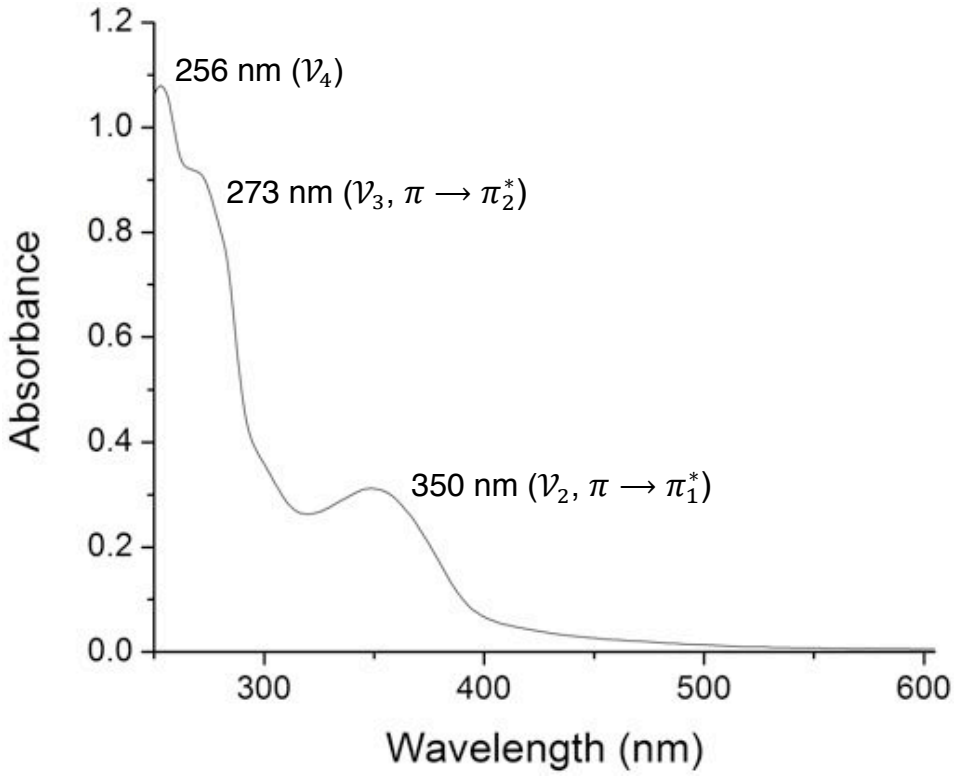

Figure 15. UV-visible absorbance spectra of **1** in THF. The band at 350 nm is characteristic of the phenolate moiety.

*2.2.3 Acid Titrations with **1***

Acids were titrated into solutions of **1** in THF and the solution stirred. The UV-visible spectra were recorded directly after each titration to investigate the effects of the acid addition on the UV-visible absorption of the complex in solution.

Acid forms of the desired anion were utilised for the titration experiments. The reason for this was two-fold; the acid form provides protons to protonate the amines, thus priming the complex for anion binding and the acid also provides the anion under investigation.

The solution of receptor **1** in THF will result in **1** initially being unprotonated. With the acids HBr, HNO_3 and $HClO_4$, once four equivalents of acid has been titrated into the solution containing **1** then the complex should be fully protonated at each of the four tertiary amine sites. In the case of H_2SO_4 however, only two equivalents of the acid will be required to fully protonate **1** since sulfuric acid has two H^+ per mole equivalent of acid to donate upon titration. From these required amounts of acid needed to fully protonate complex **1**, one would assume that four equivalents of acid (or two equivalents of sulfuric acid) would be needed to result in the highest binding strength between receptor **1** and the anion if **1** is acid (H^+) binding dependent. However, due to the software limitations of the binding modeling program SPECFIT/32^{TM} a 1:4:4 ratio or a 1:1:4 ratio of **1**:anion:H^+ (or 1:2:4 for sulfuric acid) was unable to be modeled and a corresponding association constant was unable to be calculated for the fully protonated complex **1**. What could be modeled using SPECFIT/32^{TM} was either a 1:1 ratio of **1** to anion or a 1:1 ratio of receptor **1** to acid (H^+). Modeling of either acid or anion in a 1:1 ratio with **1** gave the same result in binding constants within error of each other. This tells us that the complex is both acid and anion dependent but SPECFIT/32^{TM} could not model both the anion and H^+ with **1** at the same time. Appendix A shows the UV-vis spectra of the titrations performed between **1** and each of the four acids used. Each anion has caused a significant and differently shaped titration curve in comparison to each other.

These differently shaped titration curves for each anion tells us that the changes seen in the UV-vis spectrum are caused by the anion, and hence **1** must be mostly anion dependent in nature. If complex **1** were mostly acid (H^+) dependent then the UV-vis titration curves of all the anions tested would look more similar. From all of the above, we may conclude then that the first equivalent of anion titrated into solution most likely enters and coordinates to the metal centres in the central cavity of receptor **1** before it is fully protonated. A 1:1 ratio of complex **1** to anion was used during the titration experiments to calculate the corresponding association constants. Attempts at calculating binding constants with SPECFIT/32^{TM} using small increments of acid (i.e. 0.1 to 0.2 mole equivalents of acid) to finish with a small total mole equivalent amount of acid (i.e. 5 mole equivalents of acid or less) added to a solution of **1** resulted in SPECFIT/32^{TM} not being able to calculate any stability constants. It was found that this limitation of SPECFIT/32^{TM} could be overcome by including a larger amount of data and hence a larger change in the UV-vis spectrum to calculate the appropriate binding constants. This was carried out by titrating the anions in either 0.25 or 1.0 mole equivalents of acid to a total mole equivalents of 8 mole equivalents for H_2SO_4 and a total of 30 or 35 mole equivalents for the acids $HClO_4$, HBr or HNO_3.

No attempt was made to determine the pK_a values for the amines within the complex due to solubility issues. The helicate amines are separated from each other by at least two methylene carbons and a *p*-xylylic group. At these long distances the protonation of the amines may be considered as independent events.[57] This is supported by the polyammonium macrocycle [20]aneN_4 which contains four methylene groups separating the nitrogen atoms and is in its tetraprotonated form at neutral pH in water.[58] The larger amine – amine distances in complex **1** compared with the [20]aneN_4 macrocycle suggest greater independence of the amine protonation than was observed for [20]aneN_4.

It is assumed that protonation occurs relatively fast on the UV-visible absorbance timescale. Three additional assumptions have been made for the titration experiments, the first of which is that the titrated anion is capable of

entering the central cavity of **1** in solution. This assumption is valid as evidenced from structural studies. Secondly, that the anion of interest will locate inside the central cavity first, and thirdly that the spectral change in the UV-visible spectra is a result of the interactions of the anion within the cavity (as discussed in section 2.2.2). It is assumed that any changes that arise from any interactions with the solvent or counter anions in the exterior of the cavity to the complex are nominal. The acids titrated were; sulfuric, perchloric, nitric and hydrobromic acids.

The program SPECFIT/32^{TM} was used to determine the binding stability constants of the anions to the complex. A 1:1 binding model was used and produced good agreement between the predicted and recorded spectra. Mole-ratio plots were carried out for each anion and it was determined that a 1:1 ratio of anion to complex was optimal. This binding model was also supported by the crystal X-ray structures **3** = $[ClO_4 \subset (Cu_2L^1{}_2)](ClO_4)_3$ and **4** = $[BF_4 \subset (Cu_2L^1{}_2)](BF_4)_3$ obtained (see section 2.3.3 and 2.3.4 respectively) which both show one anion encapsulated within the cavity of each complex. It is assumed the slightly larger and smaller anions sulfate and bromide will also be able to enter the cavity.

Aliquots of the anion of interest in THF were titrated into a standard solution of **1** in dry THF. Titration experiments were carried out until three concordant binding constant results were obtained for each anion studied.

The stability constants calculated for the acids used are recorded in Table 1. Sulfuric acid exhibits the strongest binding to complex **1**, with a log *K* value of 5.53 ± 0.32, approximately 1.7 orders of magnitude higher than the other, typically weak binding anions. This high binding strength is most likely due to the coordinating ability of sulfate and its increased negative (2^-) charge over the other monovalently negative anions. H_2SO_4 is a diprotic acid and is capable of donating two protons per mole of acid, unlike the other monoprotic acids used, which can only donate one proton per mole of acid. Hence **1** will be tetraprotonated with two mole equivalents of H_2SO_4 whereas with a monovalent acid, complex **1** will only be diprotonated. This additional

protonation of helicate **1** helps to bind SO_4^{2-} more strongly at the lower mole equivalents over the monoprotic acids. The sulfate anions larger size in comparison to the other anions will also contribute towards greater anion to metal interactions as well as stronger H-bonding formations with the protonated amines and possibly stronger anion–π interactions.

The remaining anions all show the same binding strength within error of each other, relatively weak binding compared to the high sulfate binding constant (Figure 16). The crystal structures of **3** and **4** (see section 2.3.3 and 2.3.4) demonstrate that the perchlorate and tetrafluoroborate anions are encapsulated inside the cavity of **1** and show metal-anion and moderate to weak H-bond interactions stabilizing the occluded anion. The encapsulated perchlorate in **3** is weakly bound to the copper metal centres and three weak to moderate H-bonds from the protonated amines. This can be extrapolated to the complex being only just flexible enough to shrink in size to fit the anion. This is displayed by the relatively weak binding of the perchlorate anion to the complex and may also be the same reason as to the weak binding values of the nitrate and bromide anions.

The planarity of the nitrate anion means that it can possess one of two orientations. If the nitrate is in a planar orientation in relation to the square planar copper centres, as is the case in the C6 alkyl iminophenyl complex,[48] then it would only be loosely bound inside by a few weak to moderate H-bonds. If, on the other hand it adopts an up-down orientation, as is the case for the crystal structure complex of **5** ($[NO_3 \subset (Cu_2L^2_2)](NO_3)_3$, discussed in Chapter 3), then it may be possible to be weakly coordinated to the metal centres as well as having several H-bond interactions. In either case, its weak coordinating ability is shown by its low stability constant.

The bromide anion's size and spherical shape can explain why it is bound the weakest out of the anions investigated. Its smaller size would increase the distances to the protonated amines, accounting for weaker H-bond interactions and presuming that the complex is reaching its flexibility limits for contracting in size in the structures **3** and **4**, then so too would bromide have weak metal-anion interactions.

The ESI-MS spectra indicate that there are interactions occurring between helicate **1** and the corresponding anions. Each of the anions investigated showed a fragmented peak of $[L^1CuX]^+$, which contains one *p*-xylylic ligand coordinated to one Cu(II) with a single anion (X) bound. The fragments convey a sense of fragility towards the helicate complex as a whole and may break up during flight in the Mass Spectrometer. This was further shown by the mass spectrum of the anion free complex of **1** where only a main peak of $[L^1Cu]^+$ was seen. The mass spectra of complex **1** with the nitrate anion however showed a peak corresponding to the NO_3^{2-} anion bound to a whole helicate complex, presumably with the anion encapsulated within **1**.

Acid	Log K	Stoichiometry	ESI-MS Peaks
H_2SO_4	5.53 ± 0.32	1:1	$[L^1CuSO_4]^+$
$HClO_4$	3.86 ± 0.22	1:1	$[L^1CuClO_4]^+$
HNO_3	3.72 ± 0.08	1:1	$[NO_3\subset\mathbf{1}H_2]^{2+}$, $[L^1CuNO_3]^+$
HBr	3.69 ± 0.17	1:1	$[L^1CuBr]^+$

Table 1. The log *K*, stoichiometry and the main ESMS peaks observed as evidence for the binding of the anions to **1** in THF at 294 K.

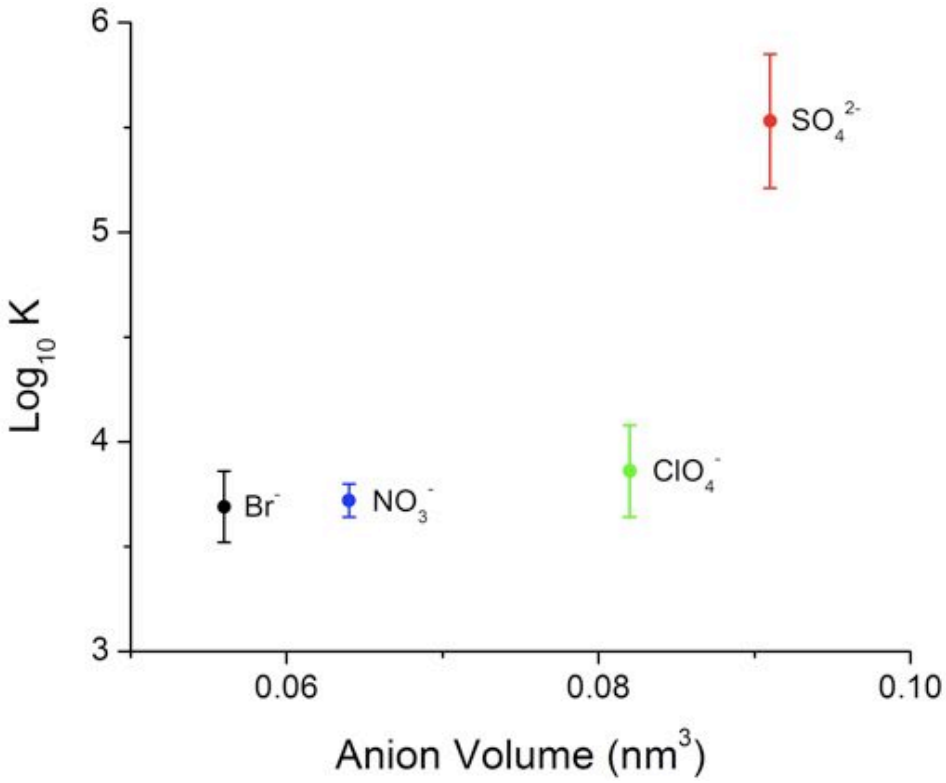

Figure 16. The calculated stability constants for anions binding within the cavity of complex **1** vs. size of the anion. The anion volumes used are from the paper by Jenkins *et al.*[59]

2.3 X-ray Crystal Structures of **1**

2.3.1 X-ray Crystal Structure of ***L*** ^{1}*.tol*

Colourless block shaped crystals of a toluene solvate of $\mathbf{L}^{1}$ suitable for X-ray diffraction were grown by the slow evaporation of toluene containing the oxime ligand and the crystal structure was determined (Figure 17). The asymmetric unit consists of one half of the complex with the other half generated by inversion, confirming the successful synthesis of the ligand.

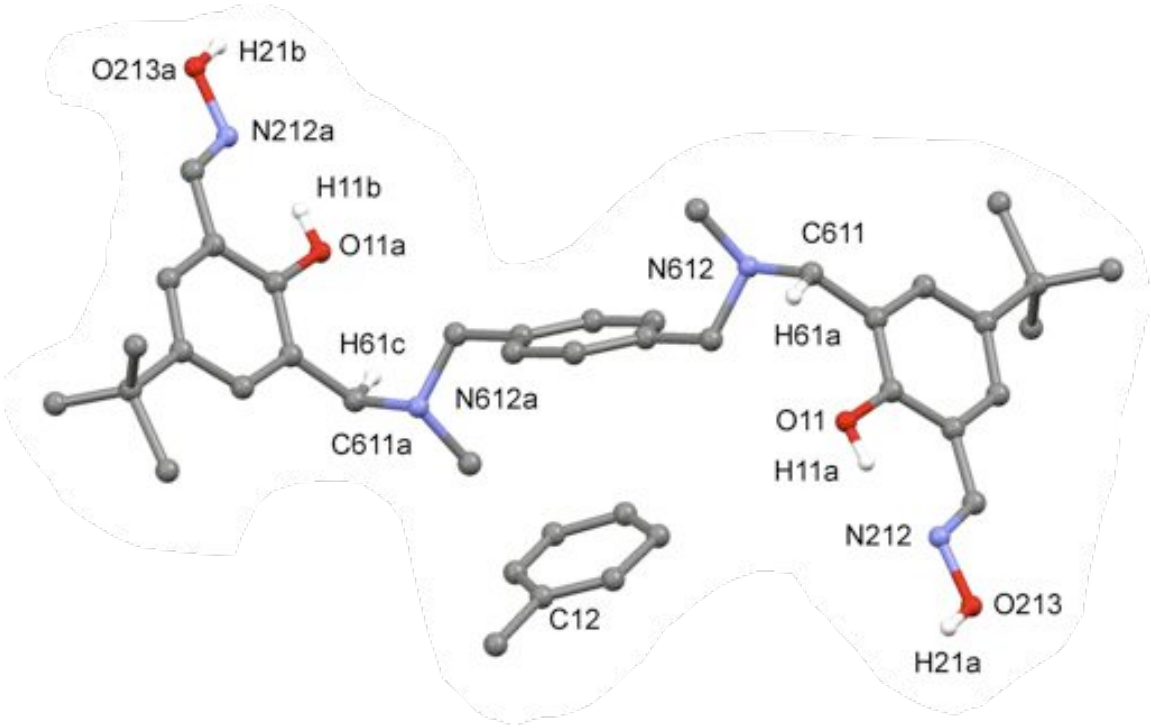

Figure 17. Perspective view of $\mathbf{L}^{1}$ with included toluene solvent molecule showing the adopted labeling scheme (hydrogen atoms have been omitted for clarity and the disordered *t*-butyl groups and disordered toluene are not shown).

The salicylaldoxime groups at each end of the molecule are orientated in opposite directions. This orientation allows a repeating inter and intramolecular hydrogen bonding network to form throughout the crystal lattice, similar to other single oxime ligand arrangements.[60] The

intermolecular interactions form between the oxime hydrogen H21a and the tertiary nitrogen atom N612 from adjacent **L**[1] molecules (Figure 18). The intramolecular interactions occur between the phenolic hydrogen H11a and the oxime nitrogen N212 and between the alkyl hydrogen H61a and the phenolic oxygen O11 (refer to Table 2 for H-bond lengths and angles).

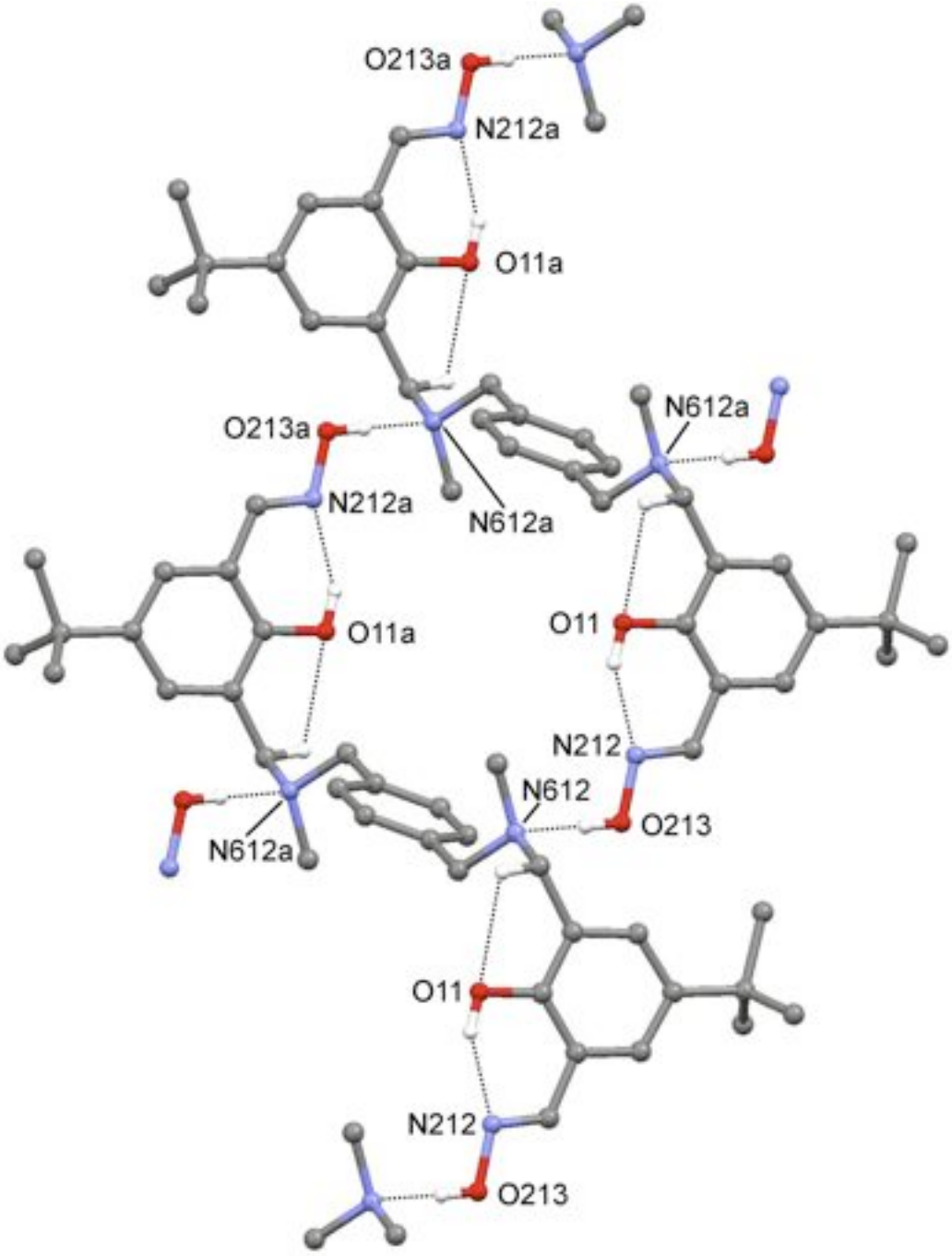

Figure 18. Perspective view of **L**[1] showing the extended intra and intermolecular H-bonding network (hydrogen atoms and the solvent toluene molecule not involved in H-bonding have been omitted for clarity).

Atoms	D–H–A distances (Å)	D–H–A angles (°)
O11-H11a … N212	2.6718(1)	149.1
C611-H61a … O11	2.8658(1)	106.0
O213-H21a … N612b	2.7296(1)	162.5

Table 2. Selected intra and inter H-bond distances for **L**[1].

Within the **L**[1] molecule, the tertiary butyl groups were found to be positionally disordered over two sites (0.67:0.33).

Some minor rotational disorder of the toluene solvent molecule exists, centered around the C12 carbon, but this was not modeled.

*2.3.2 X-ray Crystal Structure of $[Cu_2(L^1\text{-}2H)_2].CHCl_3$ (**1**)*

Brown platelet shaped crystals of **1** suitable for X-ray diffraction were grown by slow diffusion of acetone into a chloroform mix of the complex and the crystal structure was determined (Figure 19). The asymmetric unit consists of one complete complex and one chloroform solvent molecule.

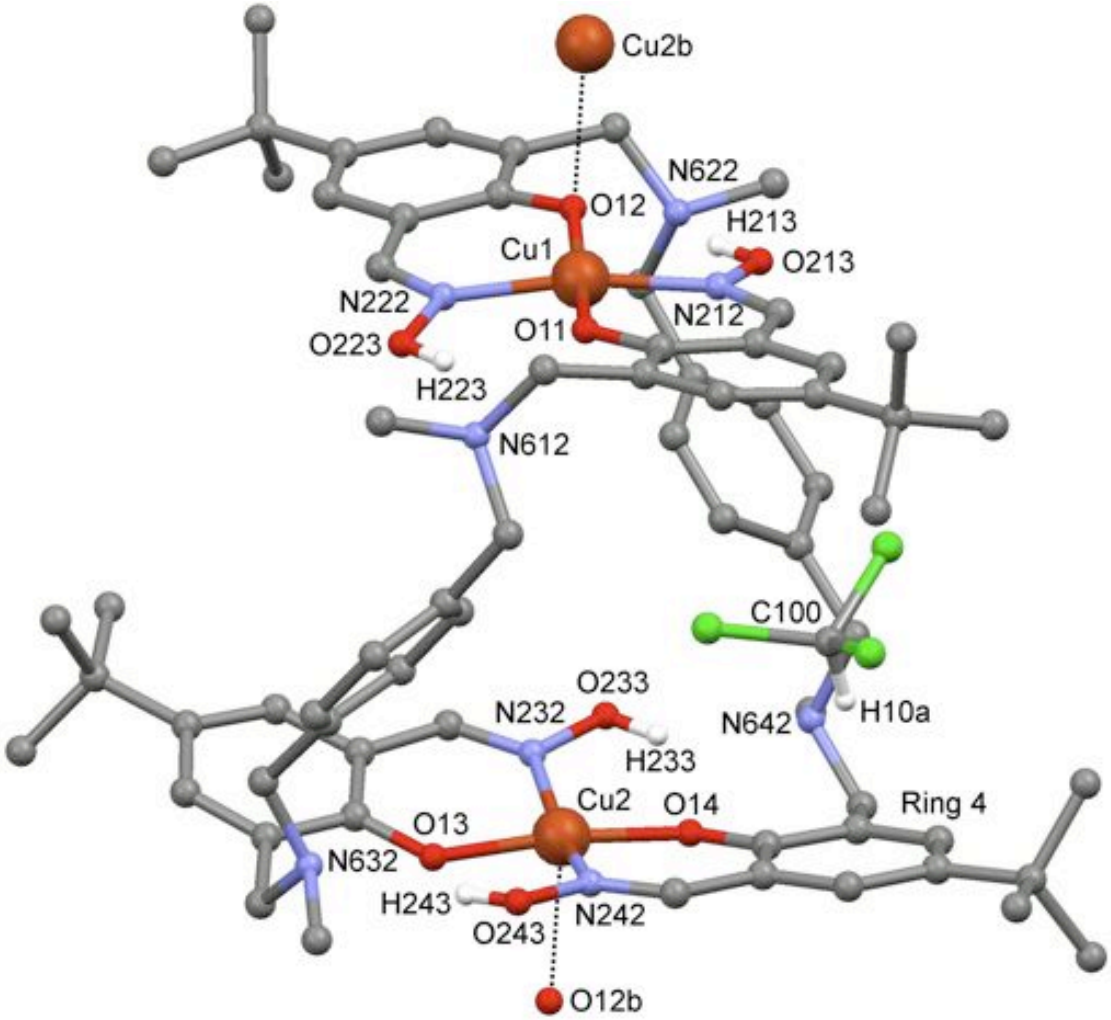

Figure 19. Perspective view of **1** and the weakly coordinated axial oxygen and Cu atoms of adjacent complexes (Hydrogen atoms not involved in H-bonding within the complex have been omitted for clarity).

The complex consists of two Cu(II) atoms coordinated to two di-anionic $\mathbf{L^1}$ molecules with each copper sharing both ligands via the phenolate and

N-oximate positions ($N_2O_2^{2-}$). The 1,4-aryl linkers give the complex enough conformational freedom to form a helical structure, where a phenolic ring of one ligand is situated above a phenolic ring of an opposing ligand. This arrangement confers a twisted square shape to the complex.

Both copper(II) centres are in differing environments due to intermolecular interactions with adjacent complex molecules. Cu1 is in a slightly distorted square planar environment while Cu2 is in a slightly distorted square pyramidal environment. With Cu2 in a 5-coordinate environment, a structural index parameter value τ (where $\tau = (\beta - \alpha)/60$) can be applied.[61] This parameter is applicable to 5-coordinate geometries and is defined as the degree of trigonality within the structural continuum between trigonal bipyramidal and square pyramidal geometries.[61] A τ value of 1 would indicate a pure trigonal bipyramidal geometry where as a τ value of 0 would indicate a purely square pyramidal geometry.[61] Cu2 has a τ value of 0.17, indicating that it is 17% along the pathway of distortion from square pyramidal towards a trigonal bipyramidal, equating to much more square pyramidal character than trigonal bipyramidal. Both copper(II) centres have four in plane donors that consist of two nitrogen donors comprised of one oxime moiety from each ligand and two oxygen donors comprised of one phenol moiety from each ligand. In addition, Cu2 has a weak fifth axial bonding interaction to a phenolic oxygen from a neighboring complex at a distance of 2.9109(1) Å (see Table 3 for a selection of bond lengths and angles around the metal centres). The distance between the two copper atoms is 8.2588(2) Å and the average helical twist angle through O–Cu–Cu–O is 78.7°. Comparing this to the C6 alkyl oxime anion free complex analogue,[46] where the linker strap contains six alkyl carbons and allows the complex to be less conformationally restricted, results in a longer distance between the two copper(II) centres at 10.191(3) Å. It also has an increase in its helical twist within the complex, with an average helical twist angle of 85.9(3)° through O–Cu–Cu–O. So the aryl spacers in **1** confer upon the complex a more compact and rigid (less-twisted) structure with a shorter Cu-Cu distance than those of the alkyl spacers.

The average torsion angle around the copper centres (e.g. through the atoms O11-N212-N222-O12) is 156.5°. In comparison, the hexylene linked analogue[46] has an average torsion angle through O-N-N-O of 157.6° which is not that much different. This suggests that the decrease in the linker flexibility has only had a very minimal influence upon the $N_2O_2^{2-}$ coordination site at the copper centre, if at all.

Atoms	Bond Lengths (Å)	X–Cu–X	Bond Angles (°)
Cu1 – O11	1.852(2)	O11–Cu1–N212	93.5
Cu1 – O12	1.870(2)	O11–Cu1–N222	87.3
Cu1 – N212	1.950(1)	O12–Cu1–N212	88.6
Cu1 – N222	1.947(1)	O12–Cu1–N222	92.6
Cu2 – O13	1.865(1)	O13–Cu2–N232	92.6
Cu2 – O14	1.863(1)	O13–Cu2–N242	87.8
Cu2 – N232	1.946(2)	O14–Cu2–N232	89.3
Cu2 – N242	1.953(2)	O14–Cu2–N242	92.6
Cu2 – O12b	2.9109(1)	O13–Cu2–O12b	86.9
		O11–Cu1–Cu2–O13	78.3
Cu1 – Cu2	8.2588(2)	O12–Cu1–Cu2–O14	79.2

Table 3. Selected bond lengths and angles for the Cu(II) centres of **1**.

The pseudo macrocyclic cavity surrounding each metal centre is completed by an oxime hydrogen bonded towards the opposing phenolate oxygen with an average O … O distance of 2.6901 Å. There is a second, weaker H-bond to the tertiary amines in the aryl linker with an average N … O distance of 2.9716 Å (refer to Table 4 for H-bond lengths and angles). In

comparison to the C6 alkyl oxime analogue, the average O … O distance is longer at 2.753 Å and the average N … O distance is shorter at 2.862 Å. This shows that this more rigid spacer imparts a tighter pseudo macrocyclic cavity around the metal centres but at the cost of having the secondary H-bonds from the amines at a longer distance.

Atoms	H-bond distances (Å)	D–H–A angles (°)
O223-H223 … O11	2.6384(1)	130.4
O213-H213 … O12	2.7241(3)	128.6
O243-H243 … O13	2.6806(3)	130.8
O233-H233 … O14	2.7172(3)	130.6
O223-H223 … N612	3.0438(3)	145.2
O213-H213 … N622	2.9864(3)	148.0
O243-H243 … N632	2.9699(2)	142.1
O233-H233 … N642	2.8864(2)	144.7

Table 4. Selected intramolecular oxime H-bond distances for **1**.

There are a number of secondary weaker and (potentially) important intermolecular H-bonds occurring between adjacent complexes (Figure 20). This is due to polarisation due to the proximity of $–CH_2–$ and $–CH_3$ groups beside an N amine.[62] The interactions occur from CH_2 hydrogens H61e and H62g from one complex and the adjacent complex oxime oxygens O243b and O233b respectively, while the CH_3 and CH_2 hydrogens H63fb and H63cb from the adjacent complex both form interactions with the first complex's oxime oxygen O223 and also the CH_2 hydrogen H64ib interacts with the other oxime oxygen O213 (refer to Table 5 for H-bond lengths and angles). These five weak interactions have pulled adjacent complexes together resulting in

the close proximity of the Cu(II) atoms from adjacent complexes with a Cu1 … Cu2b distance of 3.3038(1) Å.

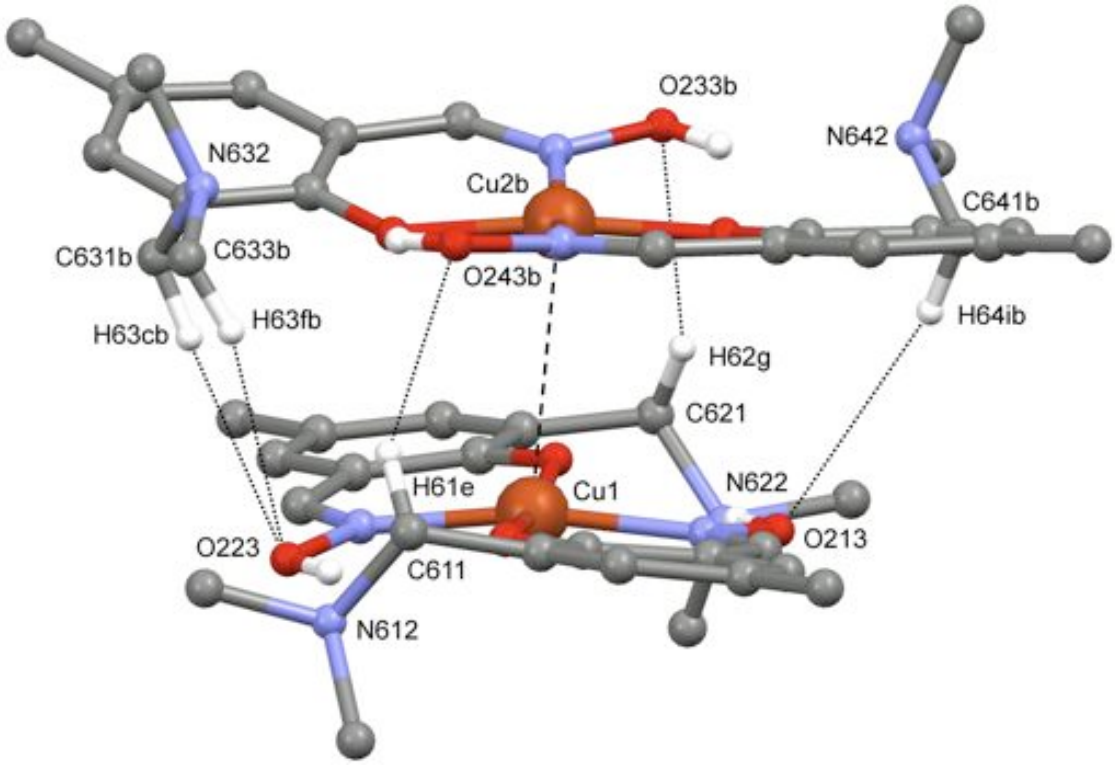

Figure 20. Perspective view of **1** showing the intermolecular H-bonding between adjacent complex molecules (Hydrogen atoms not involved in intermolecular H-bonding have been omitted for clarity).

Atoms	H-bond distances (Å)	D–H–A angles (°)
C631b-H63cb … O223	3.7123(3)	173.1
C633b-H63fb … O223	4.0491(3)	144.8
C611-H61e … O243b	3.9439(3)	148.1
C621-H62g … O233b	3.4841(2)	149.9
C641b-H64ib … O213	3.9044(2)	137.7
Cu1 … Cu2b	3.3038(1)	-

Table 5. Selected intermolecular H-bond distances between **1** and an adjacent molecule.

The aromatic rings in the aryl linker adopt an edge on position with respect to the cavity of the complex. This orientation of the aryl rings results in a partial filling of the inner cavity and thus the solvent chloroform molecule is positioned out of the central cavity but still contained within the complex. The chloroform molecule shows a weak H–π interaction between H10a and the centroid of Ring 4 with a C100 … π distance of 3.662 Å and a C100–H10a … π angle of 168.0° (Figure 21).

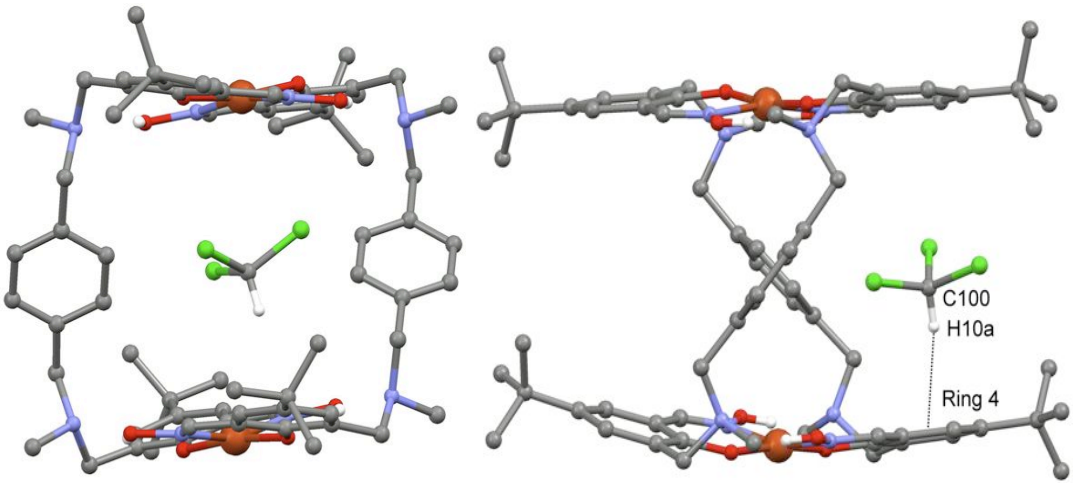

Figure 21. Perspective front and side views of **1** showing the edge on nature of the aryl linkers and positioning of the solvent molecule (Hydrogen atoms not involved in H-bonding have been omitted for clarity).

*2.3.3 X-ray Crystal Structure of $[ClO_4 \subset (Cu_2L^1{}_2)](ClO_4)_3$ (**3**)*

Green chunk shaped crystals of **3** suitable for X-ray diffraction were grown by slow diffusion of diisopropyl ether into a chloroform mix of the complex and the crystal structure was determined (Figure 22). The asymmetric unit consists of one complete protonated complex with one encapsulated perchlorate anion and three counter perchlorate anion molecules.

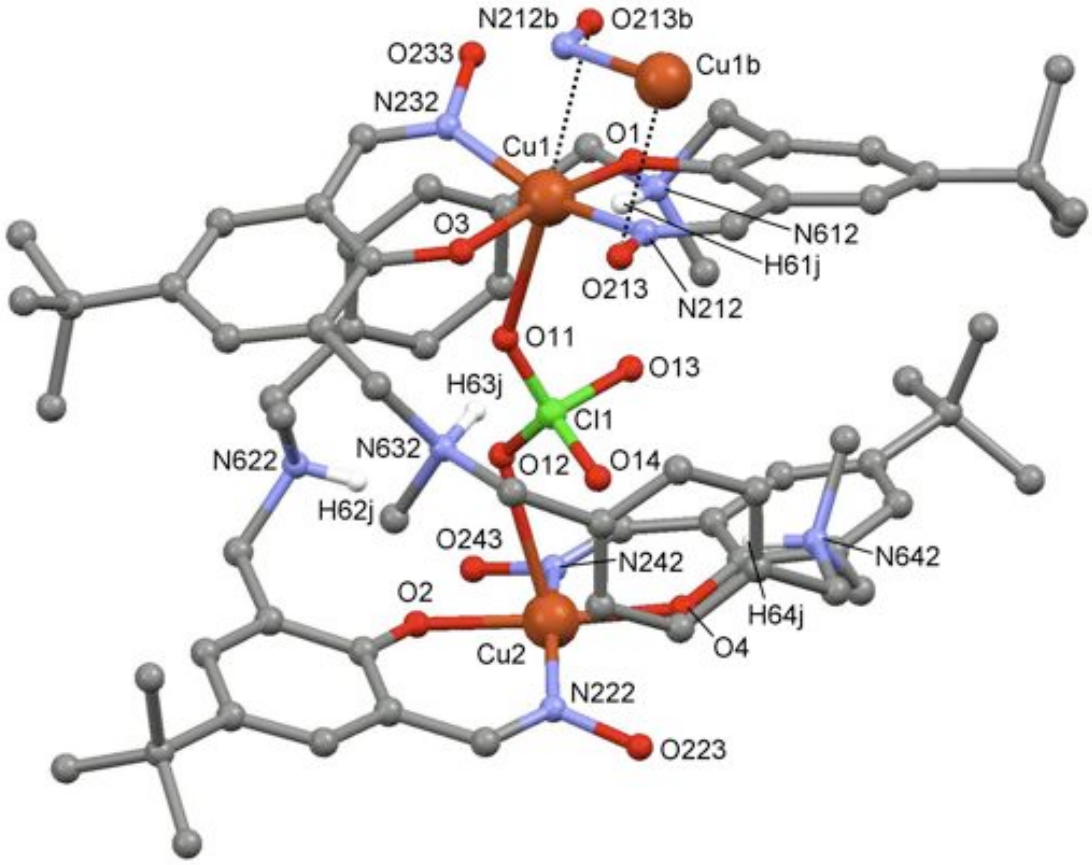

Figure 22. Perspective view of **3** with the encapsulated perchlorate anion and the weakly coordinated axial O–N–Cu atoms of an adjacent complex (Hydrogen atoms that aren't on the protonated amines, the disorder around the perchlorate anion Cl1 and the remaining three counter perchlorate anions have been omitted for clarity).

The complex consists of two Cu(II) atoms coordinated to two $\mathbf{L^1}$ molecules with each copper centre sharing both ligands via the N-oximate

and phenolate positions ($N_2O_2^{2-}$). Each **L**[1] ligand is protonated at the two tertiary amines and located within the cavity of the complex is an encapsulated ClO_4^- anion. There are three counter perchlorate anions giving rise to an overall neutral complex.

The Cu(II) centres in **3** are in differing environments due to the encapsulated ClO_4^- anion and the intermolecular interactions with adjacent complex molecules. Cu1 is in a distorted octahedral environment while Cu2 is in a distorted square pyramidal environment. Both Cu(II) centres have four donors that consist of two oxygen donors (one phenol moiety from each ligand) and two nitrogen donors (one oxime moiety from each ligand). Cu2 then has a fifth weak interaction in the axial position with O12 from the captured perchlorate molecule at a distance of 2.606(11) Å. In contrast, Cu1 has two weak axially positioned interactions; a slightly stronger interaction between O11 of the captured perchlorate anion at a distance of 2.487(11) Å and a more distant interaction between the oxygen atom O213b from an oxime moiety of an adjacent complex at a distance of 2.8530(3) Å (refer to Table 6 for bond lengths and angles for the copper centres). The Cu–O bond lengths of **3** to the perchlorate anion are significantly shorter than the hexylene linked imine analogue,[48] which are 2.668(5) Å and 2.721(3) Å. This is most likely because the Cu–Cu distance in **3** is shorter than in the C6 analog as a consequence of the more restricted aryl spacer and results in closer Cu–anion interactions.

The distance between the two copper(II) centres has decreased markedly upon complexation of the ClO_4^- anion to 7.135(2) Å and the average helical twist angle has increased to 129.0° through the O–Cu–Cu–O atoms. This shows that the more rigid aryl spacer still has sufficient flexibility to twist and shrink in size to accommodate the encapsulated ClO_4^- anion and allow interactions to both metal centres. The C6 alkyl imine analogue[48] only has a slightly longer Cu–Cu distance of 7.278(1) Å and a relatively similar helical twist angle of 133.5°, which is only a difference of 0.143 Å and 4.5° respectively. This shows that even with the more conformationally restrictive

aryl spacer in place of the more flexible alkyl spacer, **3** still has sufficient flexibility to accommodate the ClO_4^- anion.

The average torsion angle around the copper centres is 155.3°. This is only a fractionally more distorted square planar environment around the metal centres than the anion free complex **1**. This suggests that encapsulating and coordinating a perchlorate anion within the complex has relatively no effect on the square planar arrangement around the metal centres. In comparison, the C6 alkyl imine perchlorate analog[48] has an average torsion angle through the O-N-N-O planes of 133.5°. This amounts to a significant difference between the two complexes and could be because the more rigid aryl linkers in **3** prevent the salicylaldoxime units from twisting further upon complexation and therefore can only increase the helical twist to accommodate the anion.

The τ value of the 5-coordinate Cu2 is 0.22. If we consider Cu1 also 5-coordinate (ignoring the weak sixth axially coordinated oxime from the adjacent complex), then Cu1 has a τ value of 0.18. These τ values indicate that the coordination of the perchlorate anion within the cavity has caused a slight deviation from a true square pyramidal geometry, more so in Cu2 than for Cu1. Comparing these τ values to the τ value found for complex **1** (τ = 0.17) shows that the binding of the perchlorate anion has caused a slightly more distorted geometry around the metal centers.[61]

Complex **3**, like **1**, has a smaller box-like shape and a more twisted helical arrangement of the coordinated $\mathbf{L^1}$ ligands upon complexation with the perchlorate anion, with the top and bottom sides of the box being the two copper centre planes and the aryl rings of the linker making up the two sides.

Atoms	Bond Lengths (Å)	X–Cu–X	Bond Angles (°)
Cu1 – O1	1.900(4)	O1–Cu1–N212	92.7
Cu1 – O3	1.907(4)	O1–Cu1–N232	90.8
Cu1 – N212	1.942(6)	O3–Cu1–N212	87.4
Cu1 – N232	1.952(6)	O3–Cu1–N232	91.7
Cu1 – O11	2.487(11)	O11–Cu1–O1	90.0
Cu1 – O11a	2.829(15)	O11a–Cu1–O1	104.4
Cu1 – O213b	2.853(3)	O213b–Cu1–O1	84.5
Cu2 – O2	1.931(5)	O2–Cu2–N222	91.6
Cu2 – O4	1.907(4)	O2–Cu2–N242	89.6
Cu2 – N222	1.953(6)	O4–Cu2–N222	88.4
Cu2 – N242	1.933(6)	O4–Cu2–N242	91.9
Cu2 – O12	2.606(12)	O12–Cu2–O2	76.5
Cu2 – O12a	2.471(16)	O12a–Cu2–O2	79.0
		O1–Cu1–Cu2–O2	129.8
Cu1 – Cu2	7.135(2)	O3–Cu1–Cu2–O4	128.3

Table 6. Selected bond lengths and angles for the Cu(II) centres of **3**.

The encapsulated ClO_4^- anion was found to be disordered over two positions (50:50). One position of the disordered perchlorate anion (O11, O12, O13, O14) lies slightly closer towards Cu1 than to Cu2, while the other disordered position (O11a, O12a, O13a, O14a) lies closer to Cu2 than to Cu1. A search through the CCDC for complexes containing a Cu – O-ClO_3 bond resulted in an average Cu – O (perchlorate) bond length of 2.565 Å from 41 selected bond lengths.[63 – 89] This average shows that the bond length between Cu1 and O11 is comparatively short while the bond length between

Cu2 and O12 is comparatively long. This is because the anion is positioned closer to one metal centre in each disordered state and thus creates one short and one long metal to anion bond. Overall the encapsulated perchlorate anion sits relatively comfortably inside the cavity created by the complex and has caused the receptor to contract significantly so that both of the copper (II) centres are able to make weak interactions with this traditionally non-coordinating anion. All of the protonated tertiary amines of the aryl linker are angled inwards towards the central cavity so as to increase the number of intermolecular H-bonds to the captured ClO_4^- anion, giving rise to three moderate to weak hydrogen bonds for each of the disordered states (refer to Figure 23). In one disordered position, O12 and O13 have one moderately strong H-bond each to H62j and H61j respectively, while O14 has one weak H-bond to H64j. The second disordered position also has two moderate H-bonds between H63j … O11a and H64j … O14a and one weak H-bond from H61j to O13a. The average H-bond length for each of the disordered states is 3.122 Å and 3.028 Å respectively, which are very similar for the 50:50 disordered perchlorate (refer to Table 7 for H-bond distances and angles).

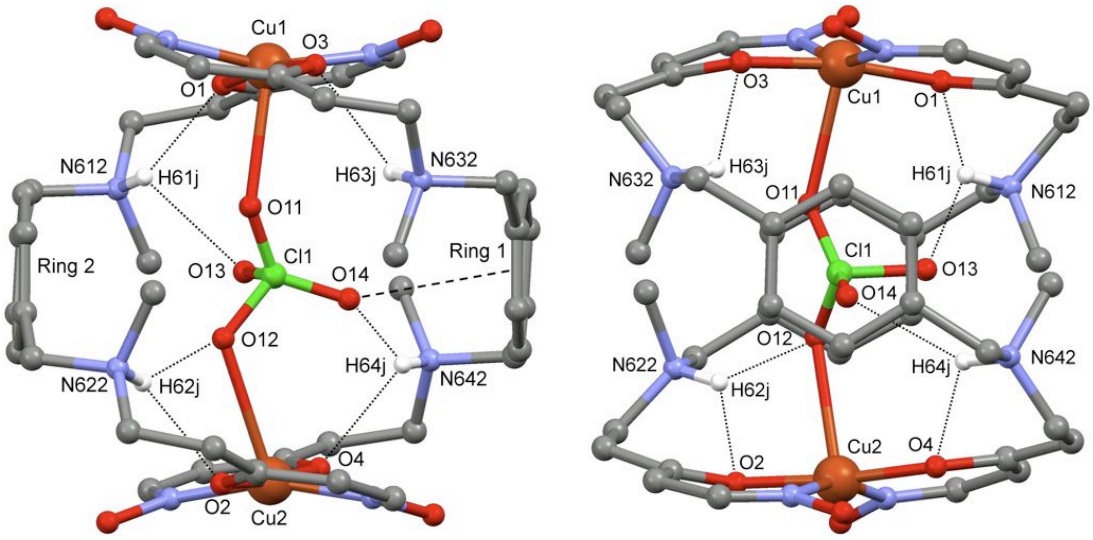

Figure 23. Perspective side views of **3** showing one disordered position of the encapsulated ClO_4^- anion and the multitude of moderate to weak interactions within the cavity, including the protonated tertiary amine H-bonds and the anion–π interaction, which shows the face-on positioning of the aryl linker (Hydrogen atoms not involved in H-bonding, the salicylaldoxime rings and *t*-butyl groups and counter anions have been omitted for clarity).

Atoms	Bond distances (Å)	D–H–A angles (°)
N622-H62j … O12	3.083(11)	143.6
N612-H61j … O13	2.988(16)	115.9
N642-H64j … O14	3.295(19)	147.7
N632-H63j … O11a	2.839(13)	145.4
N612-H61j … O13a	3.292(14)	135.0
N642-H64j … O14a	2.952(11)	128.6

Table 7. Selected H-bond distances and angles between the protonated amines and the two disordered states of the encapsulated ClO_4^- anion.

The captured ClO_4^- anion is also stabilised within the cavity by one anion–π interaction for each of the positionally disordered states (50:50). This

interaction is between one oxygen atom of the perchlorate anion and one of the aromatic ring's π systems.[27, 28, 90] For one disordered state, this is between O14 and the centroid created in Ring 1 at a distance of 3.018 Å (see Figure 23) and in the other disordered position it is between O13a and the centroid created in Ring 2 at a distance of 3.040 Å. These two anion–π distances are relatively strong compared to other perchlorate oxygen–π interactions[26] of this type, possibly as a consequence of the restricted movement this anion possesses within the cavity (refer to Table 8 for bond distances and angles).

Atoms	H-bond distances (Å)	D–H–A angles (°)
Cl1-O14 … Ring 1	3.018	151.9
Cl1-O13a … Ring 2	3.040	157.8

Table 8. Selected anion–π distances and angles for the disordered encapsulated ClO_4^- anion.

The pseudo macrocyclic cavity surrounding each metal centre is completed by an oxime hydrogen bonded towards the opposing phenolate oxygen with an average distance of 2.717 Å. This is a slightly longer average bond length than in the anion free complex **1** ($[Cu_2(L^1\text{-}2H)_2]$). There also exists a secondary H-bond to each phenolate oxygen from a protonated tertiary amine from the aryl linker with an average distance of 2.898 Å (refer to Table 9 for H-bond distances and angles).

Atoms	H-bond distances (Å)	D–H–A angles (°)
O233-H233 … O1	2.849(6)	125.8
O243-H243 … O2	2.729(7)	130.7
O213-H213 … O3	2.631(6)	132.8
O223-H223 … O4	2.659(7)	132.4
N612-H61j … O1	2.815(2)	130.3
N622-H62j … O2	2.878(2)	127.8
N632-H63j … O3	2.940(2)	125.9
N642-H64j … O4	2.957(4)	123.7

Table 9. Selected intramolecular H-bond distances and angles for **3**.

The aromatic rings of the linker have now adopted a face-on position in respect to the central cavity, allowing for a strong anion–π interaction at an average distance of 3.029 Å. This orientation of the aryl rings has freed up the central cavity of its aromatic edge and thus allowing the encapsulation of an anion within it to allow further strengthening of binding the anion through anion–π interactions (refer to Figure 23 above showing the orientation of aryl linkers).

The three counter perchlorate anions are involved in a myriad of weak H-bonding with the complex and adjacent complex molecules. One perchlorate molecule (Cl2 O21 O22 O23 O24) is positioned slightly differently than the other two counter anions and sits alongside two neighbouring complexes near the oxime functionalities, having two weak interactions with them. This is in comparison to **1**, which forms a variety of weak intermolecular H-bonds between adjacent complexes. Another perchlorate counter anion (Cl3 O31 O32 O33 O34) is similar in respects of being positioned near oxime groups of the complex and another neighboring complex. The last perchlorate counter anion (Cl4 O41 O42 O43 O44) was found to be positionally

disordered (50:50) over two positions. It was found in between the complex and another different adjacent complex.

*2.3.4 X-ray Crystal Structure of $[BF_4 \subset (Cu_2L^1_2)](BF4_4)_3$ (**4**)*

Brown platelet shaped crystals of **4** suitable for X-ray diffraction were grown by slow diffusion of diethyl ether into an acetone mix of the complex and the crystal structure was determined (Figure 24). The asymmetric unit consists of one complete protonated complex with one encapsulated tetrafluoroborate anion, three counter tetrafluoroborate anions and four acetone solvent molecules. Each of the tertiary amines are protonated, giving rise to an overall neutral complex.

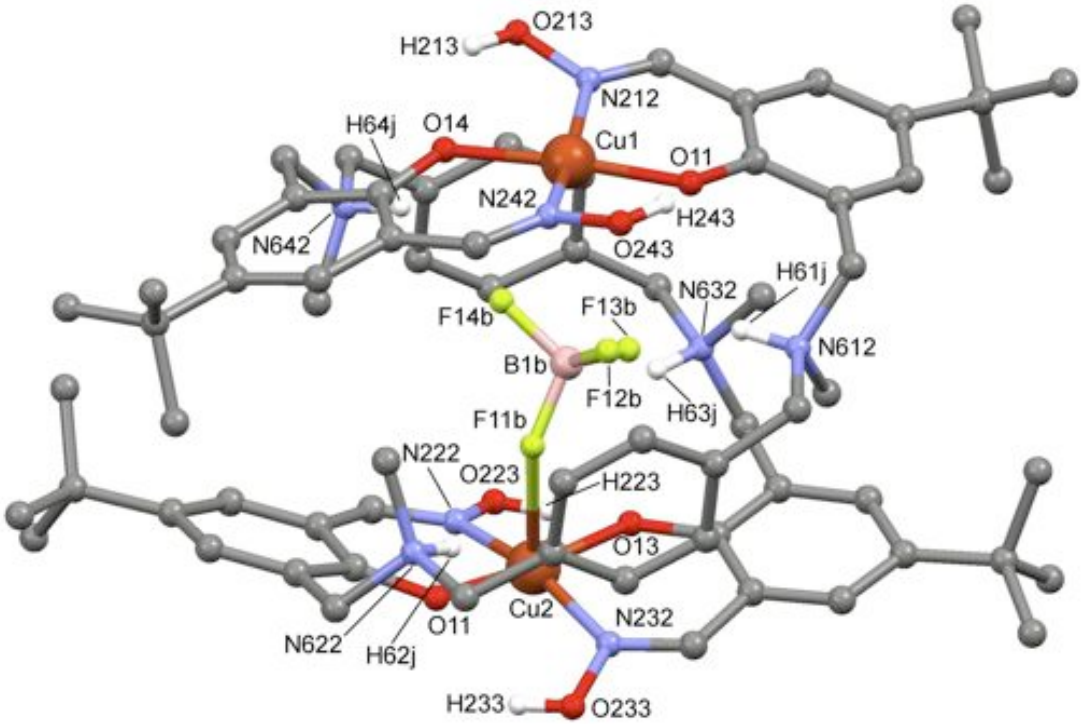

Figure 24. Perspective view of **4**, showing the encapsulation of a tetrafluoroborate anion (Hydrogen atoms not involved in H-bonding, the disorder of the encapsulated BF_4^- (40:60), the disorder of the *t*-butyl group centered at the 4° carbon of the O14 ring (50:50), the three counter tetrafluoroborate anions and the acetone solvent molecules have been omitted for clarity).

The complex consists of two Cu(II) atoms coordinated to two protonated $\mathbf{L^1}$ molecules (at the tertiary amines) with each copper centre

sharing both ligands via the N-oximate and phenolate positions ($N_2O_2^{2-}$). The complex retains a box type shape and helical nature upon complexation with the BF_4^- anion.

The Cu(II) centres in **4** are in differing environments due to the encapsulated BF_4^-. Cu1 is in a distorted square planar environment while Cu2 is in a distorted square pyramidal environment. Both Cu(II) centres have four donors that consist of two oxygen donors (one phenolate moiety from each ligand) and two nitrogen donors (one oxime moiety from each ligand). Cu2 then has a fifth weak interaction in the axial position with F11b from the captured tetrafluoroborate molecule at a distance of 2.538(21) Å (refer to Table 10 for bond lengths and angles for the copper centres). The distance between the two copper(II) centres has decreased significantly upon complexation with the BF_4^- anion to 7.212(1) Å and the average helical twist has increased significantly to 130.6°. This suggests that the complex has undergone significant conformational change to accommodate the encapsulated BF_4^- anion (compared to **1**, which has a longer distance to the copper centres and a more relaxed helical twist). Even with this drastic rearrangement of the complex, it appears that the BF_4^- anion is a sloppy fit for the cavity as evidenced by the disorder of the captured anion (40:60 for B1:B1b). One disordered state (B1b) has a short bond distance of 2.538(14) Å to Cu2 (F11b–Cu2) and a longer weaker bond distance of 3.012(8) Å to Cu1 (F12b–Cu1), while the second disordered state (B1) has moved closer to Cu1 and slightly further away from Cu2 resulting in two medium bond length distances of 2.836(21) Å and 2.626(9) Å for F11–Cu2 and F14–Cu1 respectively (refer to Table 12 for selected bond distances and angles). Overall, this results in the anion favouring one side of the cavity and is positioned closer to Cu2 resulting in a significant interaction (in the solid state) with the anion over Cu1. Clearly the BF_4^- anion (being slightly smaller than the structurally similar ClO_4^- anion[59]) does not fit as well as the perchlorate. Interestingly, the two complexes **3** and **4** have similar Cu–Cu distances and helical twist angles, differing only by 0.0770 Å and 1.6°

respectively. This suggests that the complex may be reaching its potential limits in contracting to accommodate the anion.

In comparison to the hexylene linked oxime analogue[46] which has a Cu–Cu distance of 6.938(2) Å and an average helical twist of 112.0°, **4** has a larger Cu–Cu distance and a larger average helical twist angle of 130.6°. This is because the more restrictive aryl spacers require the complex to twist further to contract in size to wrap around the anion and is potentially reaching its flexibility limits. The longer Cu–Cu distance of **4** results in longer and uneven bond distances between the encapsulated BF_4^- anion to the metal centres (see Table 11 for selected bond distances and angles for the encapsulated BF_4^- anion), compared to the C6 alkyl analogue which has a shorter Cu–Cu distance and results in shorter bond distances to the BF_4^- anion of 2.519(13) Å and 2.483(12) Å for the Cu1–F23 and Cu2–F21 bonds respectively. A search through the CCDC for complexes containing Cu–F bonds has resulted in an average Cu–F bond length of 2.56 Å.[87 – 89, 91 – 102] The Cu–F bond lengths in **4** (Table 11) are all longer than this average except for Cu2–F11b which is just shorter than the average (2.538 Å). The lengthening of these interactions in **4** are due to the fact that the BF_4^- anion does not fit comfortably inside the cavity and leaves room for the anion to move about, as evidenced by the disordered nature of the anion.

The average torsion angle around the copper centres is 158.1°. This is only a slightly less distorted square planar environment around the metal centres than the anion free complex **1** and **3**. This suggests that encapsulating and coordinating a tetrafluoroborate anion in the cavity also has relatively no effect on the square planar arrangement around the metal centres. In comparison, the hexylene linked tetrafluoroborate analogue[46] has an average torsion angle through the O-N-N-O plane of 156.7°, which is very similar. This suggests that the effect of encapsulating a BF_4^- anion makes little difference to the metal coordination site in either the akyl or aryl containing complexes.

The τ value for the 5-coordinate Cu2 metal centre is 0.18. This τ value indicates that the coordination of the tetrafluoroborate anion within the cavity

has also caused a slight deviation from a perfect square pyramidal geometry, but not as much deviation as was caused by the perchlorate anion in complex **3**. This may possibly be caused by the stronger binding of the larger anion to the metal centres. This τ value is very similar to the distortion in **1** where the Cu(II) metal centre is weakly coordinated to an adjacent phenolate oxygen atom.

Atoms	Bond Lengths (Å)	X–Cu–X	Bond Angles (°)
Cu1 – O11	1.881(4)	O11–Cu1–N212	92.1
Cu1 – O14	1.903(4)	O11–Cu1–N242	89.0
Cu1 – N212	1.955(4)	O14–Cu1–N212	88.9
Cu1 – N242	1.952(5)	O14–Cu1–N242	91.2
Cu2 – O13	1.894(3)	O12–Cu2–N222	92.3
Cu2 – O12	1.896(3)	O12–Cu2–N232	89.7
Cu2 – N222	1.951(4)	O13–Cu2–N222	88.0
Cu2 – N232	1.932(4)	O13–Cu2–N232	92.1
Cu2 – F11b	2.538(21)	F11b–Cu2–O12	76.4
		O11–Cu1–Cu2–O12	130.7
Cu1 – Cu2	7.212(1)	O14–Cu1–Cu2–O13	130.4

Table 10. Selected bond lengths and angles for the Cu(II) centres of **4**.

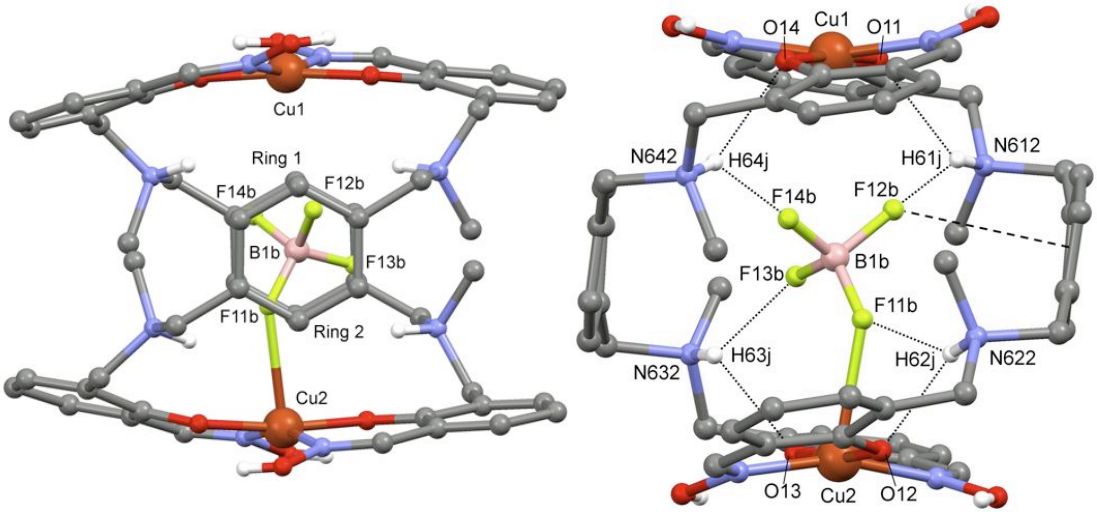

Figure 25. Perspective side views of one of the two disordered states of the encapsulated BF_4^- anion (40:60 for B1:B1b) in **4** showing the major disordered interactions and the face-on positioning of the aryl linkers (Hydrogen atoms not involved in H-bonding, the *t*-butyl groups, counter anions and solvent molecules have been omitted for clarity).

Atoms	Bond Lengths (Å)	X–Cu–X	Bond Angles (°)
F11 … Cu2	2.836(21)	O12–Cu2–F11	74.3
F11b … Cu2	2.538(14)	O12–Cu2–F11b	76.4
F12 … Cu1	3.636(11)	O11–Cu1–F12	63.1
F12b … Cu1	3.012(8)	O11–Cu1–F12b	70.7
F14 … Cu1	2.626(9)	O14–Cu1–F14	73.2
F14b … Cu1	3.102(11)	O14–Cu1–F14b	69.2

Table 11. Selected bond lengths and angles between the disordered encapsulated BF_4^- and the Cu(II) centres of **4**.

The protonated tertiary amines of the aryl linker are again angled towards the central cavity so as to make H-bonding interactions with all of the fluorine atoms of the encapsulated BF_4^- anion (refer to Figure 25 and Table 12 below for H-bond distances and angles). Both of the disordered states of

the captured anion give rise to one moderate H-bond each from one amine to a fluorine atom. With the major disorder favouring Cu2 over Cu1, this gives rise to uneven bond distances to the protonated tertiary amines. Both the B1 and B1b disorders have almost the same average H-bond distances, but the major component B1b has a shorter average bond distance of 2.995 Å over B1 disorder which has an average H-bond distance of 3.014 Å. This orientation of H-bonds to the BF_4^- anion is the same as in the C6 alkyl analog complex, where the encapsulated BF_4^- anion is also disordered over two positions but the average H-bond for each of the two disorders are longer than in **4**, which are 3.128 Å and 3.194 Å. Due to the smaller size of the BF_4^- anion over the larger ClO_4^- anion, these moderate H-bonds now play a more dominant role in stabilizing the anion inside the cavity.

Atoms	D–H–A distances (Å)	D–H–A angles (°)
N622-H62j … F11	3.010(16)	137.7
N612-H61j … F12	2.924(10)	126.3
N632-H63j … F13	2.998(10)	150.2
N642-H64j … F14	3.123(13)	146.0
N622-H62j … F11b	3.170(13)	144.1
N612-H61j … F12b	3.082(9)	149.8
N632-H63j … F13b	2.918(8)	131.2
N642-H64j … F14b	2.811(11)	135.0

Table 12. Selected H-bond distances and angles between both disordered encapsulated BF_4^- orientations and the protonated amine groups in **4**.

The captured BF_4^- anion is also stabilised within the cavity by one anion–π interaction for each of the positionally disordered states (40:60). This

is possible because the aryl rings of the linker have rotated upon complexation and so adopt a face-on position with respect to the central cavity. This leaves the centroid π system of the aryl rings facing the central cavity of the complex. The two interactions are between one fluorine atom of one disordered tetrafluoroborate anion and one of the aromatic ring's π systems,[26, 27, 90] and one fluorine atom of the second disordered anion. For the minor disorder (B1), this is between F13 and the centroid created in Ring 1 at a distance of 3.104 Å, which is a relatively strong interaction compared to other tetrafluoroborate F–π interactions.[26] For the major disordered state (B1b), it is between F12b and the centroid created in Ring 2 at a distance of 3.311 Å (see Figure 26 below), which is a relatively weak interaction compared to other tetrafluoroborate F–π interactions[26] (refer to Table 13 for bond distances and angles). Both of these anion–π interactions are weaker than the corresponding anion–π interactions in complex **3** due to the smaller size of the BF_4^- anion.

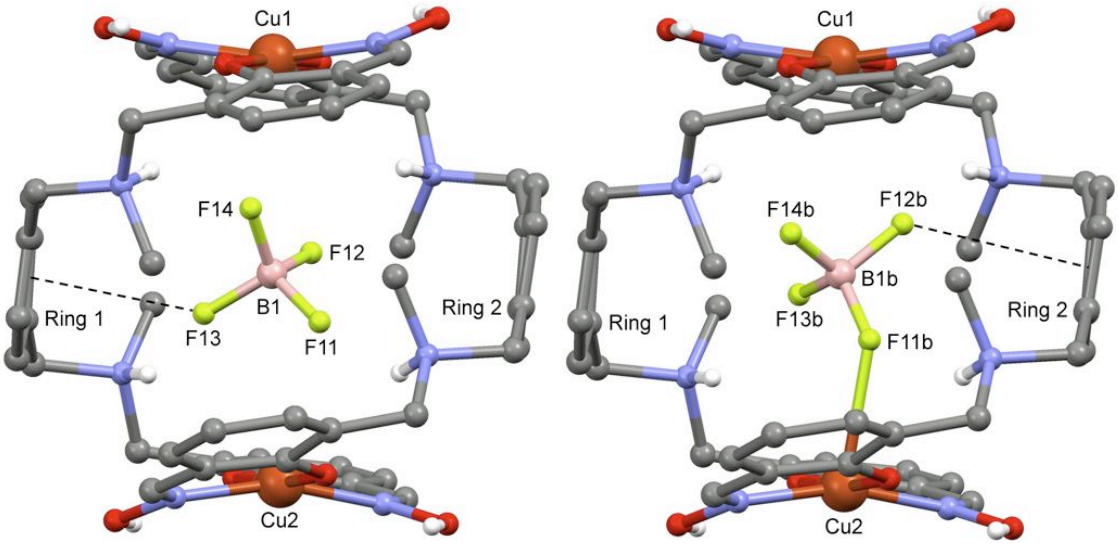

Figure 26. Perspective front-on views of complex **4** showing the two states of disorder of the encapsulated BF_4^- anion showing the anion–π interactions to the aryl rings of the linker (Hydrogen atoms not involved in H-bonding, the *t*-butyl groups and counter anions have been omitted for clarity).

Atoms	H-bond distances (Å)	D–H–A angles (°)
B1-F13 … Ring 1	3.104	133.5
B1b-F12b … Ring 2	3.311	124.0

Table 13. Selected anion–π distances and angles for the disordered encapsulated BF_4^- anion in **4**.

The pseudo macrocyclic cavity surrounding each metal centre is completed by an oxime hydrogen bonded towards the opposing phenolate oxygen with an average O … O distance of 2.701 Å, which is only just shorter than the average bond length for the perchlorate complex **3** by 0.016 Å and like **3** is also slightly longer than the average bond length for **1**. This suggests that upon coordinating to an anion this oxime to phenolate interaction is not affected. There also exists a secondary H-bond to each phenolate oxygen from a protonated tertiary amine from the aryl linker with an average distance of 2.920 Å (refer to Table 14 for H-bond distances and angles), which is only marginally longer than the average H-bond length for **3** by 0.022 Å. It is also slightly shorter than the average bond distance of **1** which can also be explained by the more coiled up nature of **4** over **1** and results in bringing the protonated amine groups closer to the phenolate oxygen groups.

Atoms	H-bond distances (Å)	D–H–A angles (°)
O243-H243 … O11	2.707(5)	129.2
O233-H233 … O12	2.755(5)	127.7
O223-H223 … O13	2.648(5)	131.1
O213-H213 … O14	2.693(5)	132.0
N612-H61j … O11	2.981(6)	126.1
N622-H62j … O12	2.818(5)	129.7
N632-H63j … O13	3.003(6)	124.4
N642-H64j … O14	2.878(5)	127.5

Table 14. Selected intramolecular H-bond distances and angles for the oxime moieties in **4**.

The tetrafluoroborate counter anions are involved in a multitude of H-bonding and close contact interactions with the complex, similar to that of the counter perchlorate anions in **3**. One of the counter tetrafluoroborate anions (B4 F41 F42 F43 F44) lies near one of the oxime moieties of the complex, an acetone molecule and the aryl ring of two adjacent complexes. The second tetrafluoroborate anion (B3 F31 F32 F33 F34) lies in between the complex and another adjacent to it by their *t*-butyl groups and near another acetone solvent. The last counter tetrafluoroborate anion (BF2 F21 F22 F23 F24) is positioned differently. It is located away from the main complex and lies between two adjacent complexes near their oxime moieties and two acetone solvent molecules.

2.4 Summary

The crystal structure of **1** $[Cu_2(L^1\text{-}2H)_2]$ obtained has helped in understanding the way the 1,4-aryl linkers in the anion free complex **1** orient themselves in the solid state. The crystal structures **3** and **4** have given an insight into the many distinct interactions involved when anions are encapsulated within the cavity of **1**, including metal-anion, H-bonding and last but not necessarily least, anion–π interactions. These have all contributed to the interpretation of the stability constants obtained in the titration experiments.

Of the anions investigated, sulfate demonstrated the strongest binding constant, approximately one and a half orders of magnitude higher than any other. This is most likely due to a number of reasons; the anion's more negative charge and larger size compared to the other anions which also account for its strong coordinating ability to the Cu(II) centres, helping maximize its ability to form stronger H-bonds to the protonated tertiary amines. The larger size of sulfate and its tetrahedral shape also aid in making closer and stronger anion–π interactions to the 1,4-aryl linkers of the complex, as evidenced by the other tetrahedral shaped anion crystal structures. There is a very weak correlation between increasing stability constant with an increase in anion size/volume. The lower and equivalent binding constants of perchlorate, nitrate and bromide anions demonstrate this weak trend, with $Br^- < NO_3^- < ClO_4^-$. This trend for **1** shows that it may not be flexible enough to shrink in size to accommodate the much smaller anions. This demonstrates that the incorporated *p*-xylylic spacers have imposed a size restriction within the complex in which anions must be a certain size (i.e. ~0.09 nm^3) to bind effectively in the cavity.

In the original anion receptor with a C6 akyl spacer, there exists a general trend whereby there is an increase in the stability constant with an increase in anion size, with the nitrate anion the exception. Upon incorporating the more restrictive 1,4-aryl spacers into **1**, this has drastically changed the anion binding properties of the complex. There is now a very

large increase in binding strength for the sulfate anion over the smaller anions studied. Another general trend is seen between the smaller anions, in which now there is no real distinction or selectivity of one over the other. This can be further emphasized with the crystal structure of the complex containing the perchlorate anion, the second largest anion tested. This anion is only held in the cavity by three weak to moderate H-bonds and bonds weakly with the copper(II) metal centres, it stands to reason that the smaller anions will exhibit weaker binding than perchlorate.

Changing the flexible alkyl linkers to more restrictive *p*-xylylic linkers in **1** has resulted in a decrease in binding strength of the anions smaller than sulfate. In contrast, the sulfate binding constant has dramatically increased relative to these anions, possibly as a result of the increased rigidity created by the aryl rings in the linker arms.

2.5 Experimental

2.5.1 Materials and Reagents

Spectrophotometric measurements in the UV-visible region were performed at 294 K using a CARY 100Bio UV-Vis spectrophotometer and 1 cm path length quartz cuvettes. The data were analysed and the stability constants were calculated using the software program SPECFIT/32^{TM} (version 3.0.40).[103 – 105] X-ray crystallographic data were recorded at low temperature with a Rigaku-Spider X-ray diffractometer. Chemicals and solvents were of AR grade unless otherwise stated and used as received. **1** was dried under vacuum for two hours prior to the preparation of the titration solutions and the titrations were prepared immediately. The synthesis of **1** is reported in Chapter 6.

2.5.2 Spectrophotometric Titrations

Solutions of **1** in dry THF:$CHCl_3$ ($CHCl_3$ less than 0.01%) (2 mL, 1.5 x 10^{-5} mol L^{-1}) were titrated with dry THF solutions of the acid of interest (2.5 x 10^{-4} mol L^{-1} – 1.0 x 10^{-3} mol L^{-1}). Spectra were recorded following the addition of each aliquot over the wavelength range of 250 to 900 nm. The acid solutions were titrated at 0.25 molar equivalent increments for H_2SO_4 and 1.0 molar equivalent increments for HNO_3, $HClO_4$ and HBr. A larger mole equivalent was required by these three acids to give a large enough change in the UV-vis spectrum in order for SPECFIT/32^{TM} to determine a formation constant between the receptor and the anion. A 1:1 anion to complex binding model was assumed for all spectrophotometric titrations (as determined by mole-ratio plots) and supported by SPECFIT/32^{TM} which was used to calculate the binding constants of **1** to the corresponding anions of the acids used. In order to ensure reliable results, titrations were repeated until at least three concordant results were obtained which were within error of each other. Binding constant errors are the standard deviations of the three concordant results.

2.5.3 Solution Preparation

All solutions were prepared using dry THF as the solvent. A pre-weighed sample of **1** was dissolved in 1 mL of $CHCl_3$ and was made up to 100 mL with THF to give a standard solution concentration of 2.0 x 10^{-4} mol L^{-1} – 3.0 x 10^{-4} mol L^{-1}. A further dilution of this solution was used to give a final concentration of 1.5 x 10^{-5} mol L^{-1} with a $CHCl_3$ content less than 0.01%. A standard ampoule of sulfuric acid (in H_2O) was made up to 500 mL with THF to give a 0.1 mol L^{-1} solution. This solution was diluted to give a 1.5 x 10^{-3} mol L^{-1} solution. Then a further dilution to give a final concentration of 2.5 x 10^{-4} mol L^{-1} with a water content less than 0.05%. A standard ampoule of nitric acid (in H_2O) was made up to 500 mL with THF to give a 1.0 mol L^{-1}

solution. This solution was diluted to give a 0.01 mol L^{-1} solution and then a further dilution to give a final concentration of 1.0 x 10^{-3} mol L^{-1} with less than 0.01% of water. A 28.3 µL aliquot of a 48% solution of hydrobromic acid (in H_2O) was made up to 50 mL with THF to give a 5.0 x 10^{-3} mol L^{-1} solution. This solution was further diluted to give a final concentration of 1.0 x 10^{-3} mol L^{-1} with less than 0.01% of water. A 43.0 µL aliquot of a 70% solution of perchloric acid (in H_2O) was made up to 50 mL with THF to give a 0.01 mol L^{-1} solution. This solution was further diluted to give a final concentration of 1.0 x 10^{-3} mol L^{-1} with less than 0.01% of water.

2.5.4 Reliability of Standard Solutions

The acid solutions of hydrobromic and perchloric acid were prepared from the dilution of concentrated aqueous acid solutions.[45] Previous work carried out to determine the reliability of these solutions where a perchloric acid solution 1) made from aqueous perchloric acid was compared to a perchloric acid solution 2) prepared from a standard solution. The titrations carried out using 2) produced spectra which were indistinguishable from those titrations done with 1) and when they were analyzed with multivariable analysis using SPECFIT/32™ program, the binding constants were within error of each other.[45] This suggested that the acid solutions prepared from concentrated aqueous acid solutions were of a comparable or of equal quality to the solutions of acids made from standard acid solutions.

Chapter 3

Titrations of $[Cu_2(L^2\text{-}2H)_2]$

3.1 Introduction

The second objective of this thesis was to investigate the solid state and solution interactions between a selection of anions and a second conformationally restricted receptor **2** (Figure 27).

This receptor has the potential for further restriction in conformational freedom and by altering the spacer group from the *p*-xylylic to an *m*-xylylic linker, the $\mathbf{L^2}$ ligand was synthesized (Figure 27). Reaction of $\mathbf{L^2}$ with copper acetate produced a neutral complex $[Cu_2(L^2\text{-}2H)_2]$, referred to as the anion free complex **2**, analogous to both **1** and the hexylene linked helicates, as evidenced by X-ray analysis (see section 3.3.2). The comparison of the binding constants of anion encapsulation for **2** against previously studied helicates and **1** will allow the effect of potential further conformational restrictions using the 1,3-aryl functionality in the structure to be analyzed. In particular, whether the rigid 1,3-aryl spacer will result in a major change in flexibility of the complex with regards to **1** and the earlier published hexylene linked analogues and how this will affect the binding strength of anions (via UV-visible and solid state evidence). As was shown in Chapter 2, the large changes in the UV-visible spectra upon the addition of acids to **2**, as well as the crystal X-ray structures obtained, suggest the encapsulation of anions and binding to **2**. Thus these techniques have been employed to study the ability of a selection of anions to bind to the tetraprotonated form of **2**.

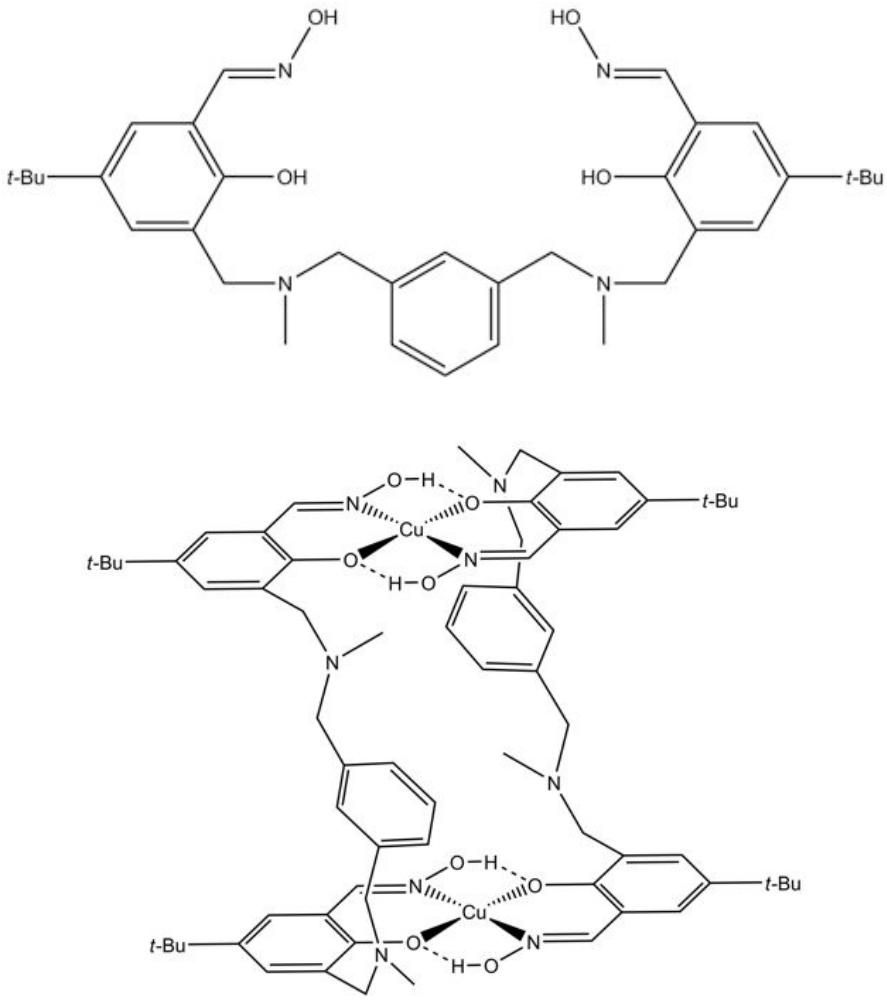

Figure 27. The *m*-xylylic oxime ligand $\mathbf{L^2}$ (top) which was used to produce $[Cu_2(L^2\text{-}2H)_2]$, the anion free dicopper complex **2** (bottom) and used in the UV-visible titrations.

3.2 Results and Discussion

3.2.1 Synthesis of Complexes

By reacting $\mathbf{L^2}$ with copper(II) acetate under the same conditions as in **1**, a neutral anion free complex **2** was produced.

As with **1**, **2** is in equilibrium between its protonated and neutral forms in solution and the H-N bonds of the protonated tertiary amines are weakened due to the proximity to the phenolate oxygen atoms. The effectively lowered pK_a of the tertiary amines thus primes the acetate to receive the protons from

the complex and results in the neutral anion free complex **2** (synthesis of complexes are further outlined in Chapter 6).

*3.2.2 Absorption Spectra of **2***

Analogous to **1** in Chapter 2, attempts to dissolve **2** in either IPA or in a 1:1 mix of IPA:DCE also resulted in un-dissolved product. When THF was added to **2**, a pale yellow coloured solution developed and **2** was dissolved, hence it was used as the solvent of choice for the UV-visible titration studies.

Chapter 2 mentioned that at lower wavelengths, between 200-250 nm, the spectra displayed unreliable bands under identical experimental conditions. This likewise occurred for complex **2** and as a result the spectrum was recorded from 900 to 250 nm, as well as for the titration experiments.

The spectrum of complex **2** (Figure 28) is almost identical to the spectrum produced by **1**. It has a broad band with a maximum at 355 nm and large shoulder bands at 272 and 255 nm. As with **1**, these peaks originate from the ligand. The 355 nm band was assigned as the phenolate related π to π_1^* electron transfer which is responsible for the yellow colour of the ligand solutions. The shoulder bands are assigned as the π to π_2^* electronic transition band.[56]

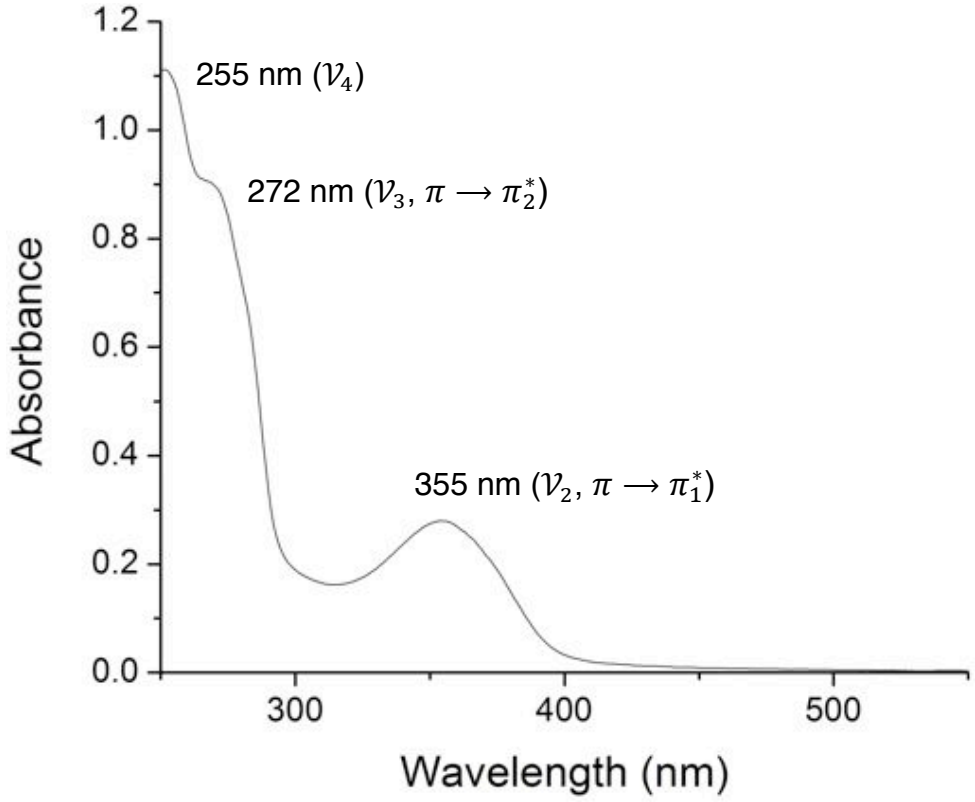

Figure 28. UV-visible absorbance spectra of **2** in THF. The broad band at 355 nm is characteristic of the phenolate moiety.

*3.2.3 Acid Titrations with **2***

As discussed in Chapter 2, the same methods of titrating were used for complex **2** in dry THF and the same important assumptions for the titration experiments are assumed for complex **2**. The acids titrated were; sulfuric, perchloric, nitric and hydrobromic acids.

As discussed in section 2.2.3, complex **2** will also be unprotonated in solution. The same modeling limitations concerning SPECFIT/32^{TM} and the same conclusions about **1** being mainly anion dependent and that the first equivalent of anion titrated into solution most likely enters and coordinates to the metal centres in the cavity of receptor **2** before it is fully protonated also apply to receptor **2**. A 1:1 ratio of complex **2** to anion was used during the titration experiments to calculate the corresponding association constants except for HBr where a 1:2 ratio of **2** to Br^- anion was used. Again, attempts

at calculating the binding constants with SPECFIT/32^{TM} using small increments of acid (i.e. 0.1 mole equivalents of acid) to finish with a small total mole equivalent amount of acid (i.e. 4 mole equivalents of acid or less) added to a solution of **2** resulted in SPECFIT/32^{TM} not being able to calculate any stability constants. Instead larger increments of acid were titrated to a higher total mole equivalent which resulted in a larger change in the UV-vis spectra which SPECFIT/32^{TM} could then calculate a binding constant. A 0.20 mole equivalent increment was used for $HClO_4$ to a total of 6 mole .equivalents, 0.25 mole equivalent increments to a total of 5 and 8 mole equivalents were used for H_2SO_4 and HBr respectively and a 1.0 mole equivalent increment to a total of 30 mole equivalents was used for HNO_3.

The program SPECFIT/32^{TM} was used to determine the binding stability constants of the anions to complex **2**. A 1:1 binding model was used to determine binding constants for all anions (except in the case of bromide), producing good agreement between the predicted and recorded spectra. Mole-ratio plots were carried out for each anion and determined that a 1:1 ratio of anion to complex was occurring except for the bromide anion. The bromide anion complex was treated differently. The crystal structures $[2Br\subset(Cu_2L^2{}_2)](Br)_2$ (**6**) and $[2Br\subset(Cu_2L^2{}_2)](BF_4)_2$ (**7**) revealed the distinct feature that the anion sits within a binding pocket with each Br^- bound to each Cu(II) centre in the solid state, suggesting a 2:1 ratio of anion:complex was more appropriate. This was further corroborated by 1) a mole-ratio plot indicating a 2:1 ratio of anion to complex and 2) good agreement between the predicted spectra produced by SPECFIT/32^{TM} and the recorded spectrum. A 1:1 binding ratio was modeled for the bromide complex using SPECFIT/32^{TM} and this resulted in an unsatisfactory predicted spectrum.

The stability constants calculated for the anions used are recorded in Table 15 below. The trend seen for the ratio of anion:complex binding is a steady stability constant between 4.5 – 4.6 for the anions bromide, perchlorate and sulfate (with their corresponding K_1 values being within error of each other) while the nitrate anion showed a comparatively weaker binding constant. The perchlorate anion exhibited the strongest binding to complex **2**,

with a log K value of 4.61 ± 0.18 for a 1:1 ratio of anion to complex **2**. From perchlorate to the larger sulfate anion the stability constant has had a slight decrease, but essentially agrees within experimental error with a binding constant of 4.49 ± 0.10. This suggests that the receptor **2** has an optimum anion binding size at approximately the size of the ClO_4^- anion (Figure 29). This observed higher binding strength of perchlorate over sulfate is likely due to the restricted nature of **2** (discussed in section 3.3). Complex **2** has a smaller cavity volume than **1**, which appears to be more easily able to accommodate the smaller ClO_4^- anion over the larger SO_4^{2-} anion. The smaller nitrate anion appears to be too small for the cavity of **2**. Attempts at growing crystalline complexes of **2** with ClO_4^- or the SO_4^{2-} anions were unsuccessful so it remains uncertain as to the reason why perchlorate exhibited the higher binding constant. The nitrate crystal structure was determined (as discussed in section 3.3.3) and demonstrates that the nitrate anion is capable of coordinating to both metal centres and has three moderate – weak H-bonds from the tertiary amines. Even with all these binding factors contributing to stabilizing the anion within the cavity, the stability constant calculated is still lower than for the larger anions.

As was mentioned above, the bromide was a special case. From the X-ray evidence it was discovered a single bromide anion binds at each Cu(II) centre of complex **2** (as discussed in section 3.3.4). This gave a combined K_1K_2 stability constant of 9.21 ± 0.07. Given the similarity in binding sites (as determined by X-ray evidence, section 3.3.4) for the two bromide anions, an estimation can be made for the individual binding constants.[106] With $\beta_{12} = \log K_1K_2 = \log K_1 + \log K_2$, and assuming $K_1 = K_2$, then $\beta_{12} = 2\log K$, which means that $K_{12}/2 = K_1 = 9.21/2 = 4.61 \pm 0.04$. It was assumed that $K_1 = K_2$ in this instance for several reasons; the first was that in the crystal structure $[2Br\subset(Cu_2L^2{}_2)](Br)_2$ (**6**), the anion binding sites are symmetrical with respect to each other, indicating that the binding of the first bromide is the same for the second bromide. Secondly, the binding sites are remote from one another and thus the binding of the first anion shouldn't have any influence upon the binding of a second anion. Lastly, when a 1:1 stoichiometry of bromide to

complex **2** was attempted, the resulting crystal structure observed again contained the binding motif of a 2:1 ratio of anion:receptor, structurally identical to the first (discussed in section 3.3.5).

The ESI-MS spectra indicate that there are interactions occurring between complex **2** and the corresponding anion. Each of the anions tested showed only a single significant fragmented peak corresponding to $[L^2CuX]^+$, which contains one *m*-xylylic ligand coordinated to one Cu(II) metal atom with a single anion (X) bound (see in Table 15), as was similarly seen for **1**. These fragments once more convey a sense of fragility of complex **2** as a whole and may break up during flight in the Mass Spectrometer. This was further shown by the mass spectrum of the anion free complex **2** where only a peak of $[L^2Cu]^+$ was seen.

Acid	Log K	Stoichiometry	ESI-MS Peaks
H_2SO_4	4.49 ± 0.10	1:1	$[L^2CuSO_4]^+$
$HClO_4$	4.61 ± 0.18	1:1	$[L^2CuClO_4]^+$
HNO_3	3.76 ± 0.09	1:1	$[L^2CuNO_3]^+$
HBr	9.21 ± 0.07 (K_{12})	1:2	$[L^2CuBr]^+$

Table 15. The log *K*, stoichiometry and the main ESMS peaks observed as evidence for the binding of anions to **2** in THF at 294K.

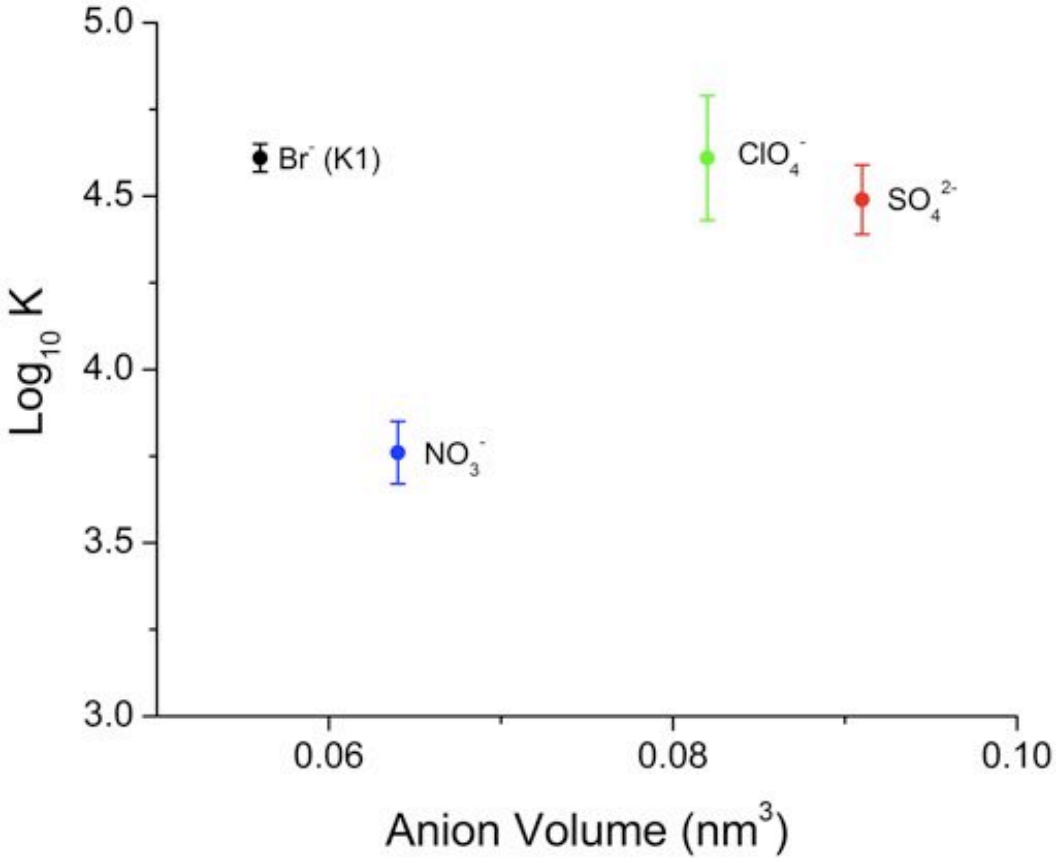

Figure 29. The calculated stability constants for anions binding to **2** vs. anion size. The anion volumes used are from the paper by Jenkins *et al.*[59]

3.3 X-ray Crystal Structures of **2**

3.3.1 X-ray Crystal Structure of L^2

Colourless platelet shaped crystals of L^2 suitable for X-ray diffraction were grown by slow diffusion of hexane into an ethyl acetate mix of the ligand and the crystal structure was determined (Figure 30). The asymmetric unit consists of one half of the ligand with the other half generated by inversion. The structure confirms the successful synthesis of L^2 and agrees with the physical data obtained for the ligand.

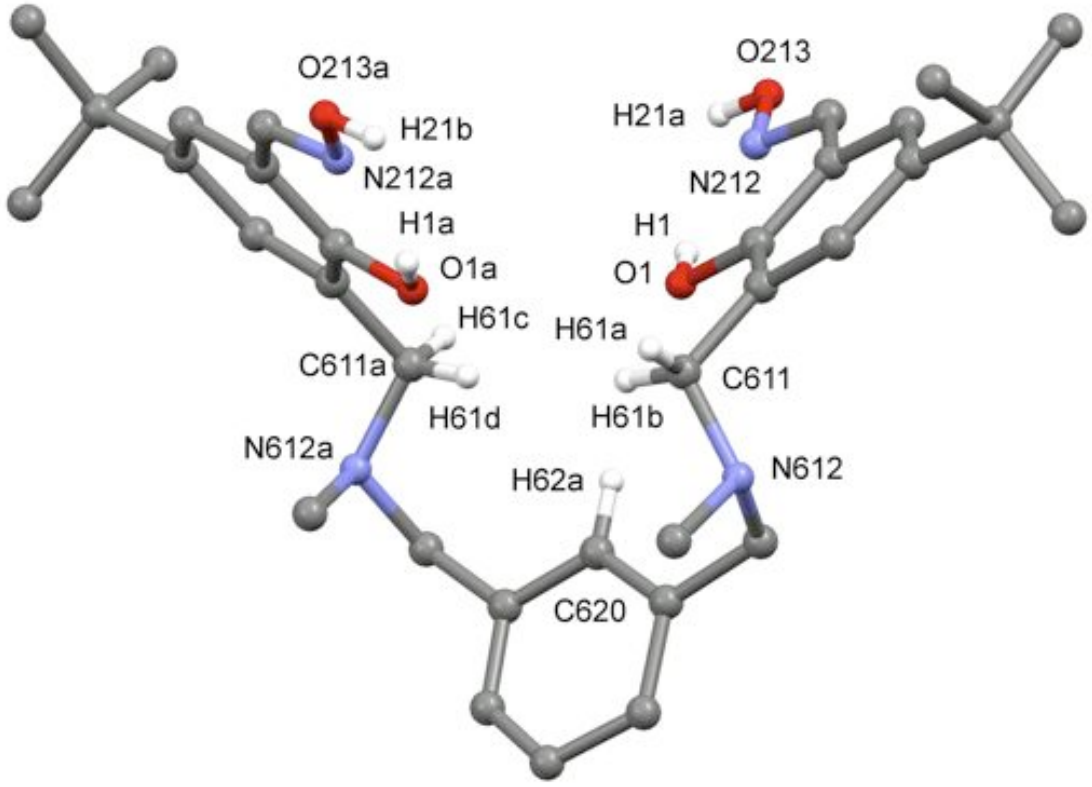

Figure 30. Perspective view and the adopted labeling scheme of L^2 (hydrogen atoms not involved in H-bonding have been omitted for clarity).

The salicylaldoxime rings in this structure are twisted away from each other and point in opposite directions. This helps in the packing of the crystal,

maximizing the number of hydrogen bonds. The phenolate has a moderately strong H-bond towards the oxime nitrogen at a distance of 2.602(3) Å and a moderate H-bond from a methylene hydrogen H61b at a distance of 2.834(4) Å. The oxime OH donor forms a moderately strong inter-hydrogen bond with a tertiary amine of an adjacent **L²** molecule at a distance of 2.692(5) Å (refer to Table 16 for H-bond lengths and angles).

Atoms	H-bond distances (Å)	D-H-A angles (°)
O1-H1 … N212	2.602(3)	146.6
C611-H61b … O1	2.834(4)	107.5
O213-H21a … N612b	2.692(5)	155.3

Table 16. Selected H-bond distances for **L²**.

The 1,3-substituted aryl linker and the methyl group on the tertiary amines are disordered between two positions (50:50). Each position of the disordered 1,3-substituted aryl linkers allows the aromatic hydrogen H62a to get closer (3.476(6) Å) to one of the phenol oxygens (O1) but further away (4.464 Å) from the other (O1a).

*3.3.2 X-ray Crystal Structure of $[Cu_2(L^2\text{-}2H)_2]$.2DIPE (**2**)*

Dark green platelet shaped crystals of **2** suitable for X-ray diffraction were grown by slow diffusion of diisopropyl ether into a THF/$CHCl_3$ (1:1) mix of the complex and the crystal structure was determined (Figure 31). The asymmetric unit consists of one half of the complex with the other half generated by an inversion at the centre of the molecule.

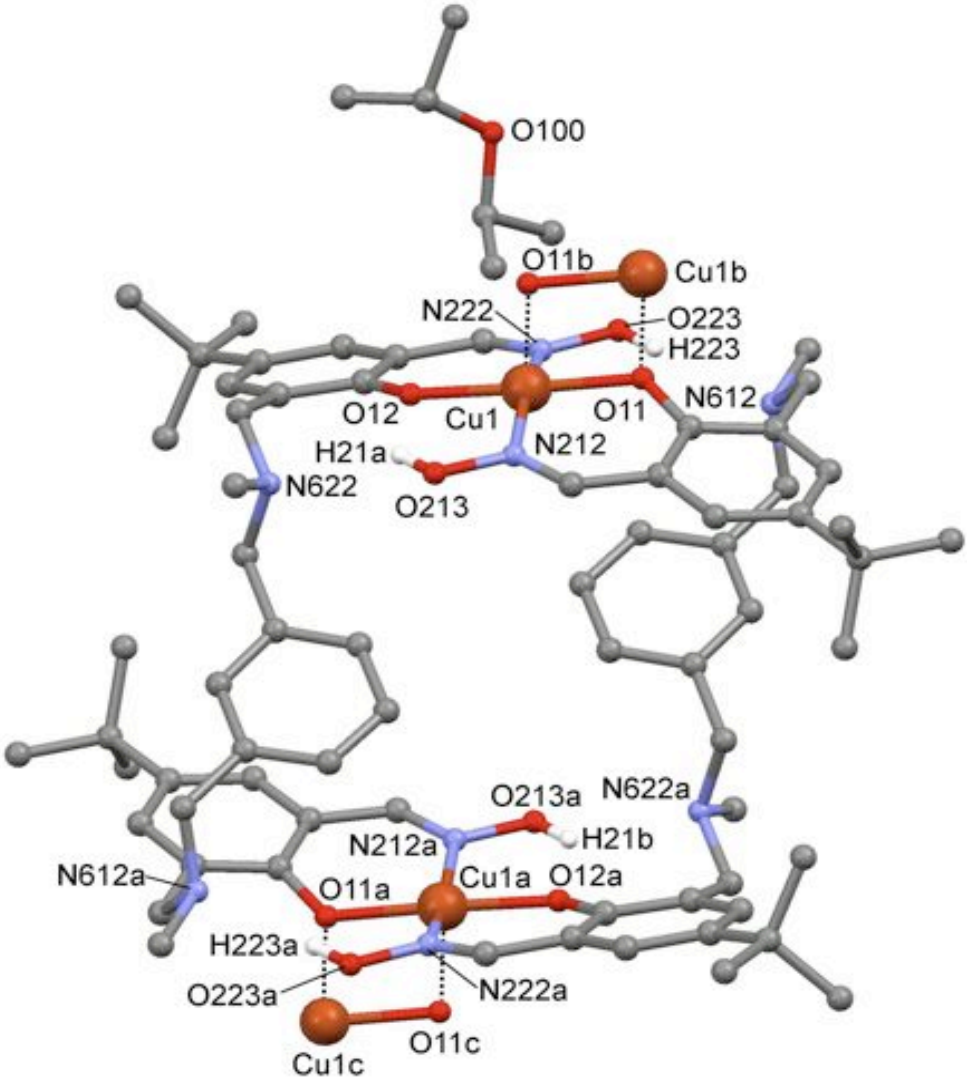

Figure 31. Perspective front view of $[Cu_2(L^2\text{-}2H)_2]$.DIPE and the axially coordinated Cu–O of the adjacent complex molecules (Non-hydrogen bonding hydrogen atoms have been omitted for clarity).

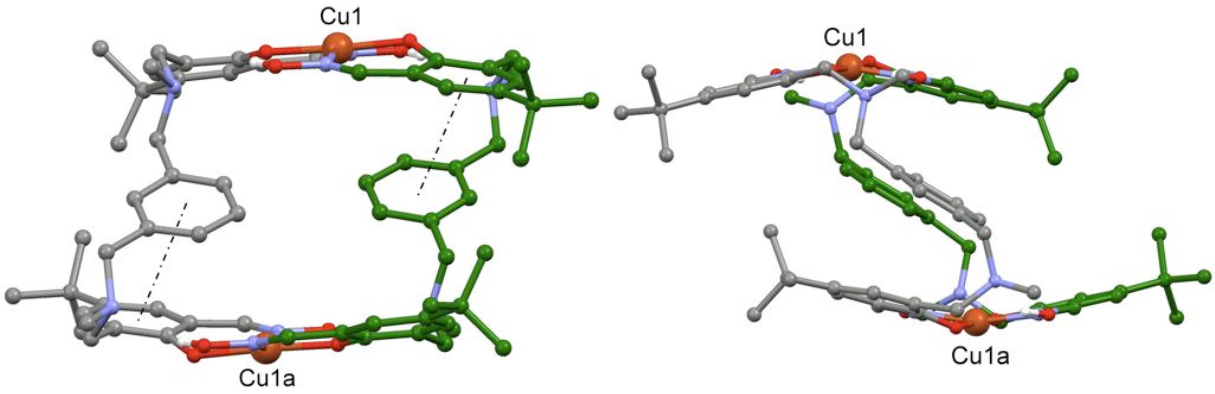

Figure 32. Perspective front and side views of complex **2** $[Cu_2(L^2\text{-}2H)_2]$, showing the close π–π stacking interactions and the edge-on positioning of the aryl rings in the strap. One ligand is coloured grey and the other green (Hydrogen atoms and solvent molecules have been omitted for clarity).

The complex consists of two Cu(II) ions coordinated to two di-anionic **L^2** molecules with each copper sharing both ligands via phenolate and N-oximate coordination ($N_2O_2^{2-}$). The reduction in conformational freedom brought about by the 1,3-aryl linkers leads the complex to adopt a non-helical, square parallelogram type structure, where one phenolic ring is above the second phenolic ring of the same ligand (demonstrated in Figure 32 with each ligand within the complex coloured a separate colour). This non-helical adopted conformation of the ligand is contrary to every other structure of this type to date.

The copper(II) centres are in a slightly distorted square pyramidal environment (refer to Table 17 for H-bond lengths and angles). As in **1**, the five donors consist of two nitrogen atoms (one oxime moiety from each ligand) and two oxygen atoms (one phenolate moiety from each ligand) and these contribute to the $N_2O_2^{2-}$ head to tail coordination mode of the in-plane donors. The fifth position consists of a weak interaction to a phenolic O atom in the axial position from a neighboring complex at a distance of 2.458(2) Å. The Cu-O distances are 1.907(2) Å and 1.894(2) Å and the Cu-N distances are 1.970(3) Å and 1.974(2) Å, which are consistent with similar complexes made previously.[44-48] The axially coordinated arrangement between

Cu1–O11b and Cu1b–O11 forms a parallelogram shaped coordination mode between the adjacent complex molecules (Figure 33).

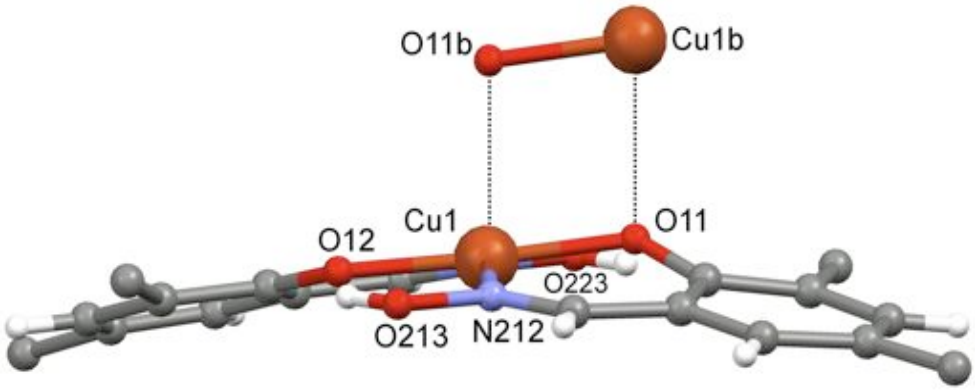

Figure 33. Perspective view of the Cu(II) centre showing the box shape of the axially coordinated Cu and oxygen atoms of an adjacent complex molecule.

The distance between the Cu(II) atoms within the same complex Cu1–Cu1a is 8.854(1) Å. The twist angle from one ligand's phenolic group through to the opposing ligand's phenolic group (O11–Cu1–Cu1a–O11a) is 180.0°. The twist angle of one ligand within the complex (O11–Cu1–Cu1a–O12a) is 2.4°. This is because the complex has relatively no twisting around of the $\mathbf{L^2}$ ligand units to it. The phenolate group of one ligand is positioned above the phenolate group of the same ligand and is orientated in the same direction (Figure 34).

The in-plane donor/metal angles are all close to 180°, emphasising the planarity of these donors and the index parameter τ value of Cu1 is 0.22. This value of 22% distortion from square pyramidal towards a trigonal bipyramidal geometry indicates that the *m*-xylylic ligands bound to the metal centres in **2** causes a slightly more distorted square pyramidal geometry around the metal centre than in **1**, which also has a distorted square pyramidal geometry with a τ value of 17%. Thus, incorporation of the *m*-xylylic spacer, while affecting the structural conformation of the complex greatly (i.e. is not a helical complex),

does not alter the inner sphere coordination environment of the copper metals.

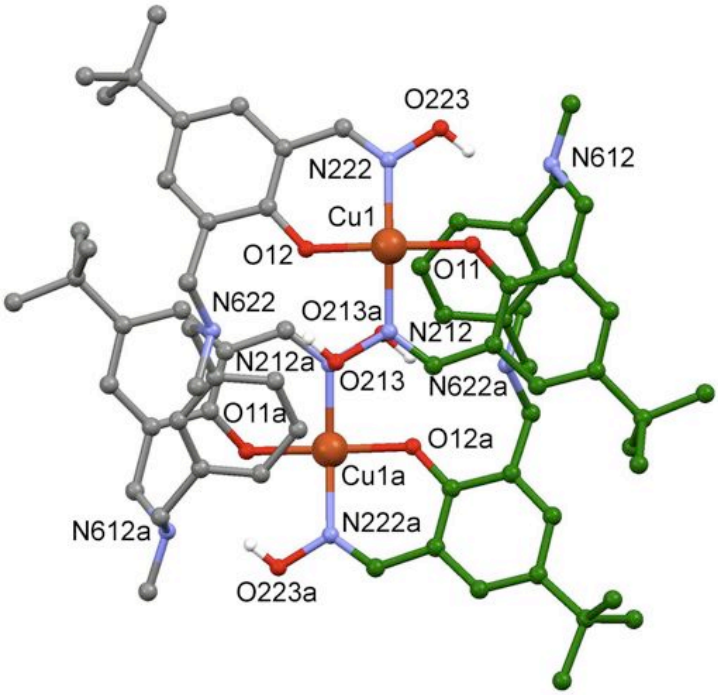

Figure 34. Perspective top view of **2**. One $\mathbf{L}^2$ ligand is coloured grey and the other is coloured green, demonstrating the orientations of the individual ligand units.

Atoms	Bond Lengths (Å)	X–Cu–X	Bond Angles (°)
Cu1 – O11	1.907(2)	O11–Cu–N212	91.6
Cu1 – O12	1.894(2)	O11–Cu–N222	90.0
Cu1 – N212	1.970(3)	O12–Cu–N222	91.4
Cu1 – N222	1.974(2)	O12–Cu–N212	87.8
Cu1 – O11b	2.458(2)	O11–Cu–O11b	82.7
Cu1 – Cu1a	8.854(1)	O11–Cu1–Cu1a–O11a	0.0

Table 17. Selected bond lengths and angles for the Cu(II) centres in **2**.

The pseudo macrocyclic cavity surrounding each metal centre is completed by an oxime hydrogen bonded towards the opposing phenolate oxygen with distances of 2.674(3) Å and 2.787(3) Å between H21a … O12 and H223 … O11 respectively, comparable to the equivalent interactions in the anion free complex **1**. There also exist secondary, weaker H-bonds to the tertiary amines in the aryl linker with distances of 2.964(4) Å and 2.847(3) Å between H21a … N622 and H223 … N612 respectively, which average out to be shorter than the corresponding distances in **1**. This could suggest that the orientation of the newly incorporated 1,3-aryl rings of the linker force the tertiary amines closer to the oximes (refer to Table 18 for H-bond lengths and angles).

Atoms	H-bond distances (Å)	D–H–A angles (°)
O213-H21A … O12	2.674(3)	132.5
O213-H21A … N622	2.964(4)	139.1
O223-H223 … N612	2.847(3)	145.6
O223-H223 … O11	2.787(3)	127.7

Table 18. Selected H-bond distances for the oxime moiety in **2**.

Each aromatic ring in the aryl linker exhibits π–π interactions with an opposing phenolic ring from the same ligand. The ring-to-ring distances are 3.688 Å at an angle of 21.3°. This orientation of the aryl rings thus results in a significant reduction in void volume between the metal centres and correspondingly the solvent molecule is located outside of the cavity, in contrast to **1**.

*3.3.3 X-ray Crystal Structure of $[NO_3 \subset (Cu_2L^2{}_2)](NO_3)_3$ (**5**)*

Green rod shaped crystals of **5** suitable for X-ray diffraction were grown by slow diffusion of diisopropyl ether into a methanol mix of the complex and the crystal structure was determined (Figure 35). The asymmetric unit consists of one complete protonated complex with one encapsulated nitrate anion and three counter nitrate anion molecules.

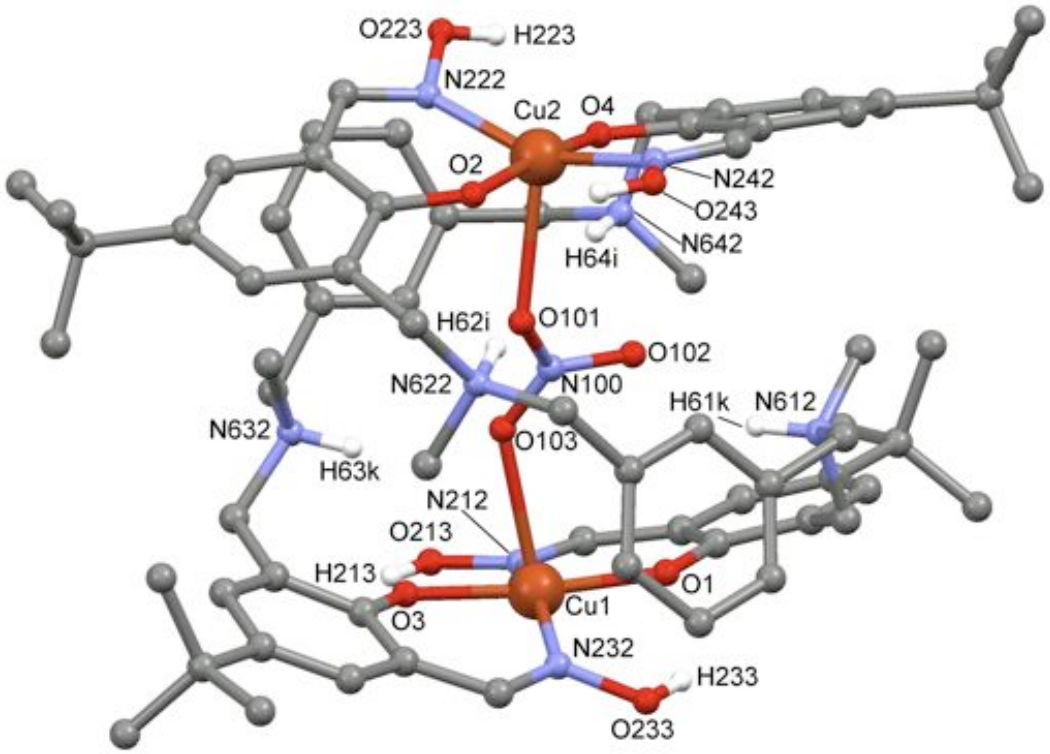

Figure 35. Perspective view of complex **5**, showing the NO_3^- anion encapsulated within the central cavity (Non H-bonding hydrogen atoms, the disorder on the *t*-butyl groups on the salicylaldoxime rings O2 (75:25) and O4 (55:45) and the three counter nitrate anions have been omitted for clarity).

The helical complex consists of two Cu(II) ions coordinated to two $\mathbf{L^2}$ molecules with each copper centre sharing both ligands via the phenolate and N-oximate positions ($N_2O_2^{2-}$). Each ligand is protonated at the tertiary amines and located within the central cavity of the complex is an encapsulated NO_3^- anion bound weakly to both copper centres. There are

three counter nitrate anions on the periphery of the complex giving an overall neutral compound.

The Cu(II) centres in **5** are in the same environment due to the encapsulated NO_3^- anion possessing a weak bond to both metal centres and there are no intermolecular bonds from either copper atom to any neighboring complex molecules. Cu1 and Cu2 have τ values of 0.23 and 0.31 respectively. These distorted square pyramidal environments around the metal centres are greater than was seen for the helicate complexes **1**, **3** and **4**. This implies that the incorporated *m*-xylylic ligands confer a more restrained geometry around the metal centers when in this helical conformation. The Cu(II) centres have four donors that consist of two oxygen donors (one phenol moiety from each ligand) and two nitrogen donors (one oxime moiety from each ligand). The fifth bond in the axial position is with an oxygen atom of the nitrate anion, with bond distances of 2.441(6) Å and 2.401(6) Å for Cu1–O103 and Cu2–O101 respectively (refer to Table 19 for bond lengths and angles). These are significantly shorter than a related copper-imine complex that also readily encapsulates a nitrate anion (Cu–O = 2.722(2) Å),[48] suggesting that this helical complex has a smaller cavity available to the anion. A search through the CCDC for other complexes containing a coordinated nitrate anion to a copper(II) complex in an $N_2O_2^{2-}$ coordinated environment revealed a large number of papers to search (greater than 400). From a selection of 29 papers, an average for the Cu–O (nitrate) bond length was calculated to be 2.369 Å.[88, 89, 100 – 102, 107 – 130] This average is a lot shorter than for the metal–anion bond lengths found in **5**. This may be due to the long distance between the Cu(II) centres in **5** and this would mean the nitrate anion is held loosely within the cavity and thus the bonds lengthened.

The encapsulated nitrate has adopted a length wise orientation within the cavity and coordinates to both copper centres, maximizing the amount of strong interactions to the anion. These are; two strong Cu-O bonds to the nitrate with bond distances of 2.441(6) Å and 2.401(6) Å to Cu1 and Cu2 respectively and three moderate NH … O H-bonds with bond distances of

2.941(14) Å, 3.009(8) Å and 3.066(9) Å to O102, O101 and O103 respectively (refer to Table 20 for bond distances and angles). This orientation and increase in the number of stronger interactions to the captured nitrate is most likely due to the significant decrease in the Cu–Cu distance (6.6615(1) Å) as a result from the restricting *m*-xylylic spacers. This shorter distance between them allows the nitrate anion to coordinate to both metal centres. It is able to form this shorter Cu–Cu distance by increasing the helical twist of the linker ligand to give an average twist through the O-Cu-Cu-O angle of 125.5°. This is in comparison to the previously discussed ClO_4^- and BF_4^- complexes **3** and **4** which both have a slightly more twisted helix twist angle (4-5°) than **5** but have relatively longer Cu–Cu distances at 7.135 Å and 7.212 Å respectively. This shows that this *m*-xylyl ligand system adopts a flatter arrangement than the *p*-xylyl linked system to encapsulate an anion. The same conclusion can also be drawn when comparing **2** to the nitrate containing hexylene-linked imine analog, which has a less contracted encapsulating cavity with a longer Cu–Cu distance of 7.020(1) Å and a helical twist angle of 130.8°**.**

In the hexylene-linked imine analog,[48] the generally weakly coordinating nitrate anion proves its worth by not having any kind of interactions to the Cu(II) centres. The hexylene units allow the complex to be more conformationally flexible than in **5** and results in a greater Cu–Cu distance (7.020(1) Å). The nitrate anion thus adopts a relatively planar orientation in the middle of the cavity with respect to the square planar copper centres and is not coordinated to the metal centres. This results in the anion having less relatively strong bonds interacting with it within the cavity compared to **5**. The nitrate encapsulated in the hexylene-linked imine complex is only bound within the cavity by six interactions. Four are NH … O H-bonds with two differently strengthened H-bonds from the protonated tertiary amines with N … O distances of 2.876(4) Å and 3.190(4) Å. The other two are close contact interactions with methyl groups off the alkyl linker, with C … O distances of 3.469(5) Å and 3.348(5) Å, as opposed to in **5** where it is bound by two strong metal-anion bonds and three moderate H-bonds.

Atoms	Bond Lengths (Å)	X–Cu–X	Bond Angles (°)
Cu1 – O1	1.890(4)	O1–Cu1–N212	92.3
Cu1 – O3	1.898(4)	O1–Cu1–N232	87.5
Cu1 – N212	1.961(5)	O3–Cu1–N212	91.6
Cu1 – N232	1.964(5)	O3–Cu1–N232	91.6
Cu1 – O103	2.441(6)	O1–Cu1–O103	94.3
Cu2 – O2	1.914(4)	O2–Cu2–N222	91.8
Cu2 – O4	1.893(4)	O2–Cu2–N242	90.0
Cu2 – N222	1.972(6)	O4–Cu2–N222	88.2
Cu2 – N242	1.935(6)	O4–Cu2–N242	93.2
Cu2 – O101	2.401(6)	O2–Cu2–O101	77.3
		O1–Cu1–Cu2–O2	125.2
Cu1 – Cu2	6.6615(1)	O3–Cu1–Cu2–O4	125.8

Table 19. Selected bond lengths and angles for the Cu(II) centres in complex **5**.

The protonated tertiary amines of the aryl linker are angled towards the central cavity so as to increase the number of intermolecular H-bonds with the captured NO_3^- anion, with three moderate H-bonds having an average distance of 3.005 Å (see Figure 36 and Table 20 below for H-bond distances and angles).

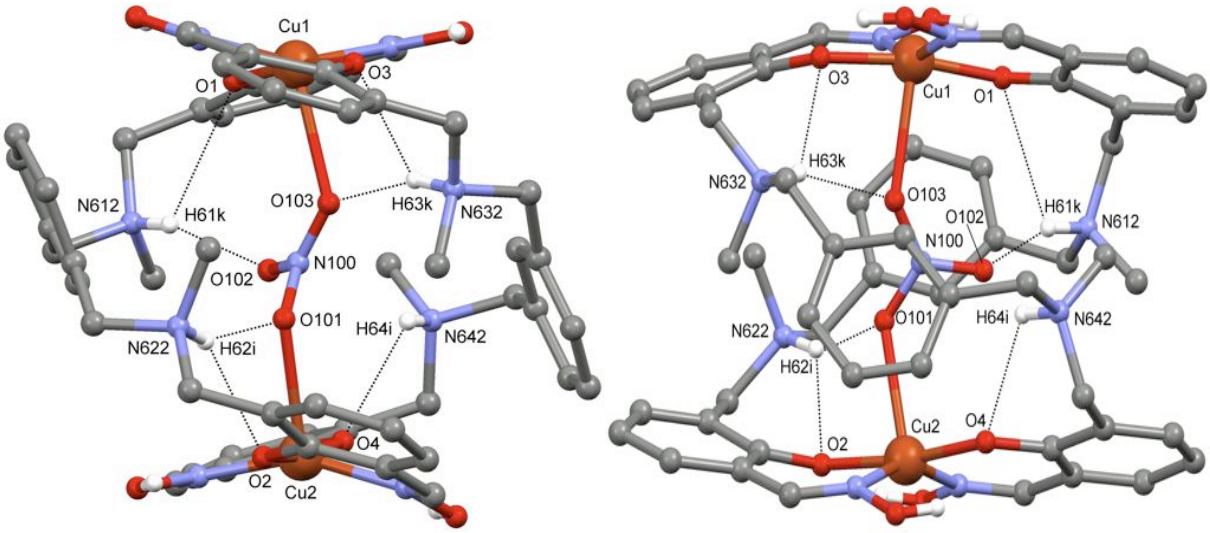

Figure 36. Perspective side-on views of the H-bonding of the protonated amines of the linker straps to the encapsulated nitrate anion and the phenolic oxygens (Non-hydrogen bonding hydrogen atoms and the *t*-butyl groups have been omitted for clarity).

Atoms	H-bond distances (Å)	D–H–A angles (°)
N612-H61k … O102	2.941(14)	154.7
N622-H62i … O101	3.009(8)	153.6
N632-H63k … O103	3.066(9)	158.9

Table 20. Selected H-bond distances and angles of the protonated tertiary amines of the aryl linker strap to the encapsulated nitrate anion in **5**.

Unlike the previous aryl strapped complexes discussed earlier (**3** and **4**), the encapsulated nitrate anion in **5** does not form anion–π interactions with the aryl rings of the linker strap. This is because the free oxygen atom on the nitrate anion is angled so as to be orientated towards, and forming a moderate H-bond to the protonated amine N612 instead (Figure 36). Clearly the H-bond interaction dominates over the weaker anion–π interaction.

Another reason as to why it is unable to have any interactions with the aromatic rings is that the aryl rings have now adopted a lop-sided face-on position in respect to the central cavity. They angle away from the nitrate

anion, distancing themselves from the central cavity so as to form π–π stacking interactions with adjacent complexes, with a centroid-centroid distance of 3.83 Å and angle of 101.1°.

The pseudo macrocyclic cavity surrounding each metal centre is completed by an oxime hydrogen bonded towards the opposing phenolate oxygen with an average OH … O distance of 2.730 Å. This is the same as the average distance for the anion free complex **2** (2.731 Å). This distance is slightly longer than the average distance for either the perchlorate complex **3** or the tetrafluoroborate complex **4**, which shows that with either of the rigid aryl ligands in a helical arrangement, these moderately strengthed interactions do not change appreciatively.

There also exists a secondary, weaker H-bond from the tertiary amines in the aryl linker to the phenolate oxygen atoms, with an average NH … O distance of 2.907 Å, which is equivalent to the analogous distances in **2**, **3** and **4**, again showing that this H-bond arrangement around the metal centres is unaltered regardless of changes at the anion binding site (refer to Table 21 for selected H-bond distances and angles).

Atoms	H-bond distances (Å)	D–H–A angles (°)
O233-H233 … O1	2.661(6)	131.1
O213-H213 … O3	2.838(6)	129.9
O243-H243 … O2	2.713(6)	133.1
O223-H223 … O4	2.706(6)	130.8
N612-H61k … O1	3.265(8)	115.2
N622-H62i … O2	2.869(8)	125.9
N632-H63k … O3	2.855(7)	124.0
N642-H64i … O4	3.131(8)	123.9

Table 21. Selected intramolecular H-bond distances and angles for **5**.

The counter nitrate anions are involved in many hydrogen bonds with the complex molecule and adjacent complexes. One of the nitrate counter anions (N300, O301, O302, O303) sits in between three adjacent complexes and makes several mainly weak interactions. The second counter nitrate anion (N400, O401, O402, O403) is similar to N300 in that it is located near the oxime regions of the complex and of two other adjacent complexes, having only minor interactions to the surrounding complexes. The last counter nitrate anion (N200, O201, O202, O203) makes only weak interactions with an adjacent complex.

These series of restricted *m*-xylyl linkers incorporated into the complexes are the first to show an anion dependent conformation. This means that upon complexation and coordinating anions, the conformation of the resulting complex undergoes a radical change in the solid state from that of the anion free complex **2**. This is further exemplified by the coordination mode shown in the crystal structures discussed next, where the complex has yet another radical change in structure from that of the nitrate encapsulating complex **5**.

*3.3.4 X-ray Crystal Structure of [2Br⊂($Cu_2L^2_2$)]($Br)_2$ (**6**)*

Green block shaped crystals of **6** suitable for X-ray diffraction were grown by slow diffusion of chloroform into a methanol/acetone (1:1) mix of the complex and the crystal structure was determined (Figure 37). The asymmetric unit consists of one complete protonated complex with two coordinated bromide anions, two counter bromide anions and two methanol solvent molecules. Each tertiary amine is protonated giving rise to an overall neutral complex.

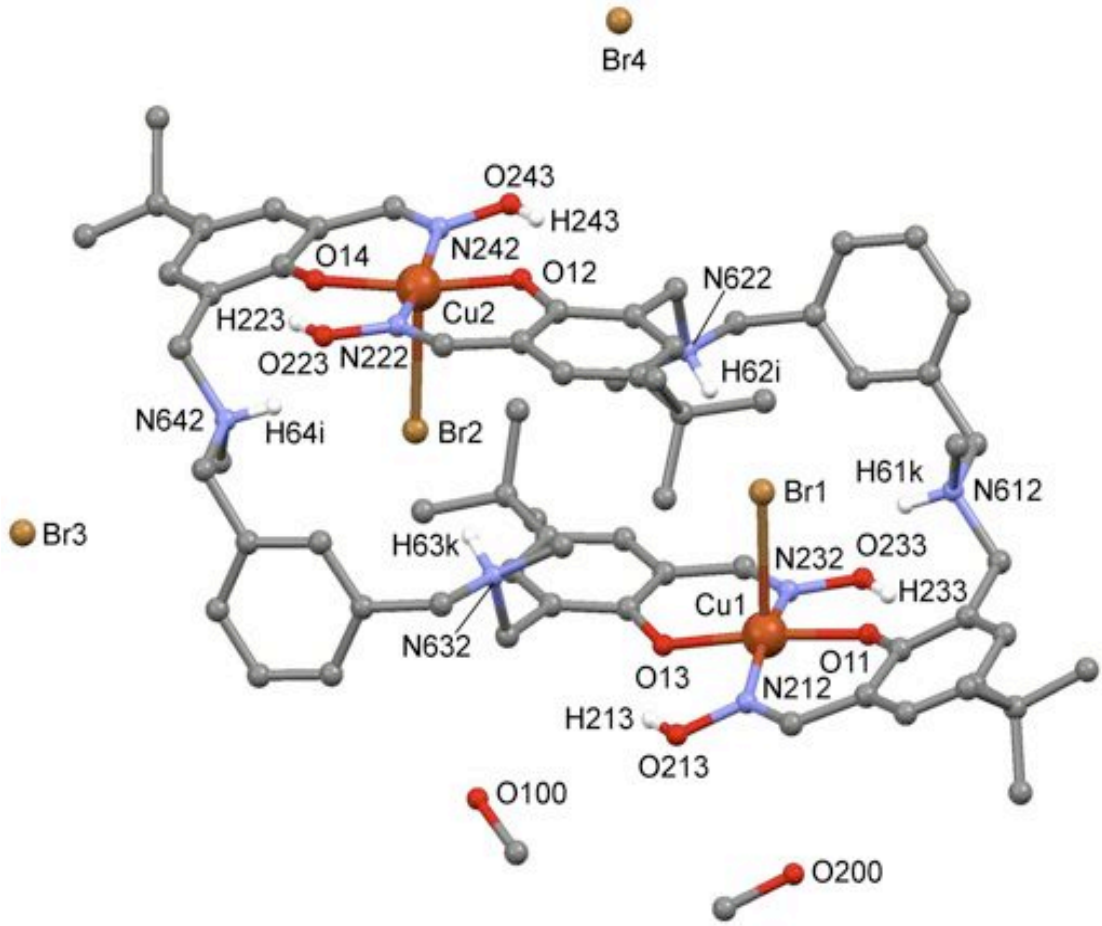

Figure 37. Perspective view of **6**, the counter bromide anions and the methanol solvent molecules (Hydrogen atoms not involved in H-bonding and the disorder on the *t*-butyl group on the salicylaldoxime ring O14 (75:25) have been omitted for clarity).

The complex consists of two Cu(II) atoms coordinated to two **L^2** molecules in the zwitterionic form (phenolate/ammonium) with each copper centre bound to N-oximate and O-phenolate donors from each ligand in a head to tail coordination mode.

The Cu(II) centres in **6** are in similar environments. Both Cu1 and Cu2 are in a slightly distorted square pyramidal arrangement. Their corresponding τ values are 0.13 and 0.05 respectively. These τ values show how close the metal centres are to true square pyramidal geometry and are the least distorted square pyramidal geometries seen within these xylylic family of complexes made.

The Cu(II) metal centres both have five donors in common, that consist of two oxygen donors (one phenol moiety from each ligand), two nitrogen donors (one oxime moiety from each ligand) and the fifth being a coordinated bromide anion in the axial position at a distance of 2.782(1) Å for Cu1-Br1 and 2.765(1) Å for Cu2-Br2. Cu1 also possess a very weak bonding interaction to a phenolate oxygen from an adjacent complex at a distance of 3.2027(1) Å (refer to Table 22 for bond lengths and angles)**.** This brings the copper centres of adjacent complexes relatively close, at a distance of 3.8720(1) Å for Cu1–Cu2b.

A search through the CCDC for other square pyramidal Cu(II) complexes with a bromide coordinated in the axial position, resulted in the Cu-Br bond distances in **6** to be slightly longer than the average (2.699 Å) for other similar complexes found.[131-140] This slight lengthening from the average found for the Cu-Br bond might be due to the bromide trying to maximize H-bonding and close contact interactions within the binding pockets (Figure 38). This arrangement of a single bromide bound to each of the copper centres makes this complex an exception to what has previously been found with these systems of oxime based helical complexes. This is caused by the more restrictive *m*-xylylic spacers incorporated into the linker, reducing the flexibility of the complex. This, coupled with the relatively small size of the Br^- anion (relative to the other anions studied), has allowed the complex to form this non-helical, flattened rectangular shaped structure as shown in Figure 37

and 38. This has then allowed a single bromide anion to coordinate to each Cu(II) centre. There are also two non-coordinating bromides on the periphery of the complex resulting in an overall neutral complex.

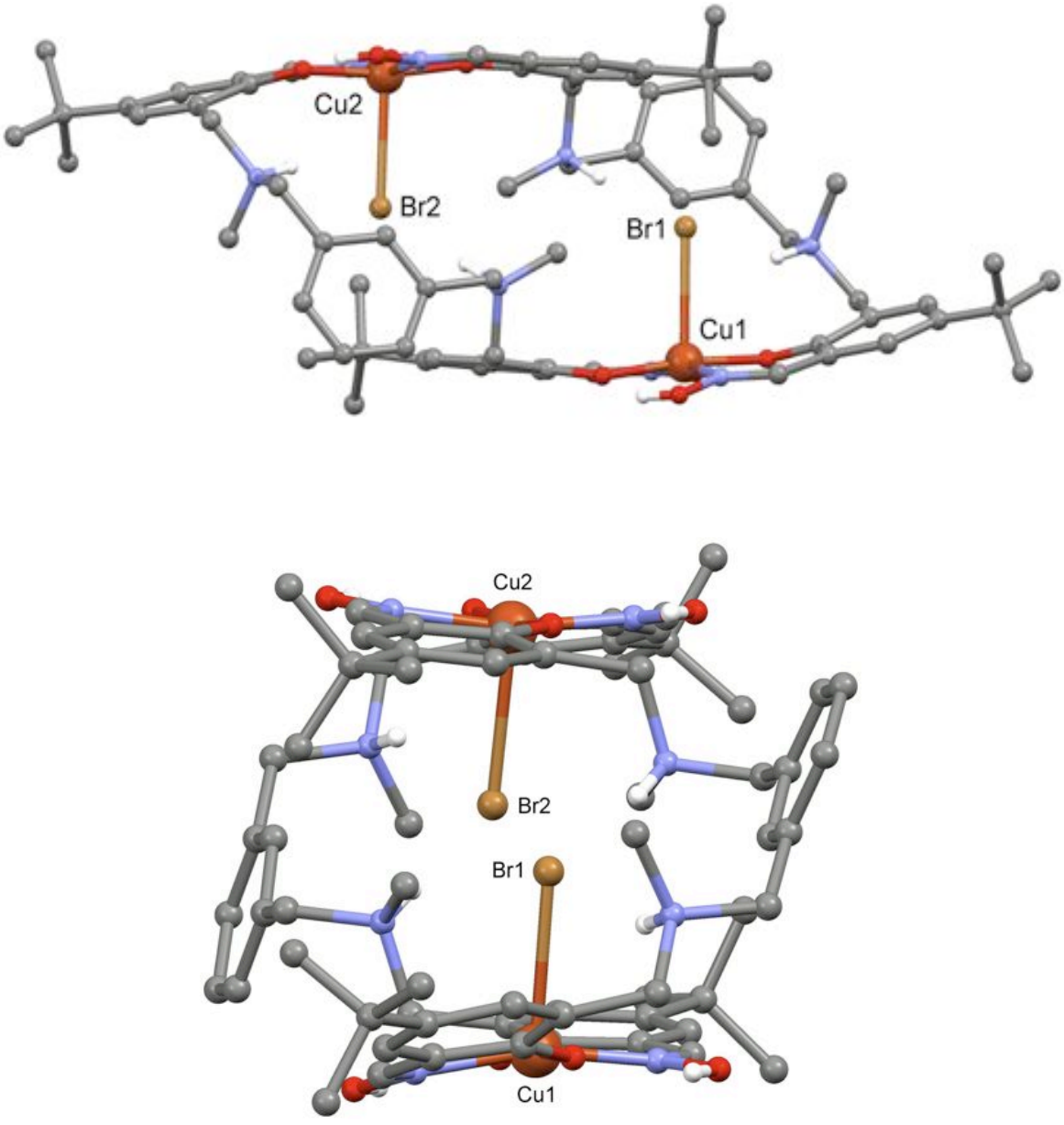

Figure 38. Perspective length and width side views showing the overall shape of complex **6** and the orientation of the aryl linkers (Hydrogen atoms not involved in H-bonding and the disorder of one of the *t*-butyl groups has been omitted for clarity).

Atoms	Bond Lengths (Å)	X–Cu–X	Bond Angles (°)
Cu1 – Br1	2.782(1)	O11–Cu1–Br1	86.0
Cu1 – O11	1.923(2)	O11–Cu1–N212	91.0
Cu1 – O13	1.918(2)	O11–Cu1–N232	87.6
Cu1 – N212	1.964(3)	O13–Cu1–N212	88.7
Cu1 – N232	1.953(3)	O13–Cu1–N232	91.2
Cu1 – O14b	3.2027(1)	O11–Cu1–O14b	93.3
Cu2 – Br2	2.765(1)	O14–Cu2–Br2	88.4
Cu2 – O12	1.914(2)	O14–Cu2–N242	91.1
Cu2 – O14	1.913(2)	O14–Cu2–N222	88.4
Cu2 – N222	1.948(3)	O12–Cu2–N222	91.5
Cu2 – N242	1.966(3)	O12–Cu2–N242	87.3

Table 22. Selected bond lengths and angles for the Cu(II) centres in **6**.

The bound bromide anions in **6** are surrounded by a multitude of weak H-bonds and weaker close contact hydrogen interactions. They include two protonated tertiary amine H-bonds and five weak close contact interactions coming from either aromatic hydrogens or methyl hydrogen groups that surround the bromide anions. The protonated tertiary amines of one linker strap are positioned so that they offer two H-bonds towards a coordinated bromide anion, while the protonated amines of the second aryl linker offer the same two H-bonds towards the other coordinated bromide anion. The average contact distances to Br1 and Br2 are 3.565 Å and 3.550 Å respectively (see Figure 39 and Table 23 for bond distances and angles).

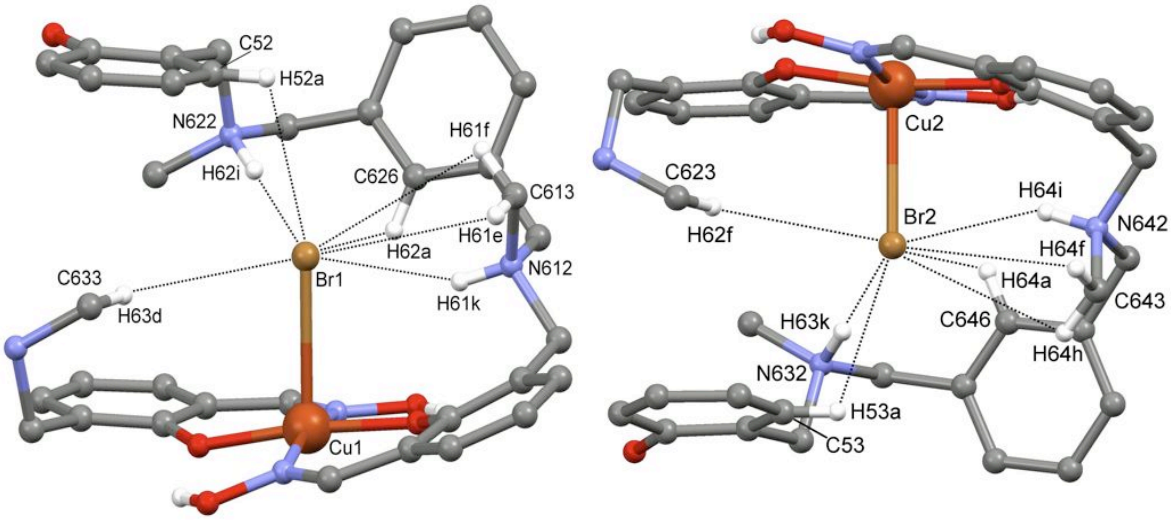

Figure 39. Partial perspective views of the binding pockets in **6**, showing the H-bonding and close contact hydrogens surrounding the coordinated Br1 and Br2 (Hydrogen atoms not involved in H-bonding or in close contact to Br1 or Br2 and the *t*-butyl groups have been omitted for clarity).

Atoms	H-bond distances (Å)	D–H–A angles (°)
	Br1	
N612-H61k … Br1	3.498(3)	151.6
N622-H62i … Br1	3.311(3)	173.6
C613-H61e … Br1	3.738(4)	88.5
C613-H61f … Br1	3.738(4)	99.4
C633-H63d … Br1	3.761(4)	120.7
C52-H52a … Br1	3.432(4)	106.9
C626-H62a … Br1	3.477(3)	109.1
	Br2	
N632-H63k … Br2	3.300(3)	177.6
N642-H64i … Br2	3.497(3)	147.9
C643-H64f … Br2	3.677(4)	87.1
C643-H64h … Br2	3.677(4)	102.4
C623-H62f … Br2	3.764(4)	120.4
C53-H53a … Br2	3.502(4)	106.5
C646-H64a … Br2	3.429(4)	101.4

Table 23. Selected H-bonds and close contact distances and angles for the bound bromide anions in **6**.

Like other Cu(II) oxime ligand complexes made, there is again a pseudo macrocyclic cavity surrounding each metal centre and it is completed by an oxime hydrogen bonded towards the opposing phenolate oxygen, with average distances of 2.635 Å and 2.624 Å for the Cu1 and Cu2 metal centres respectively (refer to Table 24 for bond distances and angles). The oxime group O213-H213 surrounding the Cu1 centre shows some moderate

H-bonding to an adjacent complex oxime moiety O223b-H223b around its Cu2b centre, with both H-bonds having distances of 2.912(4) Å (see Table 24 for bond distances and angles).

This new conformer of the $\mathbf{L^2}$ ligand has resulted in minor changes to the internal H-bonding. In **6** only one protonated tertiary amine in the linker strap is positioned to offer a secondary H-bond to one of the phenolate groups of the same ligand and to the coordinated bromide anion. The second protonated tertiary amine is now in a position so as to only offer an H-bond to the bound anion in contrast to previous receptor examples of this type (see Figure 39 and Table 24 for bond distances and angles).

Atoms	H-bond distances (Å)	D–H–A angles (°)
O233-H233 … O11	2.605(3)	135.1
O213-H213 … O13	2.665(3)	134.7
N612-H61k … O11	2.988(4)	123.2
O213-H213 … O223b	2.912(4)	109.1
O243-H243 … O12	2.604(4)	135.6
O223-H223 … O14	2.644(4)	134.2
N642-H64i … O14	2.963(4)	124.2
O223-H223 … O213b	2.912(4)	104.9

Table 24. Selected H-bond distances and angles for the oxime moieties in **6**.

The counter bromide anions surrounding the complex have no significant interactions to the complex. Br3 lies in the space between the complex and an adjacent complex, making only some close contacts to both at greater than 3.5 Å. The only significant interaction it makes is to O100b which is a methanol solvent molecule from another unit cell at a distance of

3.357(4) Å. Br4 is similar but sits in between two different adjacent complex molecules which lie above the complex. It is only surrounded by very long close contacts at distances greater than 3.5 Å.

In a further experiment, the conditions of the reaction were set up in a 1:1:0.5 ratio of L^2:$Cu(BF_4)_2$:TBABr which was hoped to favour a 1:1 binding ratio of the bromide anion to complex via helicate conformation as seen with the nitrate structure **5**. Upon crystallisation of the product, it was found that two differently shaped crystals formed. When one set of crystals was analyzed by X-ray diffraction, the structure formed was identical to the above structure, except that the counter anions were now two BF_4^- anions situated around the complex, as discussed in the next section. Unfortunately, the second set of crystals were not of sufficient quality to determine their composition.

*3.3.5 X-ray Crystal Structure of [2Br⊂($Cu_2L^2_2$)](BF_4)$_2$ (**7**)*

Green chunk shaped crystals of **7** suitable for X-ray diffraction were grown by slow diffusion of diethyl ether into a methanol/acetone (1:1) mix of the complex and the crystal structure was determined (Figure 40). The asymmetric unit consists of three half complexes with the other halves generated by inversion, six tetrafluoroborate counter anions and two acetone solvent molecules.

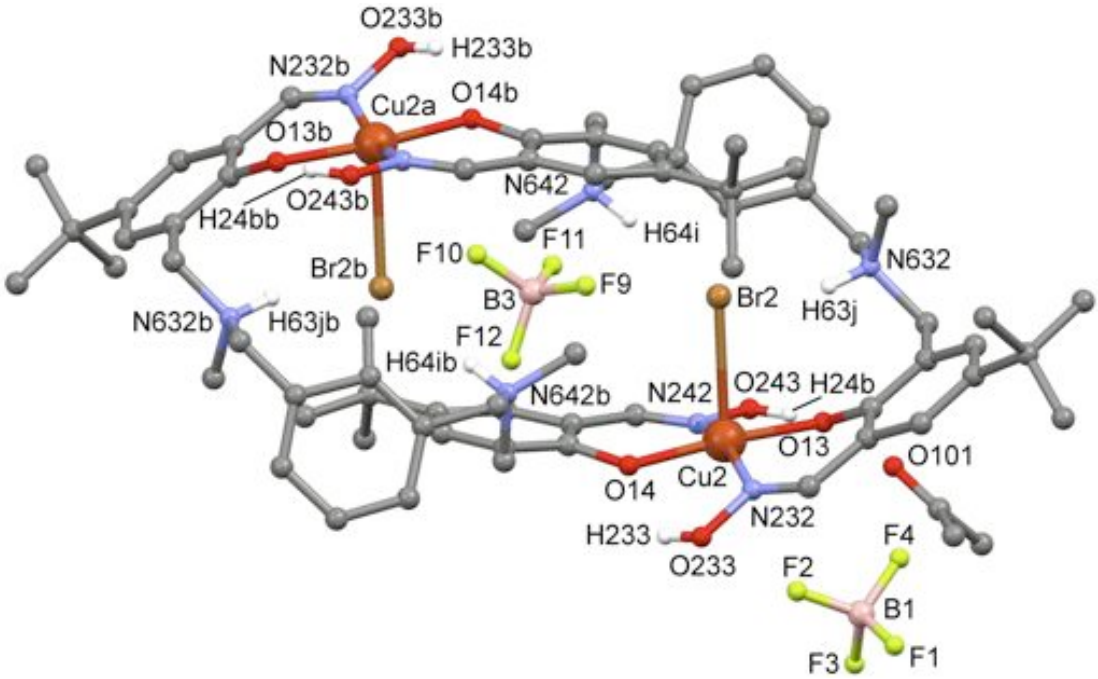

Figure 40. Perspective view of one complex within the unit cell, two of the counter tetrafluoroborate anions and an acetone solvent molecule in **7** (Hydrogen atoms not involved in H-bonding and the disorder on the tetrafluoroborate anion B3 (74:26) have been omitted for clarity).

This complex is structurally identical to the previous bromide complex **6** discussed above, but contains slightly different bond lengths and angles and a different packing arrangement in the crystal lattice. As such, a

thoroughly detailed account of this complex would serve little purpose, so only the major factors will be mentioned.

This complex also consists of two Cu(II) ions coordinated to two protonated $\mathbf{L^2}$ molecules (at the tertiary amines) with each copper centre sharing both ligands via the N-oximate and the O-phenolate positions, again forming the head to tail coordination mode. The Cu(II) centres in **7** are in the same square pyramidal environments. The τ values of the metal centres are: Cu1 = 0.29, Cu2 = 0.25 and Cu3 = 0.31. These high τ values suggest that the Cu(II) centres are in relatively highly distorted square pyramidal geometries in comparison to the Cu(II) centres found in complex **6**. This higher distortion of the metal centres in the crystal lattice maybe caused by the differently found packing arrangement with the new BF_4^- counter anion in **7** instead of the counter Br^- anions in complex **6**. Both copper centres have five donors in common that consist of two oxygen donors (one phenolate moiety from each ligand), two nitrogen donors (one oxime moiety from each ligand). The fifth position is a coordinated bromide in the axial position, with a Cu1-Br1 distance of 2.734(2) Å, a Cu2-Br2 bond distance of 2.778(2) Å and a Cu3-Br3 bond distance of 2.734(2) Å (refer to Table 25 for selected bond lengths and angles).

As was shown in section 3.3.4, the search through the CCDC for other square pyramidal Cu(II) complexes with a bromide coordinated in the axial position show that the Cu-Br bond lengths found in **7** are comparable to those in **6** and are also slightly longer than the average (2.699 Å) found for other similar complexes.[131-140] The slight lengthening of the Cu-Br bonds may again be because the bromide anions are trying to maximize the H-bonding and close contact interactions found within the binding pockets (Figure 40).

Atoms	Bond Lengths (Å)	X–Cu–X	Bond Angles (°)
Cu1 – Br1	2.734(2)	O11–Cu1–Br1	87.6
Cu1 – O11	1.934(8)	O11–Cu1–N212	90.9
Cu1 – O12	1.946(8)	O11–Cu1–N222	86.7
Cu1 – N212	1.99(1)	O12–Cu1–N212	87.8
Cu1 – N222	2.03(1)	O12–Cu1–N222	92.5
Cu2 – Br2	2.778(2)	O13–Cu2–Br2	85.2
Cu2 – O13	1.935(9)	O13–Cu2–N232	90.3
Cu2 – O14	1.927(8)	O13–Cu2–N242	90.5
Cu2 – N232	1.95(1)	O14–Cu2–N232	85.9
Cu2 – N242	2.01(1)	O14–Cu2–N242	92.1
Cu3 – Br3	2.734(2)	O15–Cu3–Br3	97.5
Cu3 – O15	1.929(8)	O15–Cu3–N252	90.2
Cu3 – O16	1.909(8)	O15–Cu3–N262	89.6
Cu3 – N252	1.94(1)	O16–Cu3–N252	87.9
Cu3 – N262	1.94(1)	O16–Cu3–N262	90.3

Table 25. Selected bond lengths and angles for each of the Cu1, Cu2 and Cu3 copper(II) centres in **7**.

The bound bromide anions in **7** are once again surrounded by a multitude of weak H-bonds and weaker close contact interactions. Each uniquely bound bromide has seven interactions binding them within the binding pockets. They include two protonated tertiary amine H-bonds from the linker strap and five weak close contact interactions coming from either aromatic hydrogens or methyl hydrogen groups. The average contact

distances to each bromide are; Br1 3.609 Å , Br2 3.517 Å and Br3 3.563 Å (see Table 26 for selected bond distances and angles).

The pseudo macrocyclic cavity surrounding the metal centres are completed by an oxime hydrogen bonded towards the opposing phenolate oxygen, as was seen and discussed in section 3.3.4 (refer to Table 27 for bond distances and angles).

Atoms	H-bond distances (Å)	D–H–A angles (°)
N612-H61k … Br1	3.62(1)	148.2
N622-H62i … Br1	3.37(1)	176.1
C613-H61d … Br1	3.81(1)	100.9
C613-H61c … Br1	3.81(1)	89.7
C623-H62c … Br1	3.69(2)	129.0
C626-H62h … Br1	3.48(1)	100.1
C52-H52a … Br1	3.48(1)	105.0
N632-H63j … Br2	3.401(11)	154.9
N642-H64i … Br2	3.345(11)	173.9
C646-H64h … Br2	3.502(13)	116.2
C633-H63e … Br2	3.687(14)	93.3
C633-H63c … Br2	3.687(14)	92.1
C54-H54a … Br2	3.439(13)	103.9
C643-H64c … Br2	3.557(14)	122.7
N662-H66i … Br3	3.52(1)	148.9
N652-H65i … Br3	3.32(1)	175.5
C663-H66c … Br3	3.73(1)	85.9
C663-H66e … Br3	3.73(1)	103.0
C653-H65d … Br3	3.66(1)	128.0
C666-H66g … Br3	3.48(1)	104.7
C55-H55a … Br3	3.50(2)	110.1

Table 26. Selected H-bonds and close contact distances and angles for the bound bromides Br1, Br2 and Br3 in **7**.

Atoms	H-bond distances (Å)	D–H–A angles (°)
O213-H21b … O12	2.65(1)	134.8
O223-H22b … O11	2.66(1)	136.6
N612-H61k … O11	2.83(1)	125.5
O233-H233 … O14	2.59(1)	130.7
O243-H24b … O13	2.84(1)	130.7
N632-H63j … O13	3.15(1)	119.1
O263-H26b … O15	2.65(1)	135.0
O253-H253 … O16	2.64(2)	131.0
N662-H66i … O16	2.95(1)	125.5

Table 27. Selected H-bond distances and angles for the oxime moieties surrounding Cu1, Cu2 and Cu3 in **7**.

The tetrafluoroborate B1 counter anion resides in the space between four complexes; the Cu1, Cu2, Cu3 complexes and another adjacent complex, making 10 total interactions with these complexes. The other counter anion B3 lies in between three adjacent complexes; the Cu2 complex and another two adjacent complexes, making five total interactions.

The acetone solvent molecule is located near an oxime functionality of the Cu2 complex. O101 has a moderate H-bond to an oxime OH group H24b at a distance of 2.95(2) Å.

At this preliminary stage, it appears that complex **2** favors this structure in the presence of bromide and is more selective for the Br^- anion over the larger BF_4^- anion.

3.4 Summary

The crystal structure of **2** has demonstrated the restrictive nature imposed by the newly incorporated 1,3-aryl linkers by forming an unexpected non-helical complex. Upon coordination of the nitrate anion however, the structure of complex **5** proved that even with the conformationally restricting *m*-xylylic linkers, $\mathbf{L^2}$ is still capable of forming an anion encapsulating helicate. The bromide structures of **6** and **7** have brought to light definitive evidence that **2** favors a 2:1 ratio of anion:receptor when the bromide anion is present and forms a different structure than **5** but similar to the anion free complex **2**. This has shown that the aforementioned nature of the *m*-xylylic linkers making $\mathbf{L^2}$ and hence **2** conformationally restrictive as accurate. It has displayed its ability to form varied structures in the solid state to accommodate the differently shaped and sized anions.

This is the first complex of this type of helicate system to show anion dependent coordination based structure and the first to bind two anions directly to the metal centres, instead of forming the typically expected encapsulating helicate structure.

During the UV-visible titration studies, it was found for a 1:1 ratio of anion:receptor that the perchlorate anion exhibited the strongest binding to complex **2**, with a log K_1 value of 4.6 ± 0.2 and sulfate coming in second strongest with a binding constant of 4.5 ± 0.1, within experimental error of each other. This outcome was unexpected considering the more strongly coordinating nature of the sulfate anion towards the Cu(II) centres seen in our previous complexes.[44] If we assume the helical complex arrangement is preferred for the larger anions as seen in complex **5**, the moderately sized perchlorate anion must possess a better fit inside the cavity of **2** over the larger sulfate, resulting in enhanced binding. The nitrate anion has a lower stability constant than both the perchlorate and sulfate anions. Presuming the interactions seen in the X-ray structure **5** also occur in solution, the nitrate coordination to the Cu(II) centres and the H-bonding must still not be optimal towards this anion, possibly due to its planar shape and orientation inside the

cavity not being able to fully engage all the protonated amine H-bonds available and to any anion–π interactions on the side of the cavity.

The bromide anion revealed to have a comparable binding strength as seen for the perchlorate and sulfate anions, with an estimated log K_1 value of 4.6. Amazingly, complex **2** has shown it is able to bind two bromide anions per receptor instead of the single loading seen with the other anions. This coordination mode was strengthened by strong coordination to the metal centres as well as a myriad of H-bonding and close contacts to each bromide anion. With this exceptional binding to complex **2**, this *m*-xylylic containing complex could be considered more efficient due to its double loading capabilities with the bromide anion. It could possibly be highly selective for this anion, as shown from the crystal structure **7** which demonstrated preferential binding of Br^- over the larger BF_4^- anion.

3.5 Experimental

3.5.1 Materials and Reagents

The same equipment and reagents were used as for **1**. **2** was dried under vacuum for two hours prior to the preparation of the titration solutions. Titrations were performed immediately after making up the complex solutions.

3.5.2 Spectrophotometric Titrations

Solutions of **2** in dry THF (2 mL, 1.5×10^{-5} mol L^{-1}) were titrated with dry THF solutions of the acid of interest (2.0×10^{-4} mol L^{-1} – 1.0×10^{-3} mol L^{-1}). Spectra were recorded following the same procedure as for complex **1**. The acid solutions were titrated at 0.20 molar equivalent increments for $HClO_4$, 0.25 molar equivalent increments for H_2SO_4 and HBr and 1.0 molar

equivalent increments for HNO_3. The higher mole equivalents of the HNO_3 acid was needed to cause a large enough change in the UV-vis spectrum so SPECFIT/32^{TM} could then calculate a formation constant. A 1:1 anion to complex binding model was used for all spectrophotometric titrations, except for HBr which a 2:1 binding model was used (as determined by mole-ratio plots). This was supported by X-ray analysis as well as the SPECFIT/32^{TM} predicted spectra which were used to calculate the binding constants of the anions titrated into solution with complex **2**.[103-105] In order to ensure reliable results, titrations were repeated until at least three concordant results were obtained. Binding constant errors are the standard deviations of the three concordant results.

3.5.3 Solution Preparation

All solutions were prepared using dry THF as the solvent. The standard acid solutions of H_2SO_4 and HNO_3 used are the same solutions as used with **1**. The standard solution of HBr in THF with a concentration of 5.0 x 10^{-3} mol L^{-1} (made up from concentrated 48% aqueous solution in H_2O) was diluted to give a final concentration of 2.5 x 10^{-4} mol L^{-1}, with less than 0.01% water content. The standard solution of $HClO_4$ in THF with a concentration of 0.01 mol L^{-1} (made up from concentrated 70% aqueous solution in H_2O) was diluted to give a final concentration of 2.0 x 10^{-4} mol L^{-1}, with less than 0.01% water content.

Chapter 4

Assessment of Anion Binding

4.1 Results and Discussion

*4.1.1 Trends in the Anion Binding Abilities of **1** vs. **2***

The anion stability constants of complexes **1** and **2** in THF are shown below (Figure 41). There is a very general trend seen for complex **1** where there is an increase in the stability constant with increasing size of the bound anion. The larger size of the anions enables them to have more efficient interactions to the protonated amines and allows for greater anion–π interactions to occur. The high stability of sulfate encapsulation within **1** will be a direct consequence of its larger size and the strong coordination to the Cu(II) centres in solution. It was also found that **1** has far greater strength of binding the sulfate anion over the smaller anions Br^-, NO_3^- and ClO_4^-, binding them all within error of each other.

In contrast, complex **2** was found to have an unexpected optimum 1:1 stability constant for the perchlorate anion, possibly as a result of the more restricting *m*-xylylic linker creating a smaller cavity size in **2**, favouring stronger interactions with the smaller anion. But, in a 2:1 ratio of anion to complex **2**, **2** is highly selective for the bromide anion over the tetrafluoroborate anion and possibly maybe over any other anion. It has also shown an ability to double load in the presence of bromide, stabilized by the multitude of H-bonds, electrostatic interactions and direct coordination to the Cu(II) centres. This makes complex **2** a potentially efficient transporter of bromide, and possibly of other spherical halide anions.

The stability constants of both **1** and **2** with nitrate are the same. This is most likely due to the typically non-coordinating nature of the nitrate anion in addition to its smaller size, meaning it has longer contact distances to the protonated amines and the aryl π systems, resulting in equally weak binding within either complex cavity.

Overall, **1**, with its incorporated *p*-xylylic linkers, possessed some conformational flexibility. The complex was able to reorientate to accommodate guest molecules (anions or solvent), shown by the crystal structures of **1** and **3**. This complex shows very high strength in binding sulfate and indiscriminate weaker binding of the other anions.

With a very slight modification in the aryl linker, essentially replacing a 1,4-aryl spacer (**1**) with a 1,3-aryl spacer (**2**), there now exists increased structural rigidity within the complex. This has resulted in the formation of new conformers. **2** displays a non-helical structure in its anion free form, a contracted helical complex upon encapsulation of nitrate in complex **5** and finally a rectangular non-helical 2:1 binding complex with bromide anions in complexes **6** and **7**. This complete turn about in structural conformation and flexibility by way of the *m*-xylylic linker is further exemplified in the anion binding results. It has resulted in a dramatic change in binding strength of the same anions under the same conditions. Presuming a comparison for a 1:1 ratio of anion to complex **2**, the perchlorate anion is now the preferred choice with the highest stability constant, while it is also now capable of double loading the Br^- anion with an estimated relatively high log K_1 binding strength comparable to the perchlorate and sulfate anions.

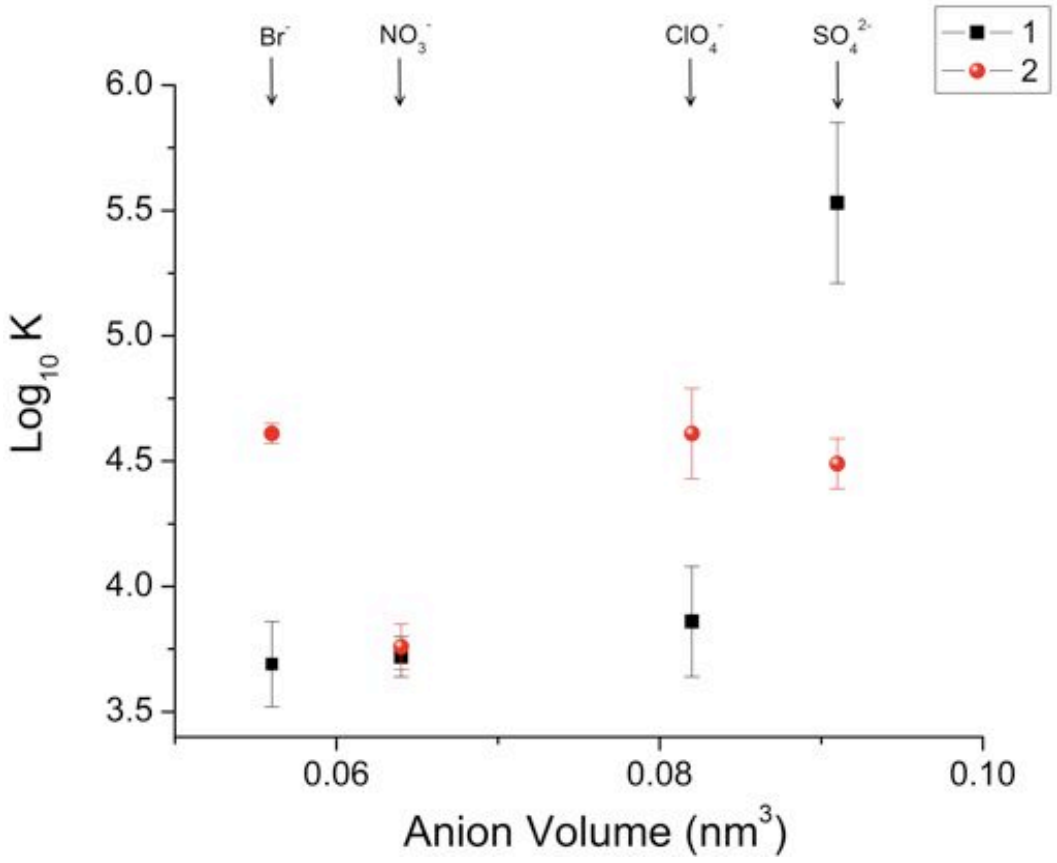

Figure 41. Comparison of the calculated stability constants for anions binding to **1** and **2** vs. the size of the anion. The anion volumes used are from the paper by Jenkins *et al.*[59]

*4.1.2 Trends in the Anion Binding Abilities of **1** vs. C6 oxime*

Figure 42 below shows a comparison of the anion binding stability constants calculated for **1** and the hexylene linked oxime helicate previously reported[46, 47] vs. anion size. It must be said that the values obtained cannot be directly compared, owing to the two complex systems having been carried out in differing solvents due to solubility issues. Therefore, with this in mind the following discussion is focused on general trends only.

There is no general trend seen for the hexylene oxime complex. Instead it shows a lack of discrimination in binding strength between these anions. This trend is also seen with complex **1** with the smaller anions (Br^-, NO_3^- and ClO_4^-) but with a clear enhancement towards binding the sulfate anion over the other anions. The larger sulfate anion must be able to have

stronger and more efficient interactions towards the complex inside the cavity. This proves that the more restricting *p*-xylylic linkers still permit adequate freedom to encapsulate an array of anions within **1**.

The stability constants show that the bromide anion is equivalently bound within each of the two different complexes within experimental error while the nitrate and perchlorate anions are more strongly bound by the hexylene linked complex. This is possibly because the hexylene linkers are more flexible than the *p*-xylylic linkers in **1** and are better suited to wrap around and accommodate the anions. In contrast, **1** binds sulfate a whole order of magnitude more strongly than the hexylene linked complex. In this regard, the more restrictive 1,4-aryl linker must be able to form a more stable structure that fits the sulfate anion very well, resulting in a higher stability constant. The crystal structure of sulfate encapsulated in the iminophenyl analogue[44] has shown that it can form strong coordinating bonds to both copper metal centres (Cu1-O1 bond distance is 2.165(4) Å and the Cu2-O2 bond distance is 2.188(10) Å) and have medium to strong H-bonds from the protonated amines (N … O distances of 2.65–3.23 Å). The enhanced binding of the sulfate anion to **1** may be explained by these same factors, in addition to being stabilised by anion–π interactions, as seen in the perchlorate and tetrafluoroborate crystal structures (section 2.3), which each have one moderate anion–π bond.

The incorporation of the more restrictive and conformationally inflexible *p*-xylylic linkers into complex **1** has therefore resulted in increased strength of binding for the sulfate anion over all the other anions tested.

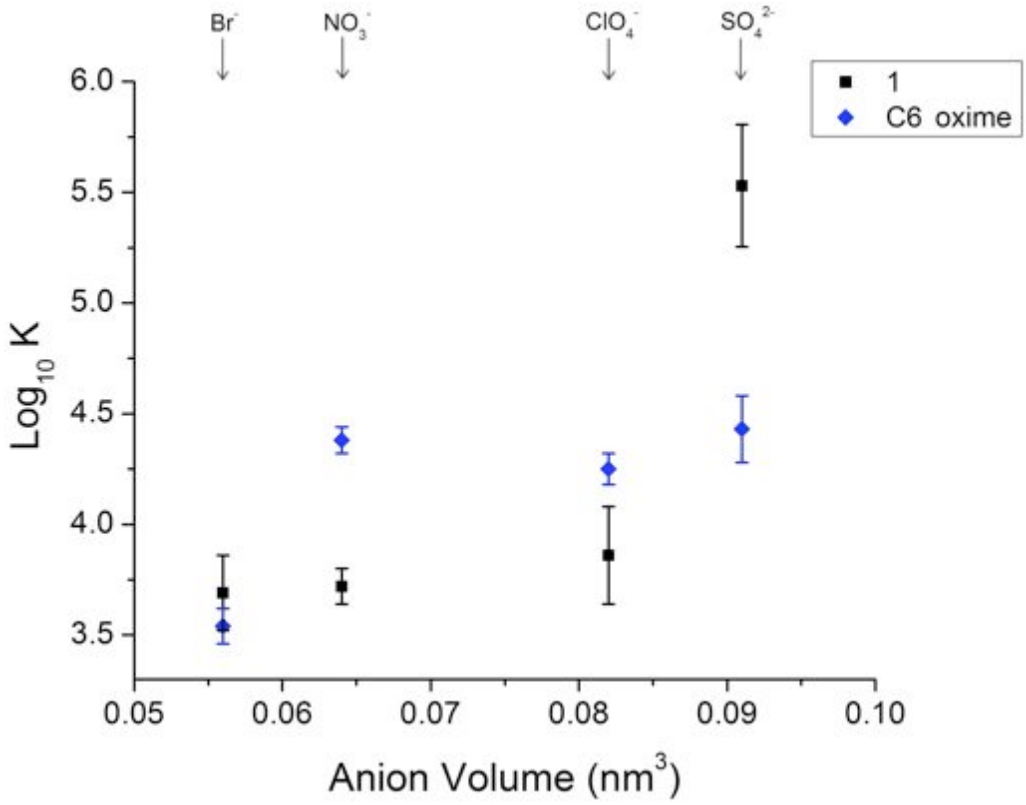

Figure 42. Comparison of the calculated stability constants for binding anions between **1** (in THF) and the hexylene linked oxime (in DCE:IPA) analogue vs. anion volume.[59]

*4.1.3 Trends in the Anion Binding Abilities of **2** vs. C6 oxime*

Figure 43 below shows the comparison of the anion binding stability constants calculated for complex **2** and the hexylene linked oxime vs. anion size. As mentioned previously, the values obtained cannot be directly compared, owing to the two complex systems having been carried out in differing solvents. Therefore, only general trends will be discussed.

As mentioned in section 4.1.2, there is no general trend seen for the hexylene linked complex (Figure 13). Instead it shows a lack of discrimination in binding strength between the nitrate, perchlorate and sulfate anions and a relatively weak binding strength for the mono-loading of bromide. Similarly, the trend seen for complex **2** is a general lack of discrimination between the perchlorate and sulfate anions and a weaker binding strength for the nitrate anion. The larger sized anions are more easily able to form shorter and hence

stronger bonds towards the metal centres and H-bonds inside the cavity of the complexes. **2** also possesses a comparable estimated mono-binding (K_1) strength for the bromide anion as the perchlorate and sulfate anions. This relatively strong binding of the bromide anion is formed not by the typically seen 1:1 ratio of anion:complex, instead by forming a double loaded complex in a 2:1 ratio of anion:receptor. This illustrates that the more restricting *m*-xylylic linker still allows moderate conformational freedom to encapsulate a variety of anions to **2**. The association constants for the sulfate anion are equivalent within experimental error. The nitrate anion is more strongly bound by the hexylene linked complex. In a surprising twist, **2** has the better binding fit for the perchlorate and bromide anions over the hexylene linked oxime complex (in a 1:1 ratio). This large change in increased strength of binding for perchlorate going from the flexible akyl to the rigid *m*-xylyl is most likely due to the smaller cavity created in **2** which will be better suited for the perchlorate anion and possibly further stabilized by additional anion–π interactions. The increased strength of binding of the bromide anion by **2** over the hexylene linked complex will be due to the direct coordination to the Cu(II) centres, the myriad of H-bonds and close contact interactions seen in the solid state.

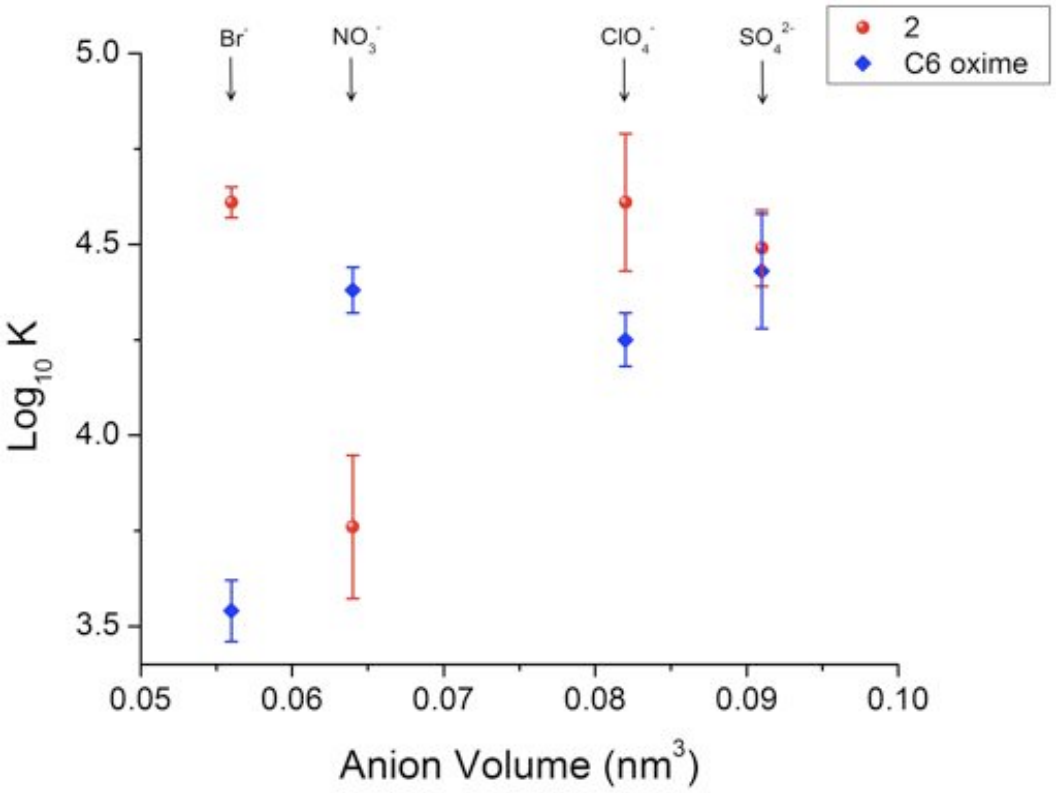

Figure 43. Comparison of the calculated stability constants for anions binding to **2** and C6 oxime vs. the size of the anion. The anion volumes used are from the paper by Jenkins *et al.*[59]

Chapter 5

Conclusions and Future Work

5.1 Conclusions

A solution and solid state study of the conformationally restricted dicopper complexes has been conducted. The stability constants for the encapsulation of four anions were determined in THF for both complex **1** and **2**. Anions encapsulated within the receptors **1** and **2** included two oxyanions sulfate and perchlorate, the trigonal nitrate anion and the spherical bromide anion. Experience in the areas of solution binding, determination of stability constants and the conformational flexibility of both **1** and **2** in the solid state was acquired. The binding studies were corroborated by the crystal structures obtained, which include the encapsulation of the perchlorate and tetrafluoroborate anions in **1** and the nitrate and two examples of bromide anion encapsulation by complex **2**. The results within this thesis have profoundly improved the knowledge of these newly formed xylyl-containing complexes **1** and **2** and their interactions with anions in solution and in the solid state.

The oxime dicopper helicate **1** was explored to determine what affect the incorporated *p*-xylylic linker would have on the complex's flexibility and how this would affect the binding and encapsulation of anions. Spectra were recorded in order to study the properties of the various anions added to **1** but due to the similarities in the absorbances of both **1** and the complexed species, a monochromatic analysis of the data was not possible. Instead, a multivariate analysis of the measured data from 900-250 nm was carried out using the SPECFIT/32^{TM} analysis program. The binding constants acquired in THF range from the weakly binding bromide and nitrate anions (log *K* values

of ~3.7) to the more spectacular binding constant for the sulfate anion which is more than 1.8 orders of magnitude stronger (log *K* value of ~5.5). The perchlorate anion was found to bind only slightly more strongly than the nitrate anion (log *K* value of 3.86 ± 0.22). The X-ray crystal structures obtained helped support the assumption that encapsulation of the anions was occurring. They also provided insight into the potential conformational limits that **1** can possess. When compared to the hexylene spaced analogue previously reported, the inclusion of the *p*-xylylic spacers in **1** have resulted in an increase in the binding strength of the sulfate anion over the other anions.

Receptor **2** was also studied to determine the extent to which the incorporated *m*-xylylic linker would have on the conformational freedom of the complex and how this change would affect anion binding. Upon changing to the *m*-xylylic linker, a drastic change in the binding properties of the anions was observed. A significant decrease in the strength of binding sulfate was shown for a 1:1 ratio of anion to receptor **2** and it now binds the perchlorate anion more strongly than sulfate. The bromide anion was found to bind as strongly to **2** as the perchlorate and sulfate anions once an estimated log K_1 was determined. Unexpectedly, as shown by the crystal structures **6** and **7**, the bromide anion is able to bind in a double loading mode to **2**, a completely new conformer for these series of anion receptors. Complex **2** may possibly be selective for the bromide anion, forming the double loaded structure even in the presence of the larger BF_4^- anion. The nitrate anion-containing crystal structure **5** proved that the $\mathbf{L^2}$ ligand system is still capable of forming a helicate structure, albeit a distorted helicate due to its limited conformational flexibility. Upon replacing the alkyl linker to the *m*-xylylic linker, there is a clear enhancement of the binding strength for the perchlorate and bromide anions over the other anions investigated.

5.2 Applications

The anions under scrutiny have a significant impact on the environment. To avert an environmental incident such as eutrophication of waterways and lakes, prevention of anions such as nitrate needs to be prevented.[1] The perchlorate anion has been used as a structural surrogate compound for the highly radioactive pertechnetate anion which is produced in nuclear fuel waste processes.[11] Sulfuric acid is one of the world's most produced industrial chemicals and is important in a wide variety of processes, including the recovery and recycling in the mining industry.[141] With these large potential environmental incidents in mind, the proficient and effective binding between receptors to anions and the research into these systems is of great importance to this area of study.

5.3 Future Explorations

The complexes studied demonstrated efficient and diverse binding to the series of anions investigated. The *p*-xylylic receptor shows exceptional binding strength for the sulfate anion while the *m*-xylylic receptor shows a preference for ClO_4^- and Br^-, but also displayed a wider range of binding modes for the anions. Future luck in growing crystals with the anions that weren't obtained over the course of this research could provide further clues as to why and how these receptors show great strength in binding certain anions. In regards to the nitrate containing structure **5**, potential future work could be done to ascertain the solution conformation of **2** with nitrate anion. This could be achieved by adding the HNO_3 acid to a solution of complex **2** in a 1:1 ratio. Crystallizing the product and analyzing by X-ray may reveal if the structure remains similar to **2** or if it completely changes to be similar to what has been found in **5**. Another X-ray analysis that can be carried out would be on the second set of crystals that formed in the reaction between $\mathbf{L^2}$, $Cu(BF_4)_2$ and TBABr. This second set was unfortunately not of sufficient quality to

determine their composition over the course of this thesis and it would be interesting to discover what this unidentified crystal contained.

Competition studies would round off this research against each of the anions investigated to discover what anions the two complexes may be selective for. Widening the study with other anions could further enhance the knowledge gained and to see how these receptors may bind differently shaped and sized anions. This could include the other halides with receptor **2** to see if an increase or decrease in the anion's size results in more effective binding. It would also be very interesting to see whether other spherical anions (F^-, Cl^- and I^-) can induce a 2:1 ratio of anion to complex binding. Investigations into the helicate's ability to remove acids or anions similarly found under industrial conditions could be achieved through phase extraction studies.

Incorporating an *o*-xylylic linker into the oxime complex to investigate its influence on conformational flexibility and the corresponding anion binding would also help complete the approach of using xylyl linkers in these systems of dicopper complexes and would complement the alkyl studies carried out by Wenzel.

Incorporating a nitrogen atom into the ring system, e.g. a pyridine group, pyrrole group or even introducing an electron poor aryl ring such as a pyridazine/pyrimidine or 1,3,5-triazine systems would provide insights into the influence of the anion–π interactions on anion binding.

Chapter 6

Synthesis of Ligands and Complexes

6.1 General Procedures

All reagents were from standard chemical suppliers and were used without further purification. Copper(II) tetrafluoroborate hydrate was dried before use. Syntheses were carried out with analytical grade solvents.

The reactant 3-(bromomethyl)-5-*tert*-butyl-2-hydroxybenzaldehyde was prepared via the procedure of Tasker and Schroder.[142] An additional step towards purifying this reactant was to recrystallise the crude oil in pentane, resulting in an amber coloured solid, which was used in the following reactions.

NMR spectra were recorded on either a Bruker Avance 400 or 500 spectrometer using the software program TopSpin version 2.1. Microanalyses were completed by the Campbell Microanalytical Laboratory at the University of Otago. Mass spectra were recorded on a Micromass ZMD 400 electrospray mass spectrometer. IR spectra were run on a Nicolet 5700 FT-IR from Thermo Electron Corporation using an attenuated total reflectance (ATR) sampling attachment. UV-vis spectra were recorded at 294 K using a CARY 100Bio UV-Vis spectrophotometer and 1 cm path length quartz cuvettes. Melting point measurements were recorded with an Electrothermal melting point apparatus, model number IA 9100. X-ray data were recorded at low temperature with a Rigaku-Spider X-ray diffractometer, comprising a Rigaku MM007 microfocus copper rotating-anode generator, high-flux Osmic monochromating and focusing multilayer mirror optics (Cu K radiation, λ = 1.5418 Å), and a curved image-plate detector. *CrystalClear*[143] was utilized for data collection and *FSProcess* in *PROCESS-AUTO*[144] for cell refinement and

data reduction. All structures were solved employing direct methods and expanded by Fourier techniques.[145] Non-hydrogen atoms were refined anisotropically. Hydrogen atoms were placed in calculated positions and refined using a riding model with fixed isotropic *U* values.

6.2 Synthesis of $\mathbf{L^1}$

*6.2.1 Synthesis of **1a***

N, N'-dimethyl-p-xylylenediamine

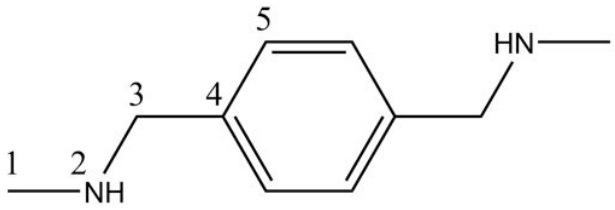

Figure 44. Labeled schematic of **1a**, the precursor of ligand **1b**.

A solution of methylamine hydrochloride (3.115 g, 46.1 mmol) in methanol (60 mL) was allowed to mix with a solution of potassium hydroxide (2.788 g, 49.7 mmol) in methanol (60 mL). The filtered solution was slowly dripped into a second solution of terephthalaldehyde (2.106 g, 15.7 mmol) in methanol (80 mL) over 1 hr. The pale yellow solution was stirred at RT for 2 hrs. Sodium borohydride (1.256 g, 33.2 mmol) was added portionwise to the stirred solution over 10 minutes, which was then left to stir for 1 hr. The solvent was removed under reduced pressure and the resulting white solid was dissolved in chloroform (70 mL) and washed with water (50 mL). The organic layer was separated and dried over anhydrous $MgSO_4$. The solvent was removed under reduced pressure, leaving a pale yellow oil, which upon standing, solidified (2.128 g, 82.6%). δ_H (500 MHz; $CDCl_3$; Me_4Si): 7.27 (4H, s, *H5*), 3.73 (4H, s, *H3*), 2.45 (6H, s, *H1*), 1.33 (2H, br s, *H2*). δ_C (125 MHz; CDCl3; Me_4Si): 139.1 (*C4*), 128.4 (*C5*), 56.0 (*C3*), 36.2 (*C1*). *m/z* (ESI) 165.45 $(\mathbf{1a})^+$. ν_{max}/cm^{-1} 3259br (N-H), 810s (Ar-H).

*6.2.2 Synthesis of **1b***

3, 3'-(1, 4-phenylenebis(methylene))bis(methylazanediyl)bis(methylene)bis(5-*tert*-butyl-2-hydroxybenzaldehyde)

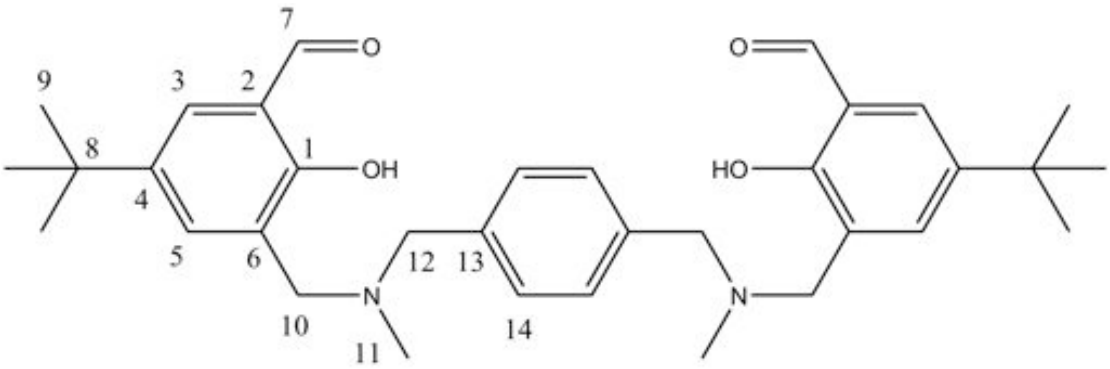

Figure 45. Labeled schematic of **1b**, the precursor to ligand $\mathbf{L^1}$.

To a stirred solution of triethylamine (1.316 g, 13.0 mmol) in dichloromethane (50 mL) were added simultaneously and slowly (over 1 hr) solutions of 3-(bromomethyl)-5-*tert*-butyl-2-hydroxybenzaldehyde (3.345 g, 12.3 mmol) in dichloromethane (50 mL) and N, N'-dimethyl-p-xylylenediamine (1.013 g, 6.5 mmol) in methanol/dichloromethane (1:20, 50 mL). The resulting mixture was left to stir at RT overnight. The reaction was monitored for completion via ^{1}H-NMR. The solvent was evaporated to dryness and the yellow solid was redissolved in chloroform (80 mL) then filtered. The organic layer was washed with water (3 x 30 mL), separated and dried over anhydrous $MgSO_4$. The solvent was removed under reduced pressure and dried *in vacuo* to give a bright yellow solid (3.262 g, 97%). δ_H (500 MHz; $CDCl_3$; Me_4Si): 10.32 (2H, s, H_7), 7.62 (2H, d, J = 2.3 Hz, H_3), 7.38 (2H, d, J = 1.8 Hz, H_5), 7.31 (4H, s, H_{14}), 3.74 (4H, s, H_{10}), 3.61 (4H, s, H_{12}), 2.26 (6H, s, H_{11}), 1.28 (18H, s, H_9). δ_C (125 MHz; $CDCl_3$; Me_4Si): 192.4 (C_7), 159.3 (C_1), 142.1 (C_4), 136.7 (C_{13}), 133.1 (C_5), 129.6 (C_{14}), 125.1 (C_3), 124.0 (C_2), 122.1 (C_6), 61.5 (C_{12}), 59.1 (C_{10}), 41.8 (C_{11}), 34.3 (C_8), 31.5 (C_9). Found: C, 74.21; H, 8.31; N, 4.78%. $C_{34}H_{44}N_2O_4 \cdot 0.25H_2O$ requires C, 74.35; H, 8.17; N, 5.10%. *m/z* (ESI) 545.71 (**1b**)$^+$. ν_{max}/cm^{-1} 2962br (C-H), 1676s (C=O), 1216s (C-O), 825s (Ar-H). Mp 129.2 - 131.1°.

6.2.3 Synthesis of ***L*^{1}**

(1*E*, 1'*E*)-5-*tert*-butyl-3-(((4-(((5-*tert*-butyl-2-hydroxy-3-((*E*)-(hydroxyimino)methyl)benzyl)(methyl)amino)methyl)benzyl)(methyl)amino)methyl)-2-hydroxybenzaldehyde oxime

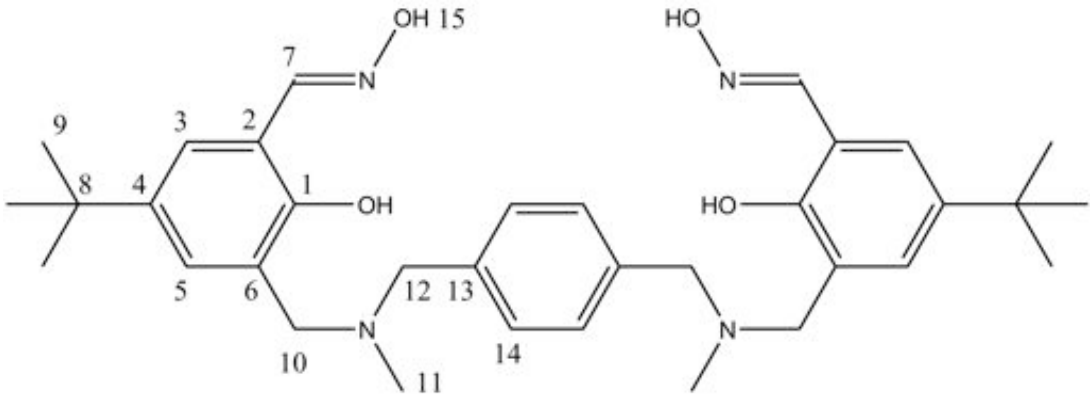

Figure 46. Labeled schematic of **L**^{1}.

A solution of hydroxylamine hydrochloride (0.400 g, 5.76 mmol) in ethanol (60 mL) was added to a solution of potassium hydroxide (0.324 g, 5.77 mmol) in ethanol (60 mL). The resulting white precipitate was removed by filtration. The filtered solution was slowly dripped into a solution of **1b** (1.032 g, 1.90 mmol) in a chloroform/ethanol mix (1:20, 100 mL) over 2 hrs. The pale yellow solution was then allowed to stir at RT overnight. The solution was removed under reduced pressure, dissolved in chloroform (50 mL) and washed with water (2 x 20 mL). The organic layer was separated and dried over anhydrous $MgSO_4$, filtered and dried to give a pale yellow solid. The product could be further purified by crystallisation from hot toluene to give colourless block shaped crystals (0.580 g, 53%). δ_H (400 MHz; $CDCl_3$; Me_4Si): 10.09 (2H, br s, H_{15}), 8.46 (2H, s, H_7), 7.44 (2H, d, J = 2.1 Hz, H_3), 7.32 (4H, s, H_{14}), 7.15 (2H, d, J = 2.1 Hz, H_5), 3.75 (4H, s, H_{10}), 3.63 (4H, s, H_{12}), 2.27 (6H, s, H_{11}), 1.30 (18H, s, H_9). δ_C (100 MHz; $CDCl_3$; Me_4Si): 154.3 (C_1), 148.7 (C_7), 141.8 (C_4), 136.3 (C_{13}), 129.7 (C_{14}), 128.2 (C_5), 123.9 (C_3), 122.5 (C_6), 117.7 (C_2), 61.2 (C_{12}), 59.3 (C_{10}), 41.6 (C_{11}), 34.1 (C_8), 31.5 (C_9).

Found: C, 72.21; H, 8.11; N, 9.22%. $C_{34}H_{46}N_4O_4 \cdot 0.5C_7H_8$ requires C, 72.55; H, 8.12; N, 9.02%. *m/z* (ESI) 575.85 $(\mathbf{L^1})^+$. ν_{max}/cm^{-1} 2955br (C-H), 1615m (C=N), 1268s (C-O), 824s (Ar-H). Mp 126 °.

Crystal data for $\mathbf{L^1}$; $C_{34}H_{46}N_4O_4$, 2(C_7H_8), M_r = 759.02, colourless block, 0.20 × 0.20 × 0.05 mm, monoclinic, P21/n, a = 10.8782(2) Å, b = 8.8537(3) Å, c = 22.8729(16) Å, β = 92.114(7)°, U = 2201.44(17) Å^3, Z = 2, μ = 0.569 mm^{-1}, F(000) = 820, T = 140(2) K. A total of 31069 reflections were collected in the range 6.7° < 2θ < 66.6°. The 3846 independent reflections [R(int) = 0.041] were used after absorption correction (T_{min} = 0.435, T_{max} = 1.000). Refinement of 286 parameters converged to R_1 = 0.0611 [for 2406 reflections having $I > 2\sigma(I)$], wR_2 = 0.2127 and goodness-of-fit of 1.14 (for all 3846 F^2 data). Peak/hole 0.26/-0.31 e Å^{-3}.

6.3 Synthesis of $\mathbf{L^2}$

*6.3.1 Synthesis of **2a***

N, N'-dimethyl-m-xylylenediamine

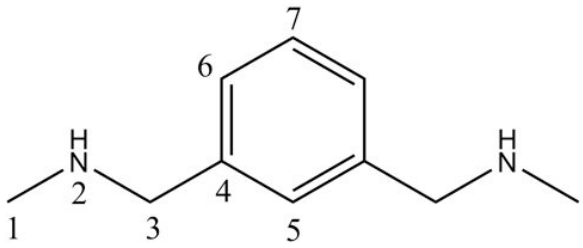

Figure 47. Labeled schematic of **2a**, the precursor of ligand **2b**.

A solution of methylamine hydrochloride (0.877 g, 13.0 mmol) in methanol (40 mL) was allowed to mix with a solution of potassium hydroxide (0.808 g, 14.4 mmol) in methanol (40 mL). The filtered solution was slowly added dropwise into a second solution of isophthalaldehyde (0.522 g, 3.89

mmol) in methanol (40 mL) over 1 hr. The pale yellow solution was stirred at RT for 2 hrs. Sodium borohydride (0.314 g, 8.30 mmol) was added portion wise to the stirred solution over 10 minutes and left to stir for 1 hr. The solvent was removed under reduced pressure and the resulting white solid was dissolved in chloroform (40 mL) and washed with water (40 mL). The organic layer was separated and dried over anhydrous $MgSO_4$. The solvent was removed *in vacuo*, leaving a pale yellow oil (0.608 g, 95%). δ_H (500 MHz; $CDCl_3$; Me_4Si): 7.28 (2H, m, $H_{5/7}$), 7.20 (2H, dd, J = 1.7, 6.9 Hz, H_6), 3.74 (4H, s, H_3), 2.45 (6H, s, H_1). δ_C (125 MHz; $CDCl_3$; Me_4Si): 140.4 (C_4), 128.6 (C_5), 128.2 (C_7), 127.0 (C_6) 56.2 (C_3), 36.2 (C_1). Found: C, 68.57; H, 9.58; N, 15.82%. $C_{10}H_{16}N_2 \cdot 0.6H_2O$ requires C, 68.61; H, 9.90; N, 16.00%. *m/z* (ESI) 165.45 (**2a**)$^+$. ν_{max}/cm^{-1} 3293brw (N-H), 2787m (C-H), 783s, 701s (Ar-H).

*6.3.2 Synthesis of **2b***

3,3'-(1,3-phenylenebis(methylene))bis(methylazanediyl)bis(methylene)bis(5-*tert*-butyl-2-hydroxybenzaldehyde)

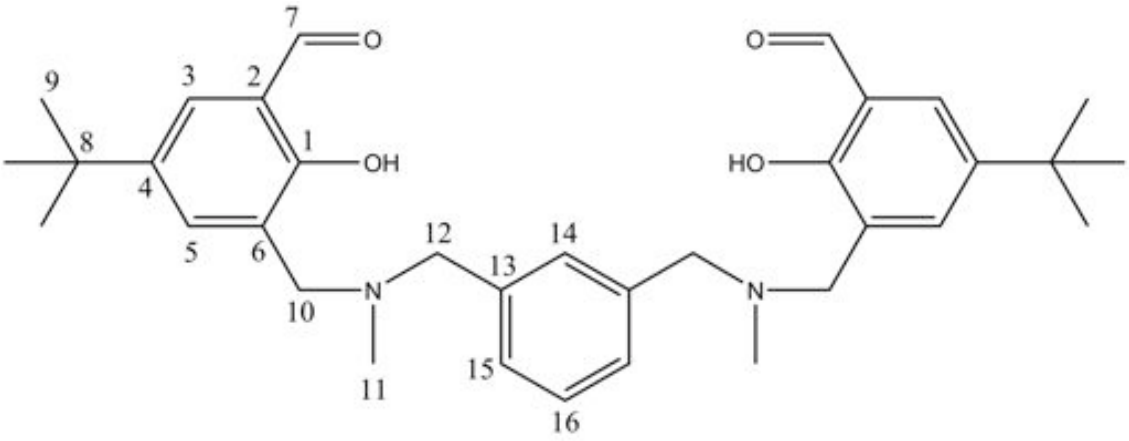

Figure 48. Labeled schematic of **2b**, the precursor to ligand **L^2**.

To a stirred solution of triethylamine (0.900 g, 8.89 mmol) in dichloromethane (60 mL) were added simultaneously and slowly (over 1 hr) solutions of 3-(bromomethyl)-5-*tert*-butyl-2-hydroxybenzaldehyde (2.007 g,

7.42 mmol) in dichloromethane (80 mL) and N,N'-dimethyl-m-xylylenediamine (0.608 g, 3.75 mmol) in dichloromethane (80 mL). The resulting mixture was left to stir at RT overnight. The reaction was monitored for completion via ^{1}H-NMR. The solvent was reduced in volume (50 mL) and the organic layer washed with water (2 x 20 mL), separated and dried over anhydrous $MgSO_4$. The solvent was removed under reduced pressure and the product was dissolved in ethyl acetate and isolated by diethyl ether diffusion. The product was collected and washed with diethyl ether and dried *in vacuo* to give a yellow solid (0.807 g, 41%). δ_H (500 MHz; $CDCl_3$; Me_4Si): 10.30 (2H, s, H_7), 7.61 (2H, d, J = 2.2 Hz, H_3), 7.38 (2H, d, J = 1.7 Hz, H_5), 7.35 (1H, t, J = 7.4 Hz, H_{16}), 7.28 (1H, s, H_{14}), 7.26 (2H, d, J = 7.1 Hz, H_{15}) 3.76 (4H, s, H_{10}), 3.64 (4H, s, H_{12}), 2.29 (6H, s, H_{11}), 1.30 (18H, s, H_9). δ_C (100 MHz; $CDCl_3$; Me_4Si): 192.5 (C_7), 159.3 (C_1), 142.1 (C_4), 137.6 (C_{13}), 133.3 (C_5), 130.4 (C_{14}), 129.1 (C_{16}), 128.8 (C_{15}), 125.2 (C_3), 123.9 (C_2), 122.0 (C_6), 61.6 (C_{12}), 58.8 (C_{10}), 41.8 (C_{11}), 34.3 (C_8), 31.5 (C_9). Found: C, 74.03; H, 8.02; N, 4.83%. $C_{34}H_{44}N_2O_4 \cdot 0.5H_2O$ requires C, 73.75; H, 8.19; N, 5.06%. *m/z* (ESI) 545.93 (**2b**)$^+$. ν_{max}/cm^{-1} 2958br (C-H), 1678s (C=O), 1217s (C-O), 746m, 731m (Ar-H).

6.3.3 Synthesis of L^2

(1*E*, 1'*E*)-5-*tert*-butyl-3-(((3-(((5-*tert*-butyl-2-hydroxy-3-((*E*)-(hydroxyimino)methyl)benzyl)(methyl)amino)methyl)benzyl)(methyl)amino)methyl)-2-hydroxybenzaldehyde oxime

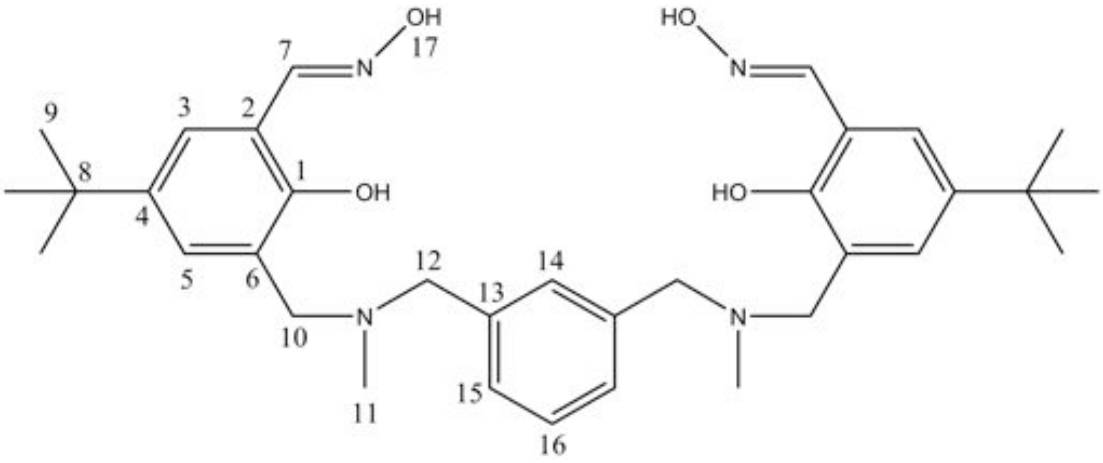

Figure 49. Labeled schematic of L^2.

A solution of hydroxylamine hydrochloride (0.714 g, 10.28 mmol) in ethanol (50 mL) was added to a solution of potassium hydroxide (0.610 g, 10.87 mmol) in ethanol (50 mL). The resulting white precipitate was removed by filtration. The filtered solution was slowly dripped into a solution of **2b** (1.851 g, 3.40 mmol) in ethanol (100 mL) over 2 hrs. The pale yellow solution was then allowed to stir at RT overnight. The solution was removed under reduced pressure, dissolved in chloroform (50 mL) and washed with water (2 x 20 mL). The organic layer was separated and dried over anhydrous $MgSO_4$. The solvent was removed under reduced pressure to give a pale yellow solid. The product was purified by recrystallisation with hexane diffusion from ethyl acetate, giving rise to colourless platelet crystals. The crystals were collected and washed with diethyl ether and dried *in vacuo* to give a white solid (0.980 g, 50%). δ_H (400 MHz; $CDCl_3$; Me_4Si): 10.16 (2H, br s, H_{17}) 8.44 (2H, s, H_7), 7.41 (2H, d, J = 2.2 Hz, H_3), 7.33-7.27 (4H, m, $H_{14/15/16}$), 7.13 (2H, d, J = 2.0 Hz, H_5), 3.74 (4H, s, H_{10}), 3.66 (4H, s, H_{12}), 2.27 (6H, s, H_{11}), 1.29 (18H, s, H_9). δ_C (100 MHz; $CDCl_3$; Me_4Si): 154.3 (C_1), 148.7

(C_7), 141.7 (C_4), 137.2 (C_{13}), 130.7 (C_{15}), 128.9 ($C_{14/16}$), 128.3 (C_5), 124.0 (C_3), 122.5 (C_6), 117.7 (C_2), 61.5 (C_{12}), 59.3 (C_{10}), 41.6 (C_{11}), 34.1 (C_8), 31.6 (C_9). Found: C, 71.01; H, 8.36; N, 8.86%. $C_{34}H_{46}N_4O_4 \cdot 0.5H_2O \cdot 0.5$Hexane requires C, 70.89; H, 8.68; N, 8.94%. *m/z* (ESI) 575.47 $(\mathbf{L^2})^+$. ν_{max}/cm^{-1} 2960br (C-H), 1613brw (C=N), 1266s (C-O), 750s, 712s (Ar-H). Mp; 168.5 – 171.0°.

Crystal data for $\mathbf{L^2}$; $C_{34}H_{46}N_4O_4$, M_r = 574.75, colourless platelet, 0.30 × 0.13 × 0.02 mm, monoclinic, C2/c, a = 25.7501(9) Å, b = 8.7686(3) Å, c = 14.9082(12) Å, β = 113.157(17)°, U = 3095.0(5) Å^3, Z = 4, μ = 0.646 mm^{-1}, F(000) = 1240, T = 123(2) K. A total of 16396 reflections were collected in the range 6.7° < 2θ < 72.1°. The 2992 independent reflections [R(int) = 0.087] were used after absorption correction (T_{min} = 0.721, T_{max} = 1.000). Refinement of 232 parameters converged to R_1 = 0.0799 [for 1476 reflections having $I > 2\sigma(I)$], wR_2 = 0.2603 and goodness-of-fit of 1.03 (for all 2992 F^2 data). Peak/hole 0.30/-0.29 e Å^{-3}.

6.4 Synthesis of the $\mathbf{L^1}$ Complex Series

6.4.1 General Cu(II) Complex Synthesis with $\boldsymbol{L^1}$

To a stirred pale yellow solution of $\mathbf{L^1}$ (9.0 mmol L^{-1}) in methanol/chloroform (10:1, 40 mL) was slowly added dropwise 1 mole equivalent of the copper(II) salt (12.00 mmol L^{-1}) in methanol (40 mL) over 30 minutes. The resulting coloured solution was stirred for 20 hr. The solvent was evaporated to dryness. The crude product was then purified by recrystallisation.

*6.4.2 $[Cu_2(L^1\text{-}2H)_2]$ (**1**) Anion-free complex*

The general method outlined above was followed using copper(II) acetate monohydrate. The crude brown product was purified by recrystallisation with diisopropyl ether diffusion from chloroform to afford brown platelet crystals. The crystals were collected and washed with diisopropyl ether (0.1134 g, 15%). Found: C, 56.49; H, 6.38; N, 7.05%. $C_{68}H_{88}N_8O_8Cu_2 \cdot 2CHCl_3 \cdot 0.5DIPE$ requires C, 56.12; H, 6.26; N, 7.17%. *m/z* (ESI) 636.79 $[(L^1\text{-}H)Cu]^+$. UV-Vis (THF, 1.5 x10^{-5} mol L^{-1}) λ_{max}/nm (ε / L mol^{-1} cm^{-1}): 350 (21 000), 273 (60 700), 256 (72 800). ν_{max}/cm^{-1} 3137brw (O-H), 1625m (C=N), 1216s (C-O), 836s (Ar-H).

Crystal data for **1**; $2(C_{68}H_{84}Cu_2N_8O_8)$, $(CHCl_3)$, M_r = 2656.39, brown platelet, 0.58 × 0.31 × 0.17 mm, triclinic, $P\bar{1}$, a = 11.4781(3) Å, b = 14.4375(3) Å, c = 25.0402(18) Å, α = 93.474(7)°, β = 98.589(7)°, γ = 113.012(8)°, U = 3744.1(4) $Å^3$, Z = 1, μ = 1.620 mm^{-1}, $F(000)$ = 1398, T = 123(2) K. A total of 48836 reflections were collected in the range 6.6° < 2θ < 62.4°. The 11657 independent reflections [R(int) = 0.058] were used after absorption correction (T_{min} = 0.389, T_{max} = 1.000). Refinement of 812 parameters converged to R_1 = 0.0761 [for 8137 reflections having $I > 2\sigma(I)$], wR_2 = 0.2462 and goodness-of-fit of 1.10 (for all 11657 F^2 data). Peak/hole 1.15/-0.88 e $Å^{-3}$.

*6.4.3 $[SO_4 \subset (Cu_2L^1{}_2)](SO_4)_3$ (**8**)*

The general method outlined above was followed using copper(II) sulfate pentahydrate. The dark green product was purified by recrystallisation with diisopropyl ether diffusion from methanol. The green precipitate was collected and washed with diisopropyl ether (0.040 g, 26%). Found: C, 48.68; H, 6.28; N, 6.42%. $C_{68}H_{92}N_8O_{24}S_4Cu_2 \cdot 2.5MeOH$ requires C, 48.64; H, 5.91; N, 6.44%. *m/z* (ESI) 734.38 $([SO_4L^1Cu])^+$. UV-Vis (THF/0.1% MeOH, 2.0 x

10^{-5} mol L^{-1}) λ_{max}/nm (ε / L mol^{-1} cm^{-1}): 310 (15 900). ν_{max}/cm^{-1} 1630brm (C=N), 1101brs (SO_4), 838w (Ar-H).

*6.4.4 [ClO_4⊂($Cu_2L^1_2$)](ClO_4)$_3$ (**3**)*

The general method outlined above was followed using copper(II) perchlorate hexahydrate. The green/grey product was purified by recrystallisation with diisopropyl ether diffusion from acetonitrile to afford green chunky crystals. The crystals were collected and washed with diisopropyl ether (0.147 g, 50%). Found: C, 47.43; H, 5.61; N, 6.49%. $C_{68}H_{92}N_8O_{24}Cl_4Cu_2 \cdot 3H_2O$ requires C, 47.25; H, 5.71; N, 6.48%. *m/z* (ESI) 736.67 $([ClO_4L^1Cu])^+$. UV-Vis (THF/0.5% MeCN, 2.0 x 10^{-5} mol L^{-1}) λ_{max}/nm (ε / L mol^{-1} cm^{-1}): 351 (8 600), 270 (26 200). ν_{max}/cm^{-1} 3132brw (O-H), 1631m (C=N), 1091brs (ClO_4), 838w (Ar-H).

Crystal data for **3**; $C_{68}H_{92}Cu_2N_8Cl_4O_{24}$, M_r = 1674.38, green chunk, 0.24 × 0.16 × 0.16 mm, triclinic, $P\bar{1}$, a = 14.7464(8) Å, b = 15.6825(8) Å, c = 21.3265(15) Å, α = 95.308(7)°, β = 109.898(8)°, γ = 104.436(7)°, U = 4405.1(6) $Å^3$, Z = 2, μ = 2.304 mm^{-1}, F(000) = 1748, T = 150(2) K. A total of 56953 reflections were collected in the range 6.5° < 2θ < 61.2°. The 13304 independent reflections [R(int) = 0.116] were used after absorption correction (T_{min} = 0.649, T_{max} = 1.000). Refinement of 1038 parameters converged to R_1 = 0.0828 [for 3644 reflections having $I > 2\sigma(I)$], wR_2 = 0.2413 and goodness-of-fit of 0.81 (for all 13304 F^2 data). Peak/hole 0.45/-0.55 e $Å^{-3}$.

*6.4.5 [NO_3⊂($Cu_2L^1_2$)](NO_3)$_3$ (**9**)*

The general method outlined above was followed using copper(II) nitrate trihydrate. The dark green product was purified by recrystallisation with diisopropyl ether diffusion from a methanol/acetonitrile (4:1) mix. The dark

green precipitate was collected and washed with diisopropyl ether (0.122 g, 37%). Found: C, 52.84; H, 6.46; N, 11.07%. $C_{68}H_{92}N_{12}O_{20}Cu_2 \cdot H_2O$ requires C, 52.94; H, 6.14; N, 10.90%. *m/z* (ESI) 699.77 $([NO_3L^1Cu])^+$, 668.22 $([L^1Cu]_2NO_3)^{2+}$. UV-Vis (THF/0.5% Acetone, 2.0 x 10^{-5} mol L^{-1}) λ_{max}/nm (ε / L mol^{-1} cm^{-1}): 338 (13 500), 289 (60 100), 260 (75 700). ν_{max}/cm^{-1} 1660s (C=N), 1295brs (NO_3), 839m (Ar-H).

*6.4.6 $[Br\subset(Cu_2L^1_2)](Br)_3$ (**10**)*

The general method outlined above was followed using copper(II) bromide. The dark brown product was purified by recrystallisation with diethyl ether diffusion from acetonitrile. The dark brown precipitate was collected and washed with diethyl ether (0.082 g, 28%). Found: C, 42.81; H, 4.97; N, 6.10%. $C_{68}H_{92}N_8O_8Br_4Cu_2 \cdot 4HBr$ requires C, 42.54; H, 5.04; N, 5.84%. *m/z* (ESI) 718.61 $([BrL^1Cu])^+$. UV-Vis (THF/0.1% MeOH, 2.0 x 10^{-5} mol L^{-1}) λ_{max}/nm (ε / L mol^{-1} cm^{-1}): 670 (825), 386 (7 300), 333 (19 300), 311 (23 100). ν_{max}/cm^{-1} 1621m (C=N), 834s (Ar-H).

*6.4.7 $[BF_4\subset(Cu_2L^1_2)](BF_4)_3$ (**4**)*

The general method outlined above was followed using copper(II) tetrafluoroborate monohydrate. The crude green product was purified by recrystallisation with diethyl ether diffusion from acetone to afford brown platelet crystals. The crystals were collected and washed with diethyl ether (0.034 g, 16%). Found: C, 50.35; H, 5.97; N, 6.64%. $C_{68}H_{92}N_8O_8B_4F_{16}Cu_2$ requires C, 50.30; H, 5.71; N, 6.90%. *m/z* (ESI) 636.16 $[(L^1\text{-}H)Cu]^+$. UV-Vis (THF/0.2% MeCN, 2.0 x 10^{-5} mol L^{-1}) λ_{max}/nm (ε / L mol^{-1} cm^{-1}): 351 (17 600), 270 (54 400), 256 (63 000). ν_{max}/cm^{-1} 1630w (C=N), 1053brs (BF_4), 838w (Ar-H).

Crystal data for **4**; $C_{68}H_{92}Cu_2B_4F_{12}N_8O_8$, $3(C_3H_6O)$, M_r = 1798.05, green platelet, 0.19 × 0.17 × 0.10 mm, triclinic, $P\bar{1}$, a = 11.7783(3) Å, b = 19.0859(5) Å, c = 20.9814(15) Å, α = 82.675(6)°, β = 77.892(5)°, γ = 75.638(5)°, U = 4453.4(4) Å^3, Z = 2, μ = 1.383 mm^{-1}, F(000) = 1876, T = 123(2) K. A total of 53358 reflections were collected in the range 6.6° < 2θ < 61.2°. The 13270 independent reflections [R(int) = 0.075] were used after absorption correction (T_{min} = 0.452, T_{max} = 0.760). Refinement of 1166 parameters converged to R_1 = 0.0881 [for 8153 reflections having $I > 2\sigma(I)$], wR_2 = 0.2718 and goodness-of-fit of 1.09 (for all 13270 F^2 data). Peak/hole 0.92/-0.91 e Å^{-3}.

6.5 Synthesis of the $\mathbf{L^2}$ Complex Series

6.5.1 General Cu(II) Complex Synthesis with $\boldsymbol{L^2}$

To a stirred pale yellow solution of $\mathbf{L^2}$ (9.0 mmolL^{-1}) in methanol (40 mL) was slowly added dropwise one mole equivalent of the copper(II) salt (9.0 mmolL^{-1}) in methanol in (40 mL) over 30 minutes. The resulting coloured solution was stirred for 20 hours. The solvent was evaporated to dryness. The crude product was then purified by recrystallisation.

*6.5.2 [$Cu_2(L^2\text{-}2H)_2$] (**2**) Anion-free complex*

The general method outlined above was followed using copper(II) acetate monohydrate. The crude brown product was purified by recrystallisation with diisopropyl ether diffusion from a tetrahydrofuran/chloroform (1:1) mix to afford brown platelet crystals. The crystals were collected and washed with diethyl ether (0.655 g, 29%). Found:

C, 63.92; H, 7.06; N, 8.67%. $C_{68}H_{88}N_8O_8Cu_2$ requires C, 64.18; H, 6.97; N, 8.81%. *m/z* (ESI) 636.79 $[(L^2\text{-H})Cu]^+$. UV-Vis (THF, 1.5 x 10^{-5} mol L^{-1}) λ_{max}/nm (ε / L mol^{-1} cm^{-1}): 355 (19 800), 272 (57 300), 255 (74 900). ν_{max}/cm^{-1} 3140brw (O-H), 1630m (C=N), 766w, 714s (Ar-H).

Crystal data for **2**; $C_{34}H_{44}CuN_4O_4$, ($C_6H_{14}O$), M_r = 738.44, brown platelet, 0.63 × 0.30 × 0.20 mm, triclinic, $P\bar{1}$, a = 11.5153(14) Å, b = 13.7564(17) Å, c = 14.434(2) Å, α = 78.740(6)°, β = 69.547(5)°, γ = 68.645(5)°, U = 1989.2(5) $Å^3$, Z = 2, μ = 1.138 mm^{-1}, F(000) = 790, T = 123(2) K. A total of 24934 reflections were collected in the range 6.5° < 2θ < 65.1°. The 6519 independent reflections [R(int) = 0.068] were used after absorption correction (T_{min} = 0.615, T_{max} = 1.000). Refinement of 452 parameters converged to R_1 = 0.0530 [for 4510 reflections having $I > 2\sigma(I)$], wR_2 = 0.1585 and goodness-of-fit of 1.14 (for all 6519 F^2 data). Peak/hole 0.62/-1.03 e $Å^{-3}$.

*6.5.3 $[SO_4\subset(Cu_2L^2{}_2)](SO_4)_3$ (**11**)*

The general method outlined above was followed using copper(II) sulfate pentahydrate. The green product was purified by recrystallisation with diethyl ether diffusion from methanol. The product was collected and washed with diethyl ether (0.078 g, 21%). Found: C, 46.45; H, 6.02; N, 6.16%. $C_{68}H_{92}N_8O_{24}S_4Cu_2{\cdot}5H_2O$ requires C, 46.65; H, 5.87; N, 6.40%. *m/z* (ESI) 734.64 $([SO_4L^2Cu])^+$. UV-Vis (THF/0.5% MeOH, 2.0 x 10^{-5} mol L^{-1}) λ_{max}/nm (ε / L mol^{-1} cm^{-1}): 359 (17 000). ν_{max}/cm^{-1} 1629brm (C=N), 1106brs, 1035brs (SO_4), 712m (Ar-H).

*6.5.4 $[ClO_4\subset(Cu_2L^2{}_2)](ClO_4)_3$ (**12**)*

The general method outlined above was followed using copper(II) perchlorate hexahydrate. The product was purified by recrystallisation with

diethyl ether diffusion from methanol. The brown product was collected and washed with diethyl ether (0.033 g, 25%). Found: C, 46.59; H, 5.61; N, 6.31%. $C_{68}H_{92}N_8O_{24}Cl_4Cu_2 \cdot 4H_2O$ requires C, 46.77; H, 5.77; N, 6.42%. *m/z* (ESI) 736.67 $([ClO_4L^2Cu])^+$. UV-Vis (THF/0.1% MeCN, 2.0 x 10^{-5} mol L^{-1}) λ_{max}/nm (ε / L mol^{-1} cm^{-1}): 353 (16 700), 271 (43 200). ν_{max}/cm^{-1} 1620m (C=N), 1097brs (ClO_4), 710s (Ar-H).

*6.5.5 $[NO_3 \subset (Cu_2L^2_2)](NO_3)_3$ (**5**)*

The general method outlined above was followed using copper(II) nitrate trihydrate. The dark green product was purified by recrystallisation with diisopropyl ether diffusion from methanol to afford green block and rod shaped crystals. The crystals were collected and washed with diisopropyl ether (0.065 g, 20%). Found: C, 51.91; H, 6.18; N, 10.61%. $C_{68}H_{92}N_{12}O_{20}Cu_2 \cdot 3H_2O$ requires C, 51.74; H, 6.26; N, 10.65%. *m/z* (ESI) 699.40 $([NO_3L^2Cu])^+$. UV-Vis (THF/0.3% MeCN, 2.0 x 10^{-5} mol L^{-1}) λ_{max}/nm (ε / L mol^{-1} cm^{-1}): 362 (12 400), 273 (36 500). ν_{max}/cm^{-1} 1627s (C=N), 1304brs (NO_3), 837m, 712s (Ar-H).

Crystal data for **5**; $C_{68}H_{92}Cu_2N_{12}O_{20}$, M_r = 1524.64, green prism, 0.43 × 0.13 × 0.10 mm, monoclinic, *P*21, *a* = 11.4408(19) Å, *b* = 20.2715(4) Å, *c* = 19.0446(13) Å, β = 106.297(10)°, *U* = 4239.4(8) $Å^3$, *Z* = 2, μ = 1.192 mm^{-1}, *F*(000) = 1604, *T* = 123(2) K. A total of 49913 reflections were collected in the range 6.5° < 2θ < 72.0°. The 14261 independent reflections [*R*(int) = 0.056] were used after absorption correction (T_{min} = 0.694, T_{max} = 1.000). Refinement of 940 parameters converged to R_1 = 0.0724 [for 9962 reflections having $I > 2\sigma(I)$], wR_2 = 0.2287 and goodness-of-fit of 1.10 (for all 14261 F^2 data). Peak/hole 0.67/-0.99 e $Å^{-3}$.

6.5.6 $[2Br\subset(Cu_2L^2{}_2)](Br)_2$ (**6**)

The general method outlined above was followed using copper(II) bromide. The dark brown product was purified by recrystallisation with chloroform diffusion from a methanol/acetone (1:1) mix to afford green block crystals. The dark green crystals were collected and washed with diethyl ether (0.102 g, 22%). Found: C, 48.68; H, 5.75; N, 6.82%. $C_{68}H_{92}N_8O_8Br_4Cu_2{\cdot}4H_2O$ requires C, 48.96; H, 6.04; N, 6.72%. *m/z* (ESI) 718.73 $([BrL^2Cu])^+$. UV-Vis (THF/0.4% MeCN, 2.0 x 10^{-5} mol L^{-1}) λ_{max}/nm (ε / L mol^{-1} cm^{-1}): 366 (10 200), 285 (24 900). ν_{max}/cm^{-1} 1611w (C=N), 710s (Ar-H).

Crystal data for **6**; $C_{68}H_{92}Br_4Cu_2N_8O_8$, 2($CH_3OH$), M_r = 1658.28, green block, 0.58 × 0.36 × 0.32 mm, monoclinic, *P*21/*c*, *a* = 22.7715(16) Å, *b* = 19.5276(4) Å, *c* = 19.8252(4) Å, β = 93.245(7)°, *U* = 8801.6(7) $Å^3$, *Z* = 4, μ = 3.132 mm^{-1}, *F*(000) = 3408, *T* = 140(2) K. A total of 90481 reflections were collected in the range 6.5° < 2θ < 72.1°. The 16757 independent reflections [*R*(int) = 0.069] were used after absorption correction (T_{min} = 0.264, T_{max} = 0.434). Refinement of 860 parameters converged to R_1 = 0.0563 [for 11558 reflections having $I > 2\sigma(I)$], wR_2 = 0.1789 and goodness-of-fit of 1.11 (for all 16757 F^2 data). Peak/hole 1.06/-1.10 e $Å^{-3}$.

6.5.7 $[2Br\subset(Cu_2L^2{}_2)](BF_4)_2$ (**7**)

The general method outlined above was followed using copper(II) tetrafluoroborate monohydrate and stirred for one hour. This was then followed by the slow addition of 0.5 mole equivalents of *t*-butyl ammonium bromide in methanol (20 mL) and left to stir for 20 hours. The product was purified by recrystallisation with diethyl ether diffusion from a methanol/acetone (1:1) mix to afford green platelets and block crystals. The green crystals were collected and washed with diethyl ether (0.050 g, 35%). Found: C, 50.68; H, 6.07; N, 6.75%. $C_{68}H_{92}N_8O_8Br_2B_2F_8Cu_2$ requires C,

50.73; H, 5.76; N, 6.96%. *m/z* (ESI) 718.73 $([BrL^2Cu])^+$, UV-Vis (THF/0.2% MeCN, 2.0 x 10^{-5} mol L^{-1}) λ_{max}/nm (ε / L mol^{-1} cm^{-1}): 367 (14 300), 285 (29 200). ν_{max}/cm^{-1} 1611w (C=N), 1058brs (BF_4), 710s (Ar-H).

Crystal data for **7**; $3(C_{68}H_{92}Br_2Cu_2N_8O_8)$, $6(BF_4)$, $2(C_3H_6O)$, M_r = 4946.20, green chunk, 0.46 × 0.28 × 0.10 mm, triclinic, $P\bar{1}$, a = 14.5994(12) Å, b = 19.6925(17) Å, c = 27.748(2) Å, α = 99.607(7)°, β = 96.215(7)°, γ = 106.635(7)°, U = 7432.9(11) $Å^3$, Z = 1, μ = 1.977 mm^{-1}, F(000) = 2554, T = 161(2) K. A total of 73025 reflections were collected in the range 6.5° < 2θ < 58.9°. The 20103 independent reflections [R(int) = 0.124] were used after absorption correction (T_{min} = 0.423, T_{max} = 0.820). Refinement of 1408 parameters converged to R_1 = 0.1108 [for 6244 reflections having $I > 2\sigma(I)$], wR_2 = 0.3336 and goodness-of-fit of 0.87 (for all 20103 F^2 data). Peak/hole 0.72/-0.70 e $Å^{-3}$.

Appendix A

Recorded UV-visible Spectra for the Acid Addition to **1** $[Cu_2(L^1\text{-}2H)_2]$.

For each spectrum, the colour transition from indigo to red indicates increasing concentration of acid.

1 + H_2SO_4

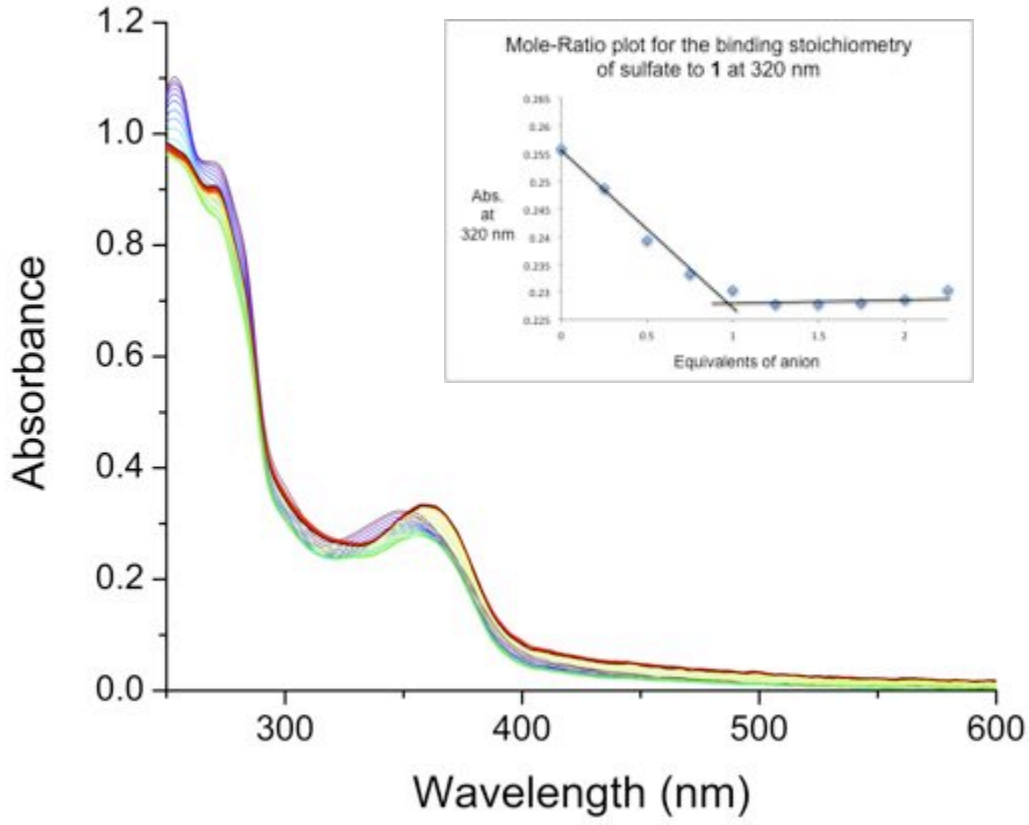

Figure A-1. Recorded UV-visible titration spectra of **1** upon titration of up to eight equivalents of H_2SO_4. Each spectrum corresponds to an addition of 0.25 equivalents.

1 + $HClO_4$

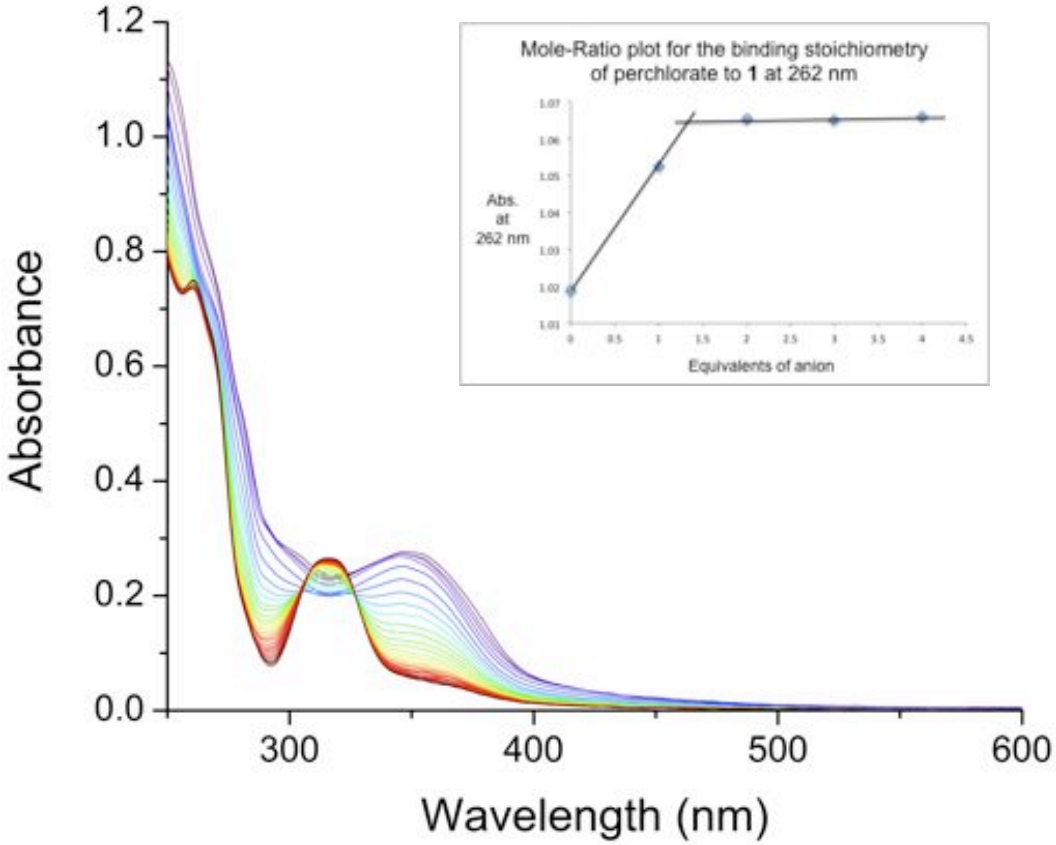

Figure A-2. Recorded UV-visible titration spectra of **1** upon titration of up to 30 equivalents of $HClO_4$. Each spectrum corresponds to an addition of 1 equivalent.

1 + HBr

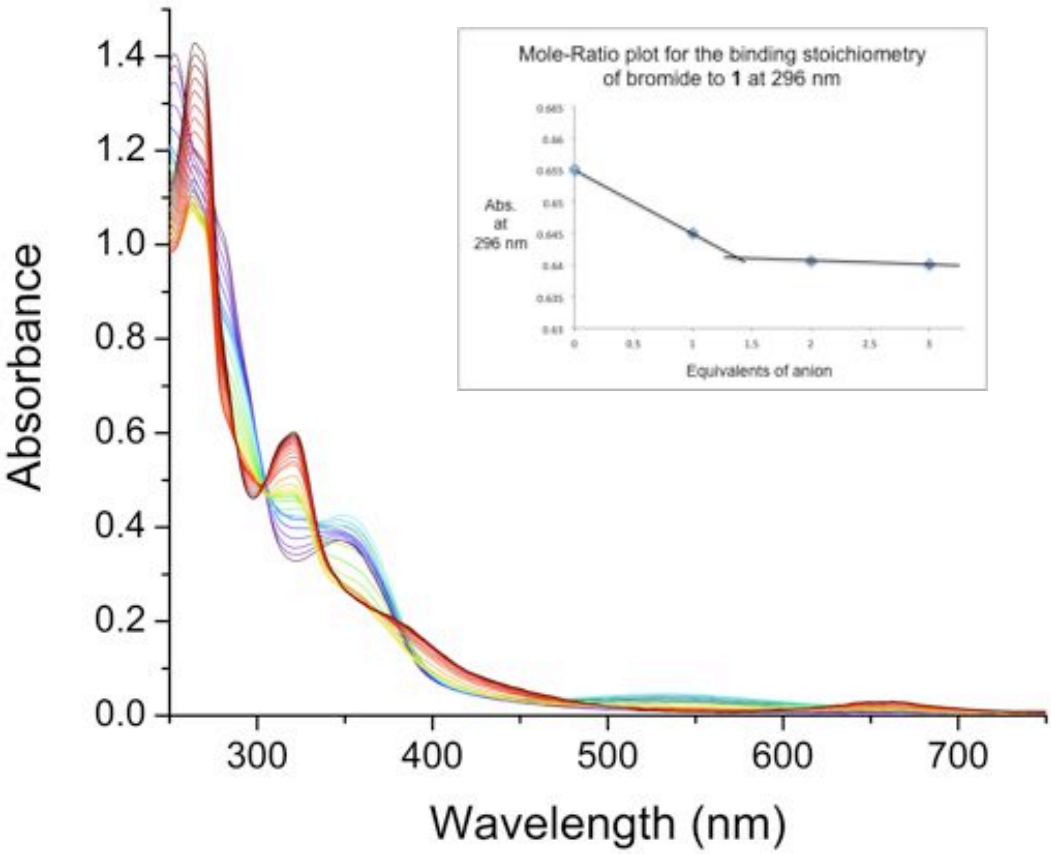

Figure A-3. Recorded UV-visible titration spectra of **1** upon titration of up to 30 equivalents of HBr. Each spectrum corresponds to an addition of 1 equivalent.

1 + HNO_3

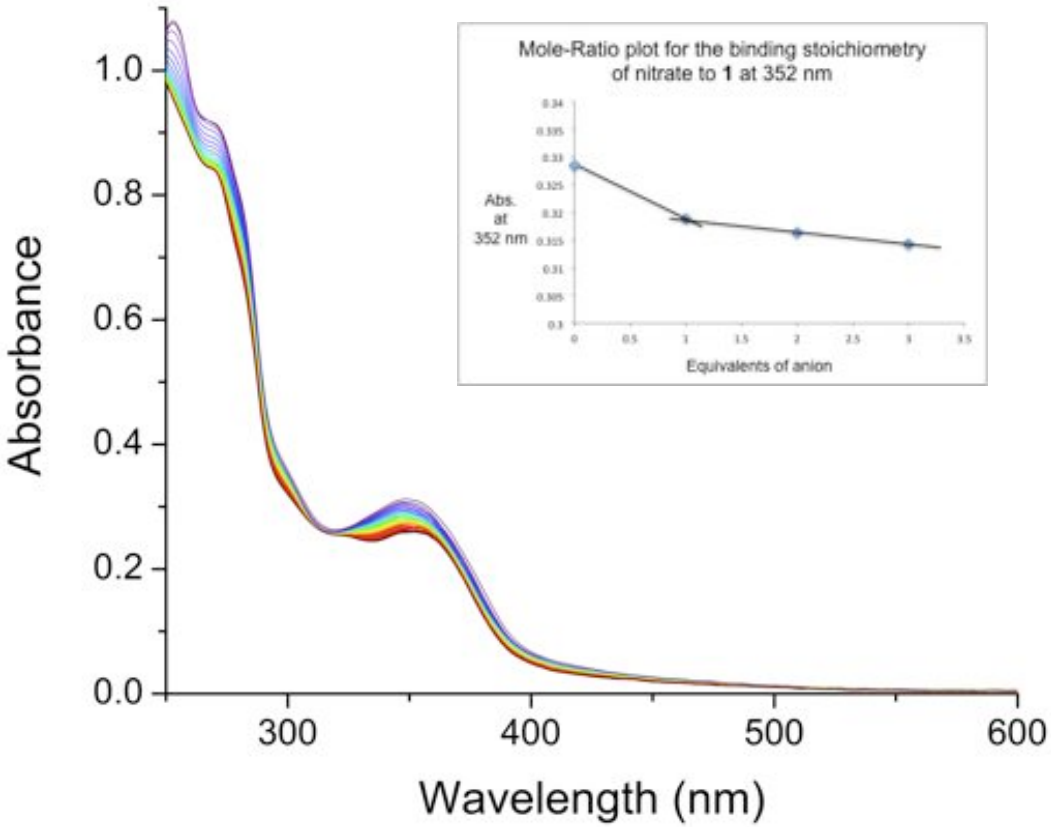

Figure A-4. Recorded UV-visible titration spectra of **1** upon titration of up to 35 equivalents of HNO_3. Each spectrum corresponds to an addition of 1 equivalent.

Recorded UV-visible Spectra for the Acid Addition to $[Cu_2(L^2\text{-}2H)_2]$.

For each spectrum, the colour transition from indigo to red indicates increasing concentration of acid.

2 + H_2SO_4

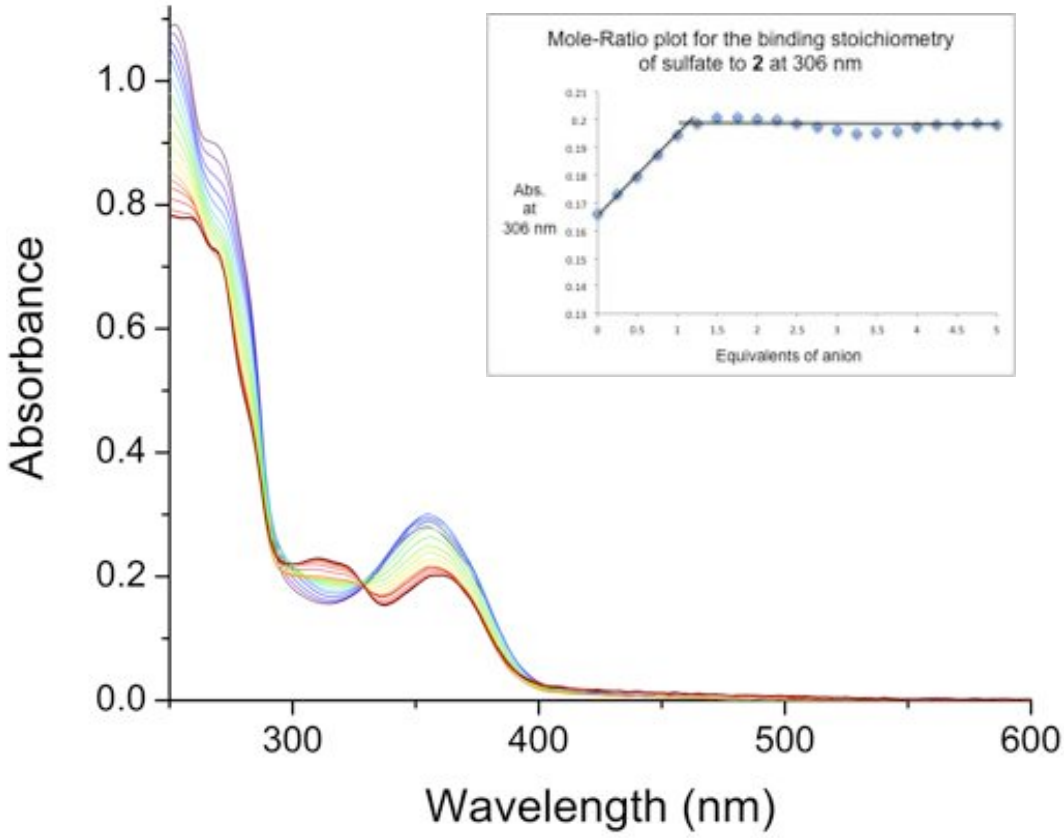

Figure A-5. Recorded UV-visible titration spectra of **2** upon titration of up to five equivalents of H_2SO_4. Each spectrum corresponds to an addition of 0.25 equivalents.

2 + $HClO_4$

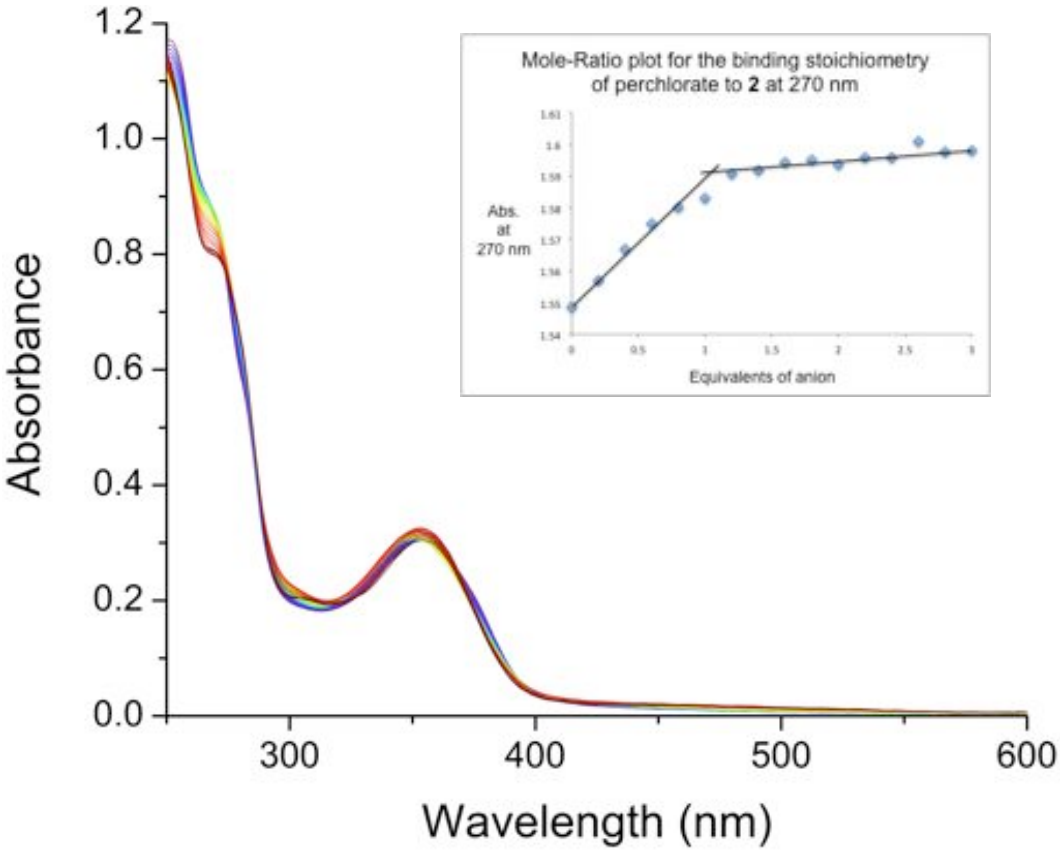

Figure A-6. Recorded UV-visible titration spectra of **2** upon titration of up to six equivalents of $HClO_4$. Each spectrum corresponds to an addition of 0.20 equivalents.

2 + HBr

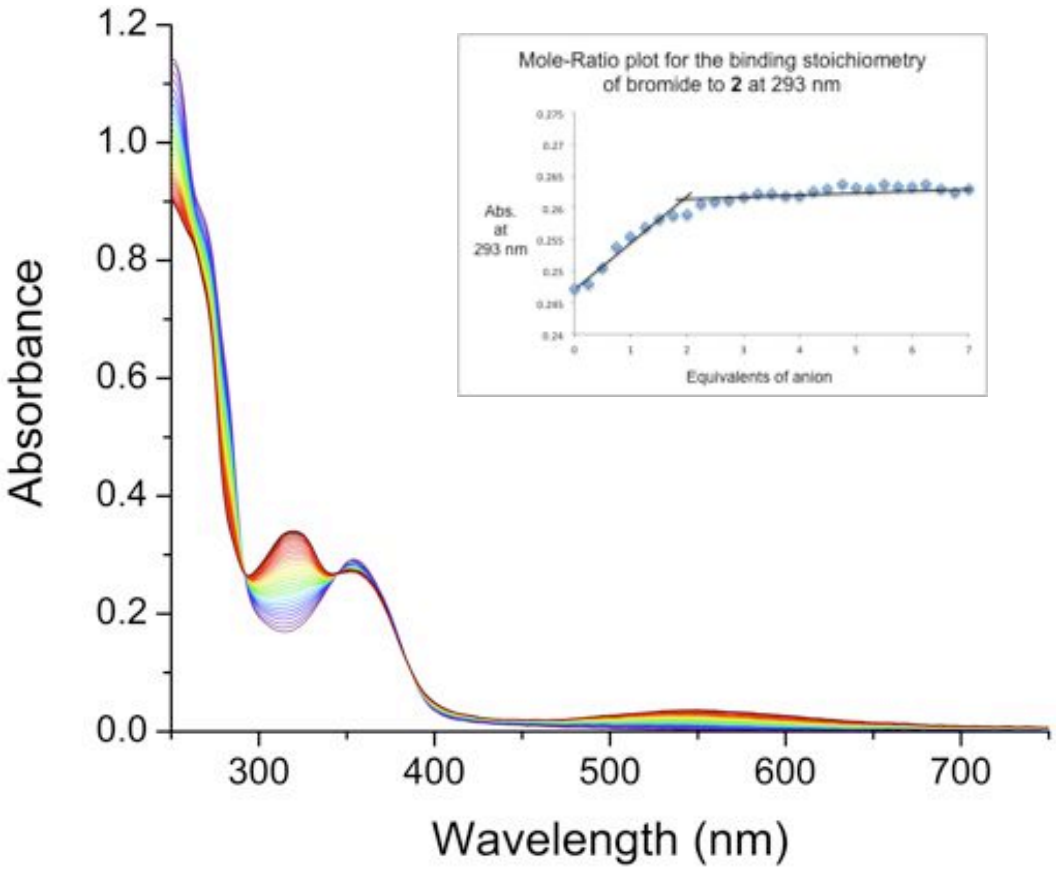

Figure A-7. Recorded UV-visible titration spectra of **2** upon titration of up to eight equivalents of HBr. Each spectrum corresponds to an addition of 0.25 equivalents.

2 + HNO_3

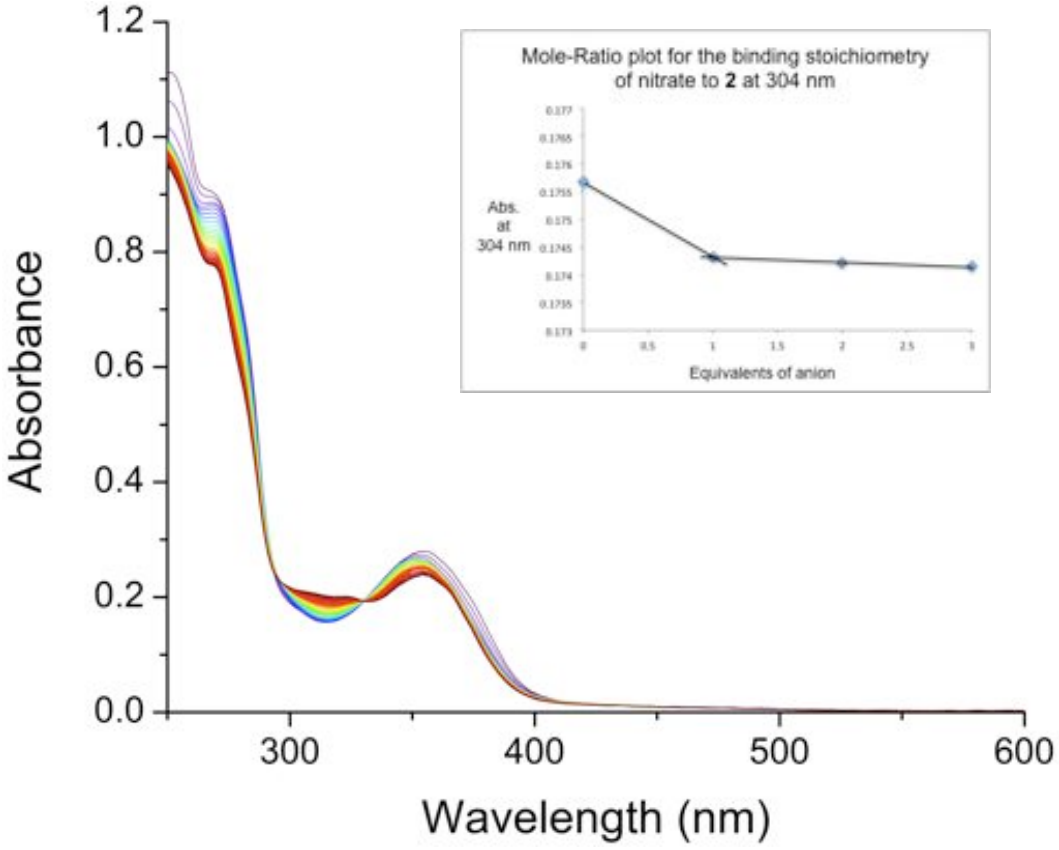

Figure A-8. Recorded UV-visible titration spectra of **2** upon titration of up to 30 equivalents of HNO_3. Each spectrum corresponds to an addition of 1 equivalent.

References

1 J. M. Holloway, R. A. Dahlgren, B. Hansen, W. H. Casey, *Nature*, 1998, **395**, 785-788.

2 G. Hanrahan, M. Gledhill, P. J. Fletcher, P. J. Worsfold, *Analytica Chimica Acta*, 2001, **440**, 55-62.

3 G. Zhu, S. Wang, Y. Wang, C. Wang, N. Risgaard-Peterson, M. S. M. Jetten, C. Yin, *The ISME J.: Multi. J. Micro. Eco.*, 2011, DOI:10.1038/ismej.2011.63.

4 D. D. Duan, *Acta Pharma. Sinica*, 2011, DOI:10.1038/aps.2011.30.

5 T. Schrader, A. D. Hamilton (Eds.) (2005), *Functional Synthetic Receptors.* Weinheim, Germany; WILEY-VCH Verlag GmbH & Co. KGaA.

6 P. Chakrabarti, *J. Mol. Biol.*, 1993, **234**, 463-482.

7 T. Yamaguchi, Y. Ikeda, Y. Abe, H. Kuma, D. Kang, N. Hamasaki, T. Hirai, *J. Mol. Biol.*, 2010, **397**, 179-189.

8 E. Pasqualetto, R. Aiello, L. Gesiot, G. Bonetto, M. Bellanda, R. Battistutta, *J. Mol. Biol.*, 2010, **400**, 448-462.

9 A. Basu, S. Mazor, J. R. Casey, *Biochem.*, 2010, **49**, 9226-9240.

10 P. A. Gale, *Acc. Chem. Res.*, 2011, **44**, 216-226.

11 E. A. Katayev, G. V. Kolesnikov, J. L. Sessler, *Chem. Soc. Rev.*, 2009, **38**, 1572-1586.

12 A. Enomoto, H. Kimura, A. Chairoungdua, Y. Shigeta, P. Jutanha, S. H. Cha, M. Hosoyamada, M. Takeda, T. Sekine, T. Igarashi, H. Matsuo, Y. Kikuchi, T. Oda, K. Ichida, T. Hosoya, K. Shimokata, T. Niwa, Y. Kanai, H. Endou, *Nature*, 2002, **417**, 447-452.

13 T. Hara, M. Ishikawa, J. Sawada, N. Ichikuni, S. Shimazu, *Green Chem.*, 2009, **11**, 2034-2040.

14 E. Noey, J. C. Curtis, S. Tam, D. M. Pham, E. F. Jones, *J. Chem. Edu.*, 2011, **88**, 793-797.

15 B. Dietrich, *Pure & Appl. Chem.*, 1993, **65**, 1457-1464.

16 E. A. Archer, H. Gong, M. J. Krische, *Tetrahedron*, 2001, **57**, 1139-1159.

17 H. Schneider, A. K. Yatsimirsky, *Chem. Soc. Rev.*, 2008, **37**, 263-277.

18 H. E. Simmons, C. H. Park, *J. Am. Chem. Soc.*, 1968, **90**, 2428-2429.

19 H. E. Simmons, C. H. Park, *J. Am. Chem. Soc.*, 1968, **90**, 2429-2431.

20 H. E. Simmons, C. H. Park, *J. Am. Chem. Soc.*, 1968, **90**, 2431-2432.

21 R. A. Bell, G. G. Christoph, F. R. Fronczek, R. E. Marsh, *Science*, 1975, **190**, 151-152.

22 P. D. Beer, P. A. Gale, *Angew. Chem. Int. Ed.*, 2001, **40**, 486-516.

23 P. Hoog, P. Gamez, I. Mutikainen, U. Turpeinen, J. Reedijk, *Angew. Chem.*, 2004, **116**, 5939-5941.

24 H. Casellas, C. Massera, F. Buda, P. Gamez, J. Reedijk, *New J. Chem.*, 2006, **30**, 1561-1566.

25 L. A. Barrios, G. Aromi, A. Frontera, D. Quinonero, P. M. Deya, P. Gamez, O. Roubeau, E. J. Shotton, S. J. Teat, *Inorg. Chem.*, 2008, **47**, 5873-5881.

26 T. J. Mooibroek, C. A. Black, P. Gamez, J. Reedijk, *Crystal Growth & Design*, 2008, 8, 1082-1093.

27 B. P. Hay, R. Custelcean, *Crystal Growth & Design*, 2009, 9, 2539-2545.

28 E. Graf, J. M. Lehn, *J. Am. Chem. Soc.*, 1976, **98**, 6403-6405.

29 J. M. Lehn, E. Sonveaux, A. K. Willard, *J. Am. Chem. Soc.*, 1978, **100**, 4914-4916.

30 P. G. Young, J. K. Clegg, M. Bhadbhade, K. A. Jolliffe, *Chem. Comm.*, 2011, **47**, 463-465.

31 A. P. Davis, J. B. Joos, *Coord. Chem. Rev.*, 2003, **240**, 143-156.

32 C. Bazzicalupi, A. Bencini, V. Lippolis, *Chem. Soc. Rev.*, 2010, **39**, 3709-3728.

33 O. A. Gerasimchuk, S. Mason, J. M. Llinares, M. Song, N. W. Alcock, K. Bowman-James, *Inorg. Chem.*, 2000, **39**, 1371-1375.

34 D. A. Nation, J. Reibenspies, A. E. Martell, *Inorg. Chem.*, 1996, **35**, 4597-4603.

35 Q. Lu, R. J. Motekaitis, J. J. Reibenspies, A. E. Martell, *Inorg. Chem.*, 1995, **34**, 4958-4964.

36 C. Anda, A. Llobet, A. E. Martell, B. Donnadieu, T. Parella, *Inorg. Chem.*, 2003, **42**, 8545-8550.

37 L. Yang, Y. Li, L. Jiang, X. Feng, T. Lu, *Cryst. Eng. Comm.*, 2009, **11** 2375-2380.

38 A. Hossain, P. Morehouse, D. Powell, K. Bowman-James, *Inorg. Chem.*, 2005, **44**, 2143-2149.

39 P. Ballester, *Chem. Soc. Rev.*, 2010, **39**, 3810-3830.

40 Y. Chen, D. Wang, Z. Huang, M. Wang, *Chem. Commun.*, 2011, **47**, 8112-8114.

41 C. R. Bondy, P. A. Gale, S. J. Loeb, *J. Am. Chem. Soc.*, 2004, **126**, 5030-5031.

42 D. J. White, N. Laing, H. Miller, S. Parsons, S. Coles, P. A. Tasker, *Chem. Commun.*, 1999, 2077-2078.

43 S. G. Galbraith, P. G. Plieger, P. A. Tasker, *Chem. Commun.*, 2002, 2662-2663.

44 P. G. Plieger, S. Parsons, A. Parkin, P. A. Tasker, *Dalton Trans.*, 2002, 3928-3930.

45 Q. W. Knapp, MSc thesis, The Spectroscopic Analysis of Di-copper Helicates as Receptors for Encapsulating Anions, 2009, Massey University.

46 M. Wenzel, G. B. Jameson, L. A. Ferguson, Q. W. Knapp, R. S. Forgan, F. J. White, S. Parsons, P. A. Tasker, P. G. Plieger, *Chem. Commun.*, 2009, 3606-3608.

47 M. Wenzel, Q. W. Knapp, P. G. Plieger, *Chem. Commun.*, 2011, **47**, 499-501.

48 M. Wenzel, S. R. Bruere, Q. W. Knapp, P. A. Tasker, P. G. Plieger, *Dalton Trans.*, 2010, **39**, 2936-2941.

49 W. Henderson and J. S. McIndoe, *Mass Spectrometry of Inorganic, Coordination and Organometallic Compounds*, John Wiley & Sons, West Sussex, 2005.

50 N. B. Cech, C. G. Enke, *Mass Spectrometry Rev.*, 2001, **20**, 362-387.

51 K. A. Conners, *Binding Constants: The Measurements of Molecular Complex Stability*, Wiley-Interscience, New York, 1987.

52 F. J. Rossotti, H. Rossotti, *The Determination of Stability Constants*, McGraw-Hill, New York, 1961.

53 B. J. Clark, T. Frost, M. A. Russell, *UV Spectroscopy: Techniques, Instrumentation, Data Handling*, Chapman & Hall, London, 1993.

54 W. Massa, *Crystal Structure Determination*, Springer-Verlag, New York, 2004.

55 N. Akkus, J. C. Campbell, J. Davidson, D. K. Henderson, H. A. Miller, A. Parkin, S. Parsons, P. G. Plieger R. M. Swart, P. A. Tasker, L. C. West, *Dalton Trans.*, 2003, 1932-1940.

56 M. R. Wagner, F. A. Walker, *Inorg. Chem.*, 1983, **22**, 3021-3028.

57 B. Dietrich, *Pure & Appl. Chem.*, 1993, **65**, 1457-1464.

58 E. Suet, H. Handel, *Tetrahedron Lett.*, 1984, **25**, 645-648.

59 H. D. B. Jenkins, H. K. Roobottom, J. Passmore, L. Glasser, *Inorg. Chem.*, 1999, **38**, 3609-3620.

60 R. S. Forgan, J. E. Davidson, F. P. A. Fabbiani, S. G. Galbraith, D. K. Henderson, S. A. Moggach, S. Parsons, P. A. Tasker, F. J. White, *Dalton Trans.*, 2010, **39**, 1763-1770.

61 A. W. Addison, T. N. Rao, J. Reedijk, J. Rijn, G. C. Verschoor, *J. Chem. Soc., Dalton Trans.*, 1984, **7**, 1349-1356.

62 K. Fakultatea, E. H. Unibertsitatea, *Chem. Rev.*, 2011, 2597-2625.

63 N. Ray, S. Tyagi, B. Hathaway, *Acta Cryst.*, 1982, **B38**, 1574-1577.

64 F. Costantino, A. Ienco, S. Midollini, A. Orlandini, L. Sorace, A. Vacca, *Eur. J. Inorg. Chem.*, 2008, 3046-3055.

65 N. R. Sangeetha, S. Pal, *J. Chem. Cryst.*, 1999, **29**, 287-293.

66 R. Gupta, S. Mukherjee, R. Mukherjee, *J. Chem. Soc., Dalton Trans.*, 1999, 4025-4030.

67 S. Roy, T. N. Mandal, A. K. Barik, S. Gupta, R. J. Butcher, M. S. E. Fallah, J. Tercero, S. K. Kar, *Polyedron*, 2008, **27**, 105-112.

68 A. W. Addison, T. N. Rao, E. Sinn, *Inorg. Chem.*, 1984, **23**, 1957-1967.

69 H. Arora, F. Lloret, R. Mukherjee, *Inorg. Chem.*, 2009, **48**, 1158-1167.

70 F. A. Mautner, F. R. Louka, S. S. Massoud, *J. Mol. Struc.*, 2009, 333-340.

71 S. Anbu, M. Kandaswamy, P. Suthakaran, V. Murugan, B. Varghese, *J. Inorg. Biochem.*, 2009, 401-410.

72 H. Arora, F. Lloret, R. Mukherjee, *Dalton Trans.*, 2009, 9759-9769.

73 J. Lorosch, H. Paulus, W. Haase, *Acta. Cryst.*, 1985, **C41**, 897-899.

74 S. Kawata, S. Kitagawa, M. Enomoto, H. Kumagai, M. Katada, *Inorg. Chim. Acta*, 1998, **283**, 80-90.

75 A. J. Rybarczyk-Pirek, M. Malecka, L. Glinka, J. Ochocki, *Acta Cryst.*, 2007, **C63**, m410-m412.

76 H. Kwong, L. Cheng, W. Lee, W. Wong, W. Wong, *Eur. J. Inorg. Chem.*, 2000, 1997-2002.

77 A. Okazawa, Y. Nagaichi, T. Nogami, T. Ishida, *Inorg. Chem.*, 2008, **47**, 8859-8868.

78 A. C. Sant'Ana, W. A. Alves, R. H. A. Santos, A. M. D. Ferreira, M. L. A. Temperini, *Polyhedron*, 2003, **22**, 1673-1682.

79 S. Naskar, S. Naskar, H. Mayer-Figge, W. S. Sheldrick, S. K. Chattopadhyay, *Polyhedron*, 2011, **30**, 529-534.

80 S. A. Komaei, G. A. Albada, J. G. Haasnoot, H. Kooijman, A. L. Spek, J. Reedijk, *Inorg. Chim. Acta*, 1999, **286**, 24-29.

81 S. Sarkar, A. Mondal, J. Ribas, M. G. B. Drew, K. Pramanik, K. K. Rajak, *Eur. J. Inorg. Chem.*, 2004, 4633-4639.

82 F. Bramsen, A. D. Bond, C. J. McKenzie, R. G. Hazell, B. Moubaraki, K. S. Murray, *Chem. Eur. J.*, 2005, **11**, 825-831.

83 C. Chou, C. Su, H. Tsai, K. Lii, *Inorg. Chem.*, 2005, **44**, 628-632.

84 F. Akagi, Y. Michihiro, Y. Nakao, K. Matsumoto, T. Sato, W. Mori, *Inorg. Chim. Acta*, 2004, **357**, 684-688.

85 K. N. Lazarou, V. Psycharis, S. P. Perlepes, C. P. Raptopoulou, *Polyhedron*, 2009, **28**, 1085-1096.

86 J. Tang, J. S. Costa, A. Golobic, B. Kozlevcar, A. Robertazzi, A. V. Vargiu, P. Gamez, J. Reedijk, *Inorg. Chem.*, 2009, **48**, 5473-5479.

87 C. Foltz, B. Stecker, G. Marconi, S. Bellemin-Laponnaz, H. Wadepohl, L. H. Gade, *Chem. Commun.*, 2005, 5115-5117.

88 G. A. Albada, I. Dominicus, I. Mutikainen, U. Turpeinen, J. Reedijk, *Polyhedron*, 2007, **26**, 3731-3736.

89 G. A. Albada, M. G. Horst, I. Mutikainen, U. Turpeinen, J. Reedijk, *Inorg. Chim. Acta*, 2008, **361**, 3380-3387.

90 L. A. Barrios, G. Aromi, A. Frontera, D. Quinonero, P. M. Deya, P. Gamez, O. Roubeau, E. J. Shotton, S. J. Teat, *Inorg. Chem.*, 2008, **47**, 5873-5881.

91 K. Youm, H. C. Kang, G. Lee, H. K. Woo, Y. J. Park, N. Lee, J. Ko, M. Jun, *Polyhedron*, 2006, **25**, 2318-2324.

92 K. Drabent, Z. Ciunik, A. Ozarowski, *Inorg. Chem.*, 2008, **47**, 3358-3365.

93 L. Wu, M. E. Keniry, B. Hathaway, *Acta Cryst.*, 1992, **C48**, 35-40.

94 J. Klingele, B. Moubaraki, K. S. Murray, J. F. Boas, S. Brooker, *Eur. J. Inorg. Chem.*, 2005, 1530-1541.

95 F. Hung;Low, K. K. Klausmeyer, *Polyhedron*, 2010, **29**, 1676-1686.

96 G. Marin, M. Andruh, A. M. Madalan, A. J. Blake, C. Wilson, N. R. Champness, M. Schroder, *Crystal Growth and Design*, 2008, **8**, 964-975.

97 C. Foltz, B. Stecker, G. Marconi, S. Bellemin-Laponnaz, H. Wadepohl, L. H. Gade, *Chem. Eur. J.*, 2007, **13**, 9912-9923.

98 B. Barszcz, T. Glowiak, J. Jerzierska, K. Kurdziel, *Inorg. Chem. Commun.*, 2002, **5**, 1056-1058.

99 C. D. Ene, C. Maxim, F. Tuna, M. Andruh, *Inorg. Chim. Acta*, 2009, **362**, 1660-1664.

100 C. Biswas, M. G. B. Drew, E. Ruiz, M. Estrader, C. Diaz, A. Ghosh, *Dalton Trans.*, 2010, **39**, 7474-7484.

101 T. Ruffer, B. Brauer, A. K. Powell, I. Hewitt, G. Salvan, *Inorg. Chim. Acta*, 2007, **360**, 3475-3483.

102 L. Carlucci, G. Ciani, A. Gramacciolo, D. M. Proserpio, S. Rizzato, *Cryst. Eng. Comm.*, 2000, **29**, 1-10.

103 H. Gampp, M. Maeder, C.J. Meyer, A. D. Zuberbuehler, *Talanta*, 1985, **32**, 95-101.

104 H. Gampp, M. Maeder, C.J. Meyer, A. D. Zuberbuehler, *Talanta*, 1985, **32**, 251-264.

105 H. Gampp, M. Maeder, C.J. Meyer, A. D. Zuberbuehler, *Talanta*, 1985, **32**, 1133-1139.

106 C. S. Tsai, *Biomacromolecules: Introduction to Structure, Function and Informatics*, John Wiley & Sons, New Jersey, 2007.

107 C. M. Fitchett, P. J. Steel, *Arkivoc*, 2006, 218-225.

108 B. Duffin, *Acta Cryst.*, 1968, **B24**, 396-400.

109 L. K. Thompson, A. W. Hanson, B. S. Ramaswamy, *Inorg. Chem.*, 1984, **23**, 2459-2465.

110 S. Ferrer, P. J. Koningsbruggen, J. G. Haasnoot, J. Reedijk, H. Kooijman, A. L. Spek, L. Lezama, A. M. Arif, J. S. Miller, *J. Chem. Soc., Dalton Trans.*, 1999, 4269-4276.

111 N. Li, S. Chen, S. Gao, *J. Coord. Chem.*, 2007, **60**, 117-123.

112 D. Ulku, L. Tatar, O. Atakol, S. Durmus, *Acta Cryst.*, 1999, **C55**, 1652-1654.

113 S. Das, C. Madhavaiah, S. Verma, P. K. Bharadwaj, *Inorg. Chim. Acta*, 2005, **358**, 3236-3240.

114 L. Vaiana, M. Mato-Iglesias, D. Esteban-Gomez, C. Platas-Iglesias, A. Blas, T. Rodriguez-Blas, *Polyhedron*, 2010, **29**, 2269-2277.

115 A. Tadsanaprasittipol, H. Kraatz, G. D. Enright, *Inorg. Chim Acta*, 1998, **278**, 143-149.

116 R. J. Majeste, E. A. Meyers, *J. Phys. Chem.*, 1970, **74**, 3497-3500.

117 J. Tang, E. Gao, W. Bu, D. Liao, S. Yan, Z. Jiang, G. Wang, *J. Mol. Struc.*, 2000, **525**, 271-273.

118 O. Castillo, I. Muga, A. Luque, J. M. Gutierrez-Zorrilla, J. Sertucha, P. Viitoria, P. Roman, *Polyhedron*, 1999, **18**, 1235-1245.

119 R. Xuan, M. Li, Y. Wan, *Acta Cryst.*, 2003, **C59**, m462-m464.

120 S. Youngme, G. A. Albada, N. Chaichit, P. Gunnasoot, P. Kongsaeree, I. Mutikainen, O. Roubeau, I. Reedijk, U. Turpeinen, *Inorg. Chim. Acta*, 2003, **353**, 119-128.

121 S. K. Padhi, V. Manivannan, *Polyhedron*, 2007, **26**, 1619-1624.

122 T. D. Coombs, B. J. Brisdon, C. P. Curtis, M. F. Mahon, S. A. Brewer, C. R. Willis, *Polyhedron*, 2001, **20**, 2935-2943.

123 J. L. Shaw, T. B. Cardon, G. A. Lorigan, C. J. Ziegler, *Eur. J. Inorg. Chem.*, 2004, 1073-1080.

124 W. S. Brotherton, P. M. Guha, H. Phan, R. J. Clark, M. Shatruk, L. Zhu, *Dalton Trans.*, 2011, **40**, 3655-3665.

125 P. Hoog, P. Gamez, M. Luken, O. Roubeau, B. Krebs, J. Reedijk, *Inorg. Chim. Acta*, 2004, **357**, 213-218.

126 B. Gole, R. Chakrabarty, S. Mukherjee, Y. Song, P. S. Mukherjee, *Dalton Trans.*, 2010, **39**, 9766-9778.

127 E. Y. Fursova, V. I. Ovcharenko, G. V. Romanenko, E. V. Tretyakov, *Tetrahedron Lett.*, 2003, **44**, 6397-6399.

128 T. Kajiwara, M. Nakano, K. Takahashi, S. Takaishi, M. Yamashita, *Chem. Eur. J.*, 2011, **17**, 196-205.

129 E. Fursova, G. Romanenko, V. Ikorskii, V. Ovcharenko, *Polyhedron*, 2003, **22**, 1957-1964.

130 T. Kajiwara, K. Takahashi, T. Hiraizumi, S. Takaishi, M. Yamashita, *Polyhedron*, 2009, **28**, 1860-1863.

131 P. Singh, V. C. Copeland, W. E. Hatfield, D. J. Hodgson, *J. Phys. Chem.*, 1972, **76**, 2887-2891.

132 L. K. Thompson, S. K. Mandel, E. J. Gabe, F. L. Lee, A. W. Addison, *Inorg. Chem.*, 1987, **26**, 657-664.

133 S. K. Mandal, L. K. Thompson, M. J. Newlands, E. J. Gabe, K. Nag, *Inorg. Chem.*, 1990, **29**, 1324-1327.

134 Z. He, J. Chaimungkalanont, D. C. Craig, S. B. Colbran, *J. Chem. Soc., Dalton Trans.*, 2000, 1419-1429.

135 M. Du, Y. Guo, X. Bu, *Inorg. Chim. Acta*, 2002, 136-140.

136 B. Yang, H. Zeng, Z. Dong, J. Mao, *J. Coord. Chem.*, 2003, **56**, 1513-1523.

137 S. G. Telfer, N. D. Parker, R. Kuroda, T. Harada, J. Lefebvre, D. B. Leznoff, *Inorg. Chem.*, 2008, **47**, 209-218.

138 O. O. E. Onawumi, O. O. P. Faboya, O. A. Odunola, T. K. Prasad, M. V. Rajasekharan, *Polyhedron*, 2008, 113-117.

139 M. M. Piepenbrock, K. M. Anderson, B. C. R. Sansam, N. Clarke, J. W. Steed, *Cryst. Eng. Comm.*, 2009, **11**, 118-121.

140 H. Yang, S. Xu, *Acta Cryst.*, 2010, **E66**, m874-m875.

141 Bala Suresh, *Sulfuric Acid*, 2009, http://www.sriconsulting.com/CEH/Public/Reports/781.5000/

142 Q. Wang, C. Wilson, A. J. Blake, S. R. Collinson, P. A. Tasker, M. Schroder, *Tetrahedron Letters*, 2006, **47**, 8983-8987.

143 Rigaku, *CrystalClear.*, Version 1.4.0, Rigaku Americas Corporation, The Woodlands, Texas, USA, 2005.

144 Rigaku, PROCESS-AUTO, Rigaku Corporation, Tokyo, Japan, 1998.

145 G. M. Sheldrick, *Acta Crystallogr., Sect. A: Found. Crystallogr.*, 2008, **64**, 112-122.